https://doi.org/10.5194/egusphere-2025-1616
Preprint. Discussion started: 10 April 2025

The Greenland-Ice-Sheet evolution over the last 24,000 years: insights from model simulations evaluated against ice-extent markers

Tancrède P.M. Leger[1,2], Jeremy C. Ely[1], Christopher D. Clark[1], Sarah L. Bradley[1], Rosie E. Archer[3], Jiang Zhu[4]

[1] School of Geography and Planning, University of Sheffield, Sheffield, S10 2TN, UK
[2] Institute of Earth Surface Dynamics, University of Lausanne, Lausanne, Switzerland
[3] Department of Geography and Environmental Sciences, Northumbria University, Newcastle, UK
[4] Climate and Global Dynamics Laboratory, NSF National Center for Atmospheric Research, Boulder, CO, USA

Correspondence: Tancrède P. M. Leger (tancrede.leger@unil.ch): personal address: tankleger@gmail.com

Abstract. Continental ice sheets possess a long-term memory that is stored within both the geometry and thermal properties of ice. In Greenland, this causes a disequilibrium between the present-day ice sheet and current climate, as the ice sheet is still adjusting to past changes that occurred over millennial timescales. Data-consistent modelling of the paleo Greenland-Ice-Sheet evolution is thus important for improving model initialisation procedures used in future ice sheet projection experiments. Additionally, open questions remain regarding the ice sheet's former volume, extent, flux, internal flow dynamics, thermal conditions, and how such properties varied in space since the last glaciation. Here, we conduct a modelling experiment that aims to produce simulations in agreement with empirical data on the extent and timing of the ice sheet's margin positions over the last 24,000 years. Due to large uncertainties in ice-sheet model parameters and boundary conditions, we apply a perturbed parameter ensemble approach and run 100 ice-sheet-wide simulations at 5 x 5 km horizontal resolution using the Parallel Ice Sheet Model. Our simulations are forced by paleo-climate and ocean simulations of the isotope-enabled Community Earth System Model. Using quantitative model-data comparison and the newly developed Greenland-wide reconstruction of former ice margin retreat (PaleoGrIS 1.0), we scored each simulation's fit across Greenland from 24,000 years ago until 1850 AD. The resulting ensemble and best-scoring simulations provide insights related to the dynamics, causes and spatial heterogeneities of the local LGM, Late-glacial, and Holocene evolution of the Greenland Ice Sheet. We for instance find that between 16 and 14 thousand years ago, the ice sheet lost most of its ice grounded on the continental shelf. This marine-sector demise, associated with up to seven times greater mass loss rates than observed today, was predominantly caused by ocean warming while air temperatures possibly remained too cold to generate surface melt. We specifically detail and showcase results from our model-data comparison procedures, including regional heterogeneities in model-data fit and the sensitivity of model-data agreement scores to certain parameter configurations, that will likely prove useful for others working on paleo-ice-sheet modelling experiments. Finally, we report on the remaining model-data misfits in ice

https://doi.org/10.5194/egusphere-2025-1616
Preprint. Discussion started: 10 April 2025

extent, here found to be largest in northern, northeastern, and central-eastern Greenland, and discuss possible causes for such spatial heterogeneity in model-data agreement.

1 Introduction

Due to anthropogenic climate change, the Greenland Ice Sheet (GrIS) is losing mass at an increasing rate and is now a major contributor to global mean sea level rise (Meredith et al., 2019). Its future contribution remains uncertain, however, and projections show important discrepancies between models/studies, with most estimations ranging between ~70 and ~190 mm of sea level rise contribution by the year 2100 under the RCP 8.5 / SSP5-85 emission scenarios (Aschwanden et al., 2019; The IMBIE Team., 2019; Goelzer et al., 2020; Edwards et al., 2021). Reducing uncertainties in GrIS projections is not only crucial for estimating future sea level rise and Greenland-wide environmental changes, but also for anticipating future global climate change, in part due to the ice-sheet's impact on ocean circulation and the potential slowdown of the Atlantic Meridional Overturning Circulation (AMOC) following increasing freshwater releases (Yu et al., 2016; Martin et al., 2022; Sinet et al., 2023). A major source of uncertainty in future ice-sheet projections relates to the model initialisation procedures required to obtain an appropriate initial state, *i.e.* the model 'spinup' (Rogozhina et al., 2011; Seroussi et al., 2019). This is a challenge mainly because ice sheets are not in equilibrium with contemporary climate but are instead still affected by past climate changes that occurred over thousands of years (Oerlemans et al., 1998; Yan et al., 2013; Calov et al., 2015; Yang et al., 2022). While paleo spinups are more appropriate to capture this ice-sheet memory, they generally fail at representing the present-day ice sheet conditions as accurately as inversion schemes used in equilibrium spinups (Goelzer et al., 2017), due in part to the greater uncertainties in forcings, model parameterisations and boundary conditions in the paleo realm (Aschwanden et al., 2013). Hence, there is a need to reduce such uncertainties by producing ensembles of higher-resolution paleo model simulations that are quantitatively scored against empirical reconstructions of past GrIS evolution. Although rare, such investigations may help obtain more appropriate initialisation procedures that better capture the ice-sheet's long-term memory while accurately modelling its present-day state (Pittard et al., 2022).

Numerous open research questions remain regarding the past behaviour of the GrIS between the global Last Glacial Maximum (LGM), which occurred ~25 - 21 thousand years before present (kyr BP), and the present-day. For instance, the maximum GrIS volume during the last glaciation remains debated and differs by a factor of up to 2.5 between modelling studies (*e.g.* Bradley et al., 2018; Quiquet et al., 2021; Yang et al., 2022). The maximum GrIS extent, while constrained empirically in certain regions (*e.g.* Ó Cofaigh et al., 2013), is still unknown in numerous locations due to the difficulty of accessing and obtaining offshore geomorphological and geochronological constraints on ice retreat, making existing data of this nature somewhat sparse (Funder et al., 2011; Sinclair et al., 2016; Leger et al., 2024). The timing, magnitude and

https://doi.org/10.5194/egusphere-2025-1616
Preprint. Discussion started: 10 April 2025

rates of ice margin retreat and mass loss experienced during the last deglaciation, while essential to contextualise present-day mass loss, are also poorly known and challenging to determine empirically. The magnitude of ice margin retreat behind its present-day margins in response to the Holocene Thermal Maximum (HTM: ~10-5 kyr BP), a warmer period often used as an analogue for expected warming in the coming decades, also remains undetermined (Briner et al., 2021). A final rationale for 3D modelling of the former GrIS is that numerous characteristics of the past ice sheet, impacting former climate, ocean conditions, landscape evolution, biodiversity and human history, are highly challenging (if not impossible) to constrain with field data alone. This is for instance the case for paleo changes in ice-sheet discharge, velocity, ice temperature, calving fluxes, mass balance, basal conditions, and their spatio-temporal variations.

Addressing some of the above knowledge gaps, and providing a present-day GrIS state that contains the appropriate long-term memory of past climate changes, requires: i) to force a three-dimensional and thermo-mechanical ice-sheet model with a paleoclimate, and ii) to produce paleo GrIS model simulations that agree (within error) with the available empirical data on former ice-sheet geometry and behaviour, while keeping the model physically-consistent and respecting mass conservation. Combining these requirements is a major challenge and has yet to be achieved. To this day, few studies modelling the GrIS evolution since the LGM have applied a quantitative model-data comparison scheme to constrain a set of simulations using geological field observations (*e.g.* Huybrechts, 2002; Lecavalier et al., 2014; Born & Robinson, 2021). Of those that did, the empirical datasets used were mainly relative sea level indicators, ice-core derived thinning curves (Vinther et al., 2009), and englacial stratigraphic isochrones (Born & Robinson, 2021; Rieckh et al., 2024). The paleo sea-level community, in particular, has pioneered the production of Greenland-wide datasets (*e.g.* Gowan, 2023) reconstructing the magnitude and rate of relative sea level drop during the Late-glacial and early-to-mid Holocene, when deglacial retreat caused the Greenland peripheral lithosphere to rebound. Such records have been used to assess GrIS-wide simulations by comparing modelled versus empirical uplift rates and relative sea level change (*e.g.* Simpson et al., 2009). However, relative sea level indicators and other previously used datasets are indirect proxies of former ice-sheet geometry, and do not provide a robust constraint on the position and shape of the former grounded GrIS margin retreat through time. With relative-sea-level-based comparisons, moreover, the quality of model-data fit is heavily dependent on parameterisations of the Earth and glacial isostatic adjustment (GIA) models. On the other hand, moraine ridges, glacial erratic boulders, trimlines, till units and other ice-contact landforms/deposits are directly deposited and/or exposed at the ice-sheet terminal or lateral margins. When dated, such records provide a more direct mean of reconstructing former ice-sheet extent and thickness through time. The recent production and release of the PaleoGrIS 1.0 database and ice-extent isochrone reconstruction provides, for the first time, such a dataset at the GrIS-wide scale (Leger et al., 2024). Thus, despite remaining uncertainties due to the spatially and temporally heterogeneous nature of field observations, we now have the opportunity to compare numerical model outputs against a different, arguably more detailed and direct reconstruction of former grounded ice extent, and thus of former ice-sheet geometry.

https://doi.org/10.5194/egusphere-2025-1616
Preprint. Discussion started: 10 April 2025

We present a perturbed parameter ensemble of 100 simulations using the Parallel Ice Sheet model (PISM: Winkelmann et al., 2011) forced by transient paleoclimate and ocean simulations of the isotope-enabled Community Earth System Model (iCESM: Brady et al., 2019). The ice-sheet simulations model the entire GrIS between 24 kyr BP and 1850 AD at a horizontal resolution of 5 x 5 km which, for such long timescales and large simulation numbers, is unprecedented. Each ensemble simulation is quantitatively scored against i) empirical data on the maximum size and extent of the ice sheet (local LGM extent), ii) the PaleoGrIS 1.0 reconstruction of ice-margin retreat during the last deglaciation (Leger et al., 2024), and iii) the present-day GrIS extent. Unlike several paleo GrIS modelling experiments of similar design (*e.g.* Simpson et al., 2009; Lecavalier et al., 2014), empirical data is here not used to force the model or as a constraint during simulations. Instead, model-data fit is quantified after the simulation is complete to ensure simulations remain consistent with ice-flow physics (within model approximations) and mass conservation (e.g. Ely et al., 2024). The results of our ensemble, as well as best-fit simulations, provide numerous insights into the LGM-to-present evolution of the ice sheet and present interesting heterogeneities in model-data fit. We report and discuss these findings along with our experiment methodology below.

2 Methods

2.1 The ice-sheet model setup

To model the last 24 kyrs of GrIS evolution, we use PISM version 2.0.5, an open-source, three-dimensional and thermo-mechanical model used widely to simulate ice-sheet systems (Winkelmann et al., 2011; Aschwanden et al., 2016; Albrecht et al., 2020; Clark et al., 2022; Ely et al., 2024; Khroulev & The PISM authors, 2020). Our overall approach is to run an ensemble of 100 PISM simulations over the entire Greenland Ice Sheet (GrIS) at 5 x 5 km horizontal resolution (Fig. 1), from 24 kyr BP to the Pre-Industrial era (PI: 1850 AD). Within the ensemble, we vary 10 key model parameters (Table 1). Each ensemble simulation is scored against empirical data on the timing of ice extent using PaleoGrIS 1.0 (Leger et al., 2024) and model-data comparison procedures (e.g. ATAT 1.1; Ely et al., 2019), enabling us to isolate best-fit simulations. Together with the full ensemble, these are analysed further to provide quantitative results presented and discussed in sections 3 and 4 (Fig. 2). In the Methods sections below, we describe our model setup and input data used as forcings to the spin-up and transient simulations. For a full description of PISM and its capabilities, the reader is referred to the complete manual (https://www.pism.io/docs/; Khroulev & The PISM authors, 2020).

https://doi.org/10.5194/egusphere-2025-1616
Preprint. Discussion started: 10 April 2025

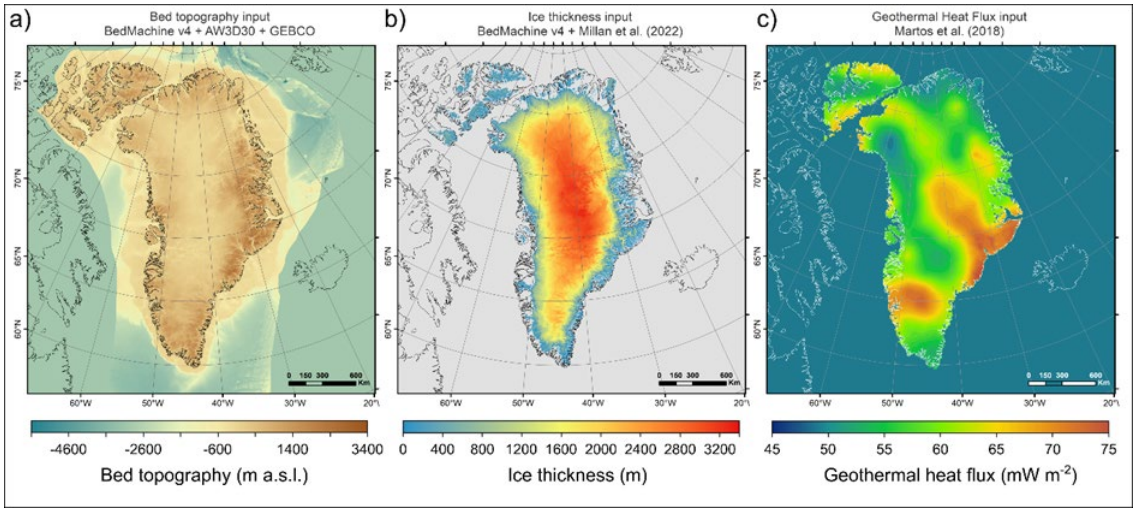

Figure 1. Time-independent and two-dimensional forcing fields used as inputs for present-day bed elevation (panel a), ice thickness (panel b; Morlighem et al., 2017**;** Millan et al., 2022**), and geothermal heat flux (panel c;** Martos et al., 2018**). Bed elevation (panel a) is estimated by merging several products. Topography under the contemporary GrIS is from BedMachine v4 (**Morlighem et al., 2017**; spatial resolution: 150 m). For terrestrial regions with no GrIS cover, we use the ALOS World 3D 30 m Digital Elevation Model (DEM;** Tadono et al., 2014**). Present-day periphery ice is removed using thickness estimates from** Millan et al. (2022)**. For other regions (ice-free ocean and other landmasses), we use the 15 arc-second resolution General Bathymetric Chart of the Oceans** (GEBCO Bathymetric Compilation Group 2022, 2022)**. These datasets are resampled (to 5 x 5 km) using cubic convolution** (Keys, 1981)**.**

https://doi.org/10.5194/egusphere-2025-1616
Preprint. Discussion started: 10 April 2025

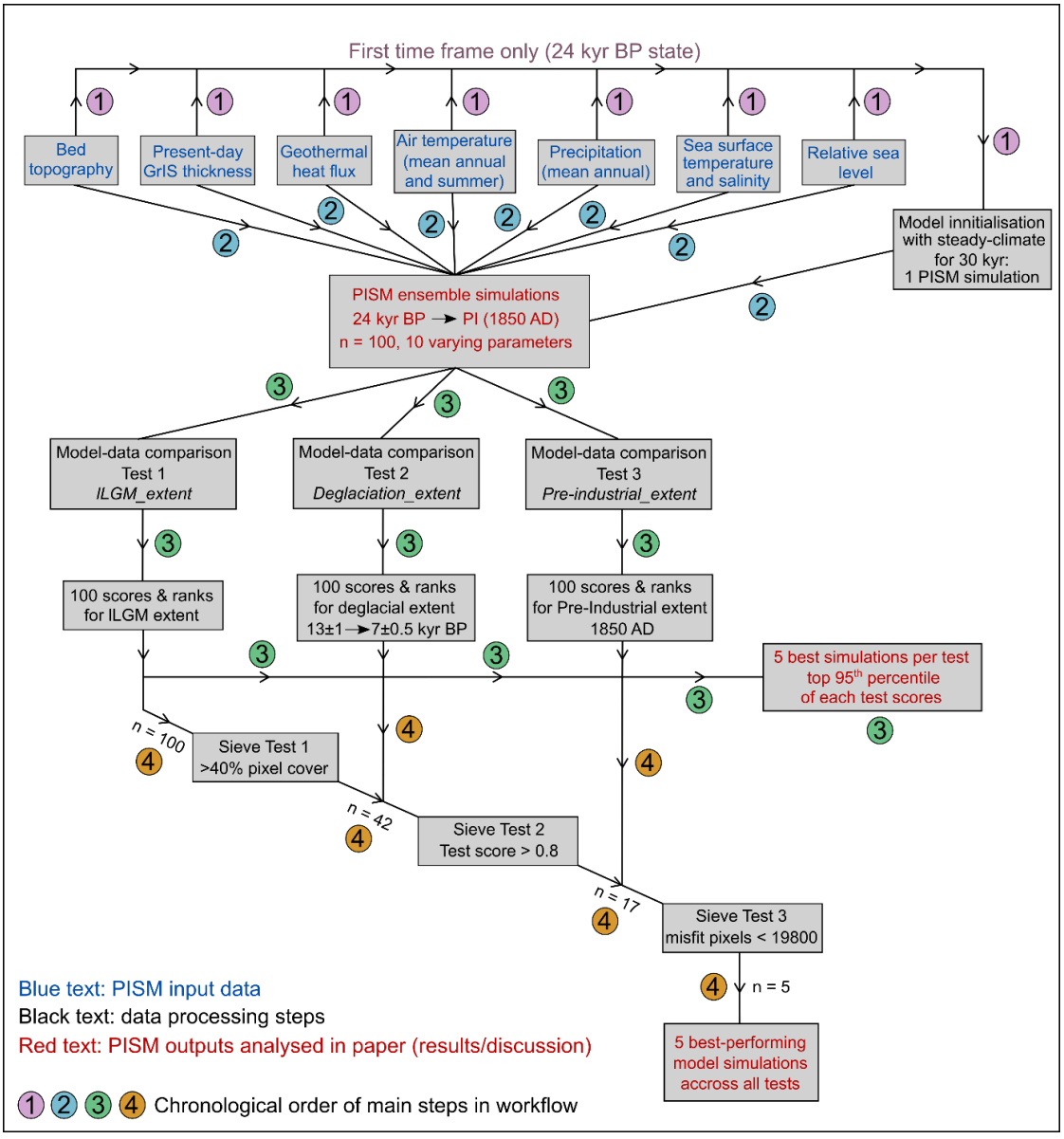

Figure 2. Flowchart diagram illustrating the methodological workflow followed in this study's modelling experiment including input datasets (step 1), model initialisation (step 1), transient ensemble simulations modelling (step 2) and post-processing steps including model-data comparison (3) and ensemble sieving (4). The reader is referred to the methods section for more details.

https://doi.org/10.5194/egusphere-2025-1616
Preprint. Discussion started: 10 April 2025

2.1.1 Ice flow

To model ice flow, PISM uses a hybrid stress balance scheme that combines the Shallow Ice Approximation (SIA) and the Shallow Shelf Approximation (SSA) (Bueler and Brown, 2009). PISM also features an enthalpy-based and three-dimensional formulation of thermodynamics enabling to model polythermal ice and basal melt (Aschwanden et al., 2012). For ice rheology ($\dot{\epsilon}$), we use the default Glen-Paterson-Budd-Lliboutry-Duval flow law,

$$\dot{\epsilon}_{i,j} = E \, . A(T, \omega) \, \tau_e^{n-1} \, \tau_{i,j} \, , \tag{1}$$

where n is the flow-law exponent, E a flow enhancement factor, A the Arrhenius factor (ice softness) determined by the liquid water content, ω, and ice temperature, T, while τ and τ_e represent the deviatoric and effective stresses, respectively (Aschwanden et al., 2012). In our ensemble, we vary E uniformly for both the SIA and SSA (see section 2.3) and keep $n = 3$ as default.

2.1.2 Boundary conditions

The ice-bed interface

We use the slip law of Zoet and Iverson (2020), which considers both mechanisms of glacier sliding over rigid beds and subglacial till deformation with minimal parameterisation and no required knowledge of the bed type. In PISM, this law is formulated as

$$\boldsymbol{\tau}_b = -\tau_c \frac{\boldsymbol{u}}{(|\boldsymbol{u}| + u_t)^q |\boldsymbol{u}|^{1-q}} \, , \tag{2}$$

where $\boldsymbol{\tau}_b$ is the basal shear stress, τ_c the basal yield stress, $\boldsymbol{u}$ the slip velocity and u_t the threshold velocity at which shear stress equals the Coulomb shear strength of the till. In our simulations, u_t is kept constant at 50 m yr^{-1} (Khroulev and The PISM authors, 2020; Zoet and Iverson, 2020) while q varies between simulations (see section 2.3). We account for space- and time-dependent yield stress, τ_c, controlled by: **1**) a simple hydrology model (Tulaczyk et al., 2000) which determines the effective pressure, N_{till}, from the till-pore water content obtained by storing basal melt locally up to a threshold (here set to 2 m); and **2**) the till friction angle, ϕ, *i.e.* the frictional strength of basal till materials (Cuffey and Paterson, 2010)

$$\tau_c = \tan(\phi) \, N_{till} \, . \tag{3}$$

https://doi.org/10.5194/egusphere-2025-1616
Preprint. Discussion started: 10 April 2025

By assuming basal materials in valley troughs are generally weaker than towards mountain tops, we parameterise ϕ as a piece-wise linear function of bed elevation, b, (after Aschwanden et al., 2013; 2016; Huybrechts and de Wolde, 1999)

$$\phi(x,y) = \begin{cases} \phi_{min}, & b(x,y) \le b_{min}, \\ \phi_{min} + (b(x,y) - b_{min})M, & b_{min} < b(x,y) < b_{max}, \\ \phi_{max}, & b_{max} \le b(x,y), \end{cases} \quad (4)$$

where $M = (\phi_{max} - \phi_{min}) / (b_{max} - b_{min})$. We set upper and lower elevation thresholds (b_{min}, b_{max}) to -400 and 500 m a.s.l., respectively, while ϕ thresholds (ϕ_{min}, ϕ_{max}) are simulation-dependent (Table 1, see section 2.3). This parameterisation was shown to produce flow velocities consistent with observations for major GrIS glaciers (Aschwanden et al., 2016).

Bed elevation is estimated by merging several products including BedMachine v4 (Morlighem et al., 2017), the ALOS World 3D 30 m Digital Elevation Model (DEM; Tadono et al., 2014), and the General Bathymetric Chart of the Oceans (GEBCO Bathymetric Compilation Group 2022, 2022). The reader is referred to Figure 1 for more details regarding these data. To avoid modelling large non-Greenlandic ice bodies, Iceland and Baffin Island are manually removed (Fig. 1). Modelling the Innuitian Ice Sheet (IIS) together with the GrIS is important as the two ice sheets coalesced (Jennings et al., 2011) and thus dynamically interacted each other (Bradley et al., 2018). We thus include Ellesmere Island in our domain, with local modern icecaps removed using present-day ice thickness estimates from Millan et al. (2022). Finally, we use a two-dimensional and time-independent geothermal heat flux data from Martos et al. (2018) (Fig. 1). This dataset ranges from 0.049 to 0.073 W m^{-2}, and is consistent with a plume track (the Iceland hotspot) that crossed Greenland from NW to SE. We run PISM at the horizontal resolution of 5 x 5 km (grid size: 620 x 620), with 101 vertical ice layers using quadratic concentration towards the base.

https://doi.org/10.5194/egusphere-2025-1616
Preprint. Discussion started: 10 April 2025

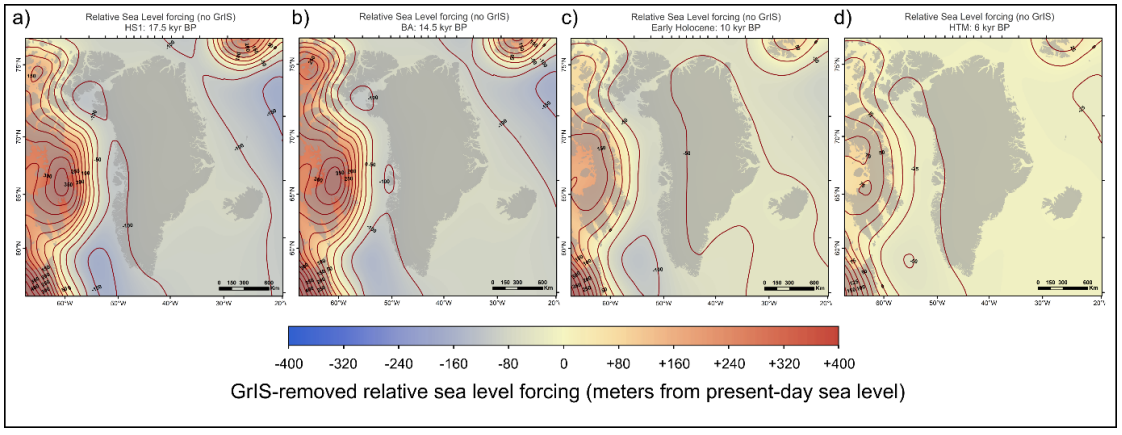

Figure 3. GrIS-removed (non-local components) relative sea-level forcing data for four different time slices and given as input to our transient ensemble simulations. These snapshots show the relative sea-level prior to adding the GrIS-specific contribution to GIA-induced relative sea-level change during our transient ensemble simulations (see methods section). Positive offset values (red) indicate isostatic bed depression relative to present and thus higher relative sea-levels than today, while negative offset values (blue) indicate isostatic bed uplift relative to present (*e.g.* on a peripheral bulge) and thus lower relative sea-levels than today. Snapshots are shown for the the HS 1 cooling event (panel a), the BA warming event (panel b; 14.5 kyr BP), the early Holocene (panel c; 10 kyr BP), and the HTM warming event (panel d; 6 kyr BP). All model input data fields are re-projected to EPSG:3413 and resampled to a 5 x 5 km resolution using cubic convolution.

https://doi.org/10.5194/egusphere-2025-1616
Preprint. Discussion started: 10 April 2025

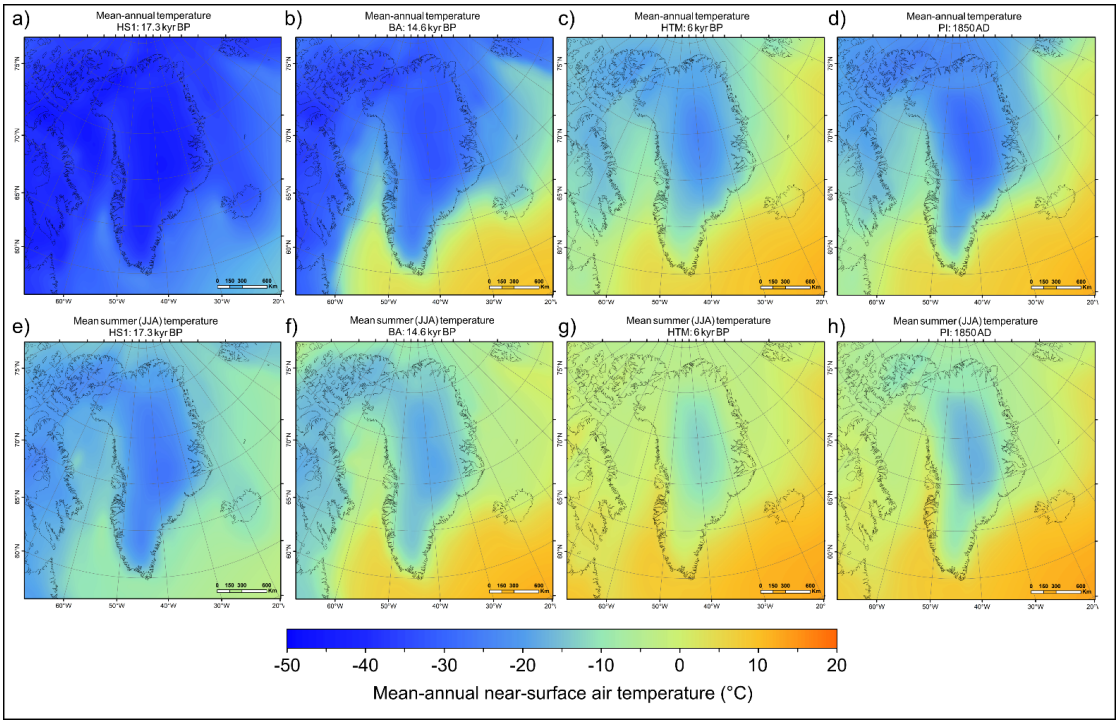

Figure 4. Two-dimensional fields of reference height mean-annual (panels a-d) and mean-summer (JJA mean; panels e-h) temperature data used as input in our modelling experiment, derived from iCESM transient and equilibrium time slice simulations (see methods section), and shown as snapshots for the HS 1 cooling event (panels a, e), the BA warming event (panels b, f), the HTM warming event (panels c, g), and the PI (1850 AD; panels d, h). All climate input data fields are re-projected to EPSG:3413 and resampled to a 5 x 5 km resolution using cubic convolution.

https://doi.org/10.5194/egusphere-2025-1616
Preprint. Discussion started: 10 April 2025

The ice-atmosphere interface

To compute Surface Mass Balance (SMB) from two-dimensional fields of time-dependent reference height temperature and precipitation (see section 2.1.3), we use PISM's default Positive-Degree-Day (PDD) model (Calov and Greve, 2005; Ritz, 1997). Precipitation when temperature is above 2 °C and under 0 °C is interpreted as rain and snow, respectively, with a linear transition between. The fraction of surface melt that refreezes is set to 60% (EISMINT-Greenland value; Ritz, 1997). Spatio-temporal variations in the standard deviation, σ, of daily temperature variability influences SMB (Arnold and MacKay, 1964). We parameterise σ to be a linear function of reference height air temperature T (and indirectly, of ice surface elevation)

$$\sigma = aT + b. \tag{5}$$

We assign b a value of 1.66 (after Seguinot and Rogozhina, 2014) and vary a as part of our ensemble (see section 2.3).

The ice-ocean interface

For floating sectors of the modelled GrIS, sub-shelf melt is obtained by computing basal melt rate and temperature from thermodynamics in a boundary layer (Hellmer et al., 1998; Holland and Jenkins, 1999). This requires time-dependent two-dimensional fields of potential temperature and practical salinity (see section 2.1.3.). Calving was likely a predominant ablation mechanism during the local LGM (~21-15 kyr BP) and throughout the Late-Glacial, when the GrIS was mostly marine-terminating (Funder et al., 2011a). Although physical calving processes remain poorly understood, we here model it following similar PISM parameterisations as Albrecht et al. (2020) and Pittard et al. (2022). Firstly, floating ice at the calving front thinner than a given threshold is automatically calved (see section 2.3). Secondly, we use the strain-rate-based eigen calving law (Albrecht and Levermann, 2014; Levermann et al., 2012) to determine the average calving rate, c, based on the horizontal strain rate, $\dot{\epsilon}_{\pm}$, derived from SSA-velocities, and a constant, K, integrating ice material properties at the calving front

$$c = K\,\dot{\epsilon}_{+}\,\dot{\epsilon}_{-}\,, \quad \dot{\epsilon}_{\pm} > 0. \tag{6}$$

We assign K a value of 5 x 10^{17} m s^{-1} (after Albrecht et al., 2020; Pittard et al., 2022). While a von Mises stress - type calving law may be more appropriate for fjord-terminating glaciers (*e.g.* Aschwanden et al., 2019), the GrIS expanded over continental shelves and was entirely marine-terminating during the local LGM, thus forming wide ice shelves comparable to Antarctica today (Jennings et al., 2017). As the ice sheet was in this configuration for more than half our simulated timeframe, we rely on the eigen calving law

https://doi.org/10.5194/egusphere-2025-1616
Preprint. Discussion started: 10 April 2025

throughout our simulations. Following Albrecht et al. (2020), we further restrict ice-shelf extent by calving ice when bathymetry exceeds 2 km, with the exception of Baffin Bay.

The grounding line location is determined by computing a floatation criterion (Khroulev and The PISM authors, 2020). This criterion depends on water depth, defined as the vertical distance between the geoid and the solid earth surface (Mitrovica and Milne, 2003). Around Greenland, and for the timeframe of interest (24-0 kyr BP), spatio-temporal variations in water depth result from changes in the global mean sea level and GIA-induced deformation of the solid earth (Rovere et al., 2016). The latter can result from variations in GrIS mass (local sources), and the influence of the neighbouring Laurentide Ice Sheet (LIS) and IIS, responsible for spatially and temporally variable sea level around Greenland (non-local sources)(Bradley et al., 2018). During and following glaciations, non-local contributions can be significant, as Greenland is located on the eastern peripheral forebulge generated by the LIS (Simpson et al., 2009; Lecavalier et al., 2014) (Fig. 3). Here, we account for this interplay and combine at each time step the non-local relative sea level signal calculated from an offline GIA model with the local GrIS-driven signal, enabling to compute the final water depth and resulting floatation criterion (Fig. 3).

For the local GrIS signal, we use PISM's Lingle-Clark-type viscoelastic deformation model (Lingle and Clark, 1985; Bueler et al., 2007). We use default lithosphere flexural rigidity and mantle density values of 5 x 10^{24} N m^{-1} and 3300 kg m^{-3}, respectively. For mantle (half-space) viscosity, we use a value of 5 x 10^{20} Pa s^{-1}, consistent with Lambeck et al. (2017). To calculate the non-local sea level change across the region of interest, we run an offline GIA model. This model was run at a resolution of 512° and solves the generalized sea level equation (Mitrovica & Milne, 2003; Kendall et al., 2005) accounting for sea level change in regions of retreating marine-based ice, perturbations to the Earth's rotation vector, and time-varying shoreline migration. For the input ice sheet reconstruction, we use a hybrid reconstruction (Lambeck et al., 2014; 2017), where the GrIS is removed from the North American ice sheet reconstruction. We use a 1D viscoelastic earth model with a lithosphere thickness of 96 km and upper and lower mantle viscosities of 5 x 10^{20} Pa s^{-1} and 1 x 10^{22} Pa s^{-1}, respectively.

https://doi.org/10.5194/egusphere-2025-1616
Preprint. Discussion started: 10 April 2025

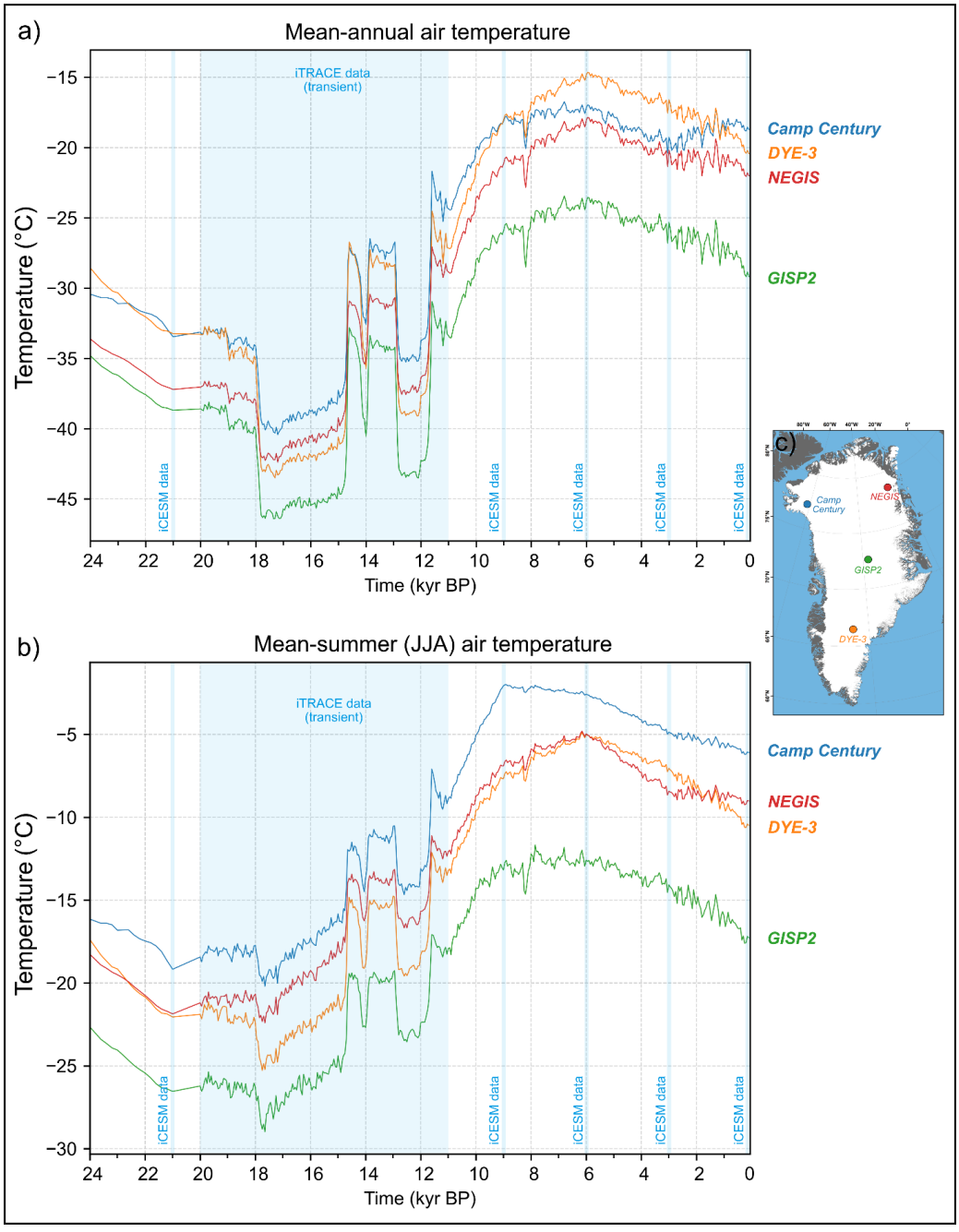

Figure 5. Time series of reference height mean-annual (panel a) and mean-summer (JJA-mean; panel b) air temperature data used as forcing in our ensemble simulations, at 4 different locations of the ice sheet (shown on inset: panel c). Transparent blue bands highlight time windows covered by iCESM climate data. In between these data points, forcing fields are approximated using a glacial index (see methods section).

https://doi.org/10.5194/egusphere-2025-1616
Preprint. Discussion started: 10 April 2025

2.1.3 Atmospheric and oceanic forcings

Air temperature and precipitation

SMB is forced with two-dimensional and time-dependent fields of reference height air temperature and total precipitation (Figs. 4-8). We use pre-existing simulations from iCESM (Brady et al., 2019) versions 1.2 and 1.3, run at a horizontal resolution of 1.9° in latitude and 2.5° in longitude for the atmosphere and a nominal 1° for the oceans. We use simulations ran with full forcing, *i.e.* including ice sheet (from ICE-6G: Peltier et al., 2015), orbital (Berger, 1978), greenhouse gases (Lüthi et al., 2008) and meltwater forcings. Between 20 and 11 kyr BP, we use data from the iTRACE experiment, ran with iCESM 1.3 (He et al., 2021a, b). Thanks to an improved climate model, higher resolution, and the addition of water isotopes, iTRACE simulates a climate over Greenland that is more data-consistent (He et al., 2021a) than the former CESM simulation of the last deglaciation TRACE-21 (Liu et al., 2009). Additionally, we use equilibrium time-slice simulations ran at 21 kyr BP and PI (1850 AD) (iCESM 1.3), and at 9, 6, and 3 kyr BP (iCESM 1.2). To create continuous forcing over remaining data gaps, we use a glacial index approach (Niu et al., 2019; Clark et al., 2022) and linearly scale our climate fields proportionally to variations in independent climate reconstructions (Fig. 5). For data gaps between 21 kyr BP and the PI (*e.g.* 11 - 9 kyr BP), we use the seasonally-resolved Greenland-wide temperature and precipitation reconstruction of Buizert et al. (2018) as glacial index. Between 24 and 21 kyr BP, we use surface air temperature and $\delta^{18}O$ reconstructions of Osman et al. (2021) to scale variations in temperature and precipitation fields, respectively. The results are time-dependent, two-dimensional fields of mean annual and mean summer (JJA) reference height air temperature and mean precipitation rate, continuous between 24 kyr BP and PI (Fig. 4-8). From mean annual and mean summer temperatures, our SMB scheme reads a cosine yearly cycle generating an idealised seasonality signal.

Ocean temperature and salinity

To compute sub-shelf melt, the chosen parameterisation (Holland and Jenkins, 1999) requires time-varying two-dimensional fields of potential ocean temperature and salinity data (see section 2.1.2). For the ocean temperature, we use the LGM-to-present ensemble-mean sea surface temperature (SST) reconstruction of Osman et al. (2021), yielding a 200-year temporal resolution and nominal 1° spatial resolution (Figs. 6, 7). This re-analysis uses Bayesian proxy forward models to perform an offline data assimilation (using 573 globally-distributed SST records) on climate model priors; *i.e.* a set of iCESM 1.2 and 1.3 simulations (Zhu et al., 2017; Tierney et al., 2020). For ocean surface salinity, we use iCESM outputs, following the same methodology as described above. We however use linear interpolation rather than a glacial index to bridge data-gaps in salinity data.

https://doi.org/10.5194/egusphere-2025-1616
Preprint. Discussion started: 10 April 2025

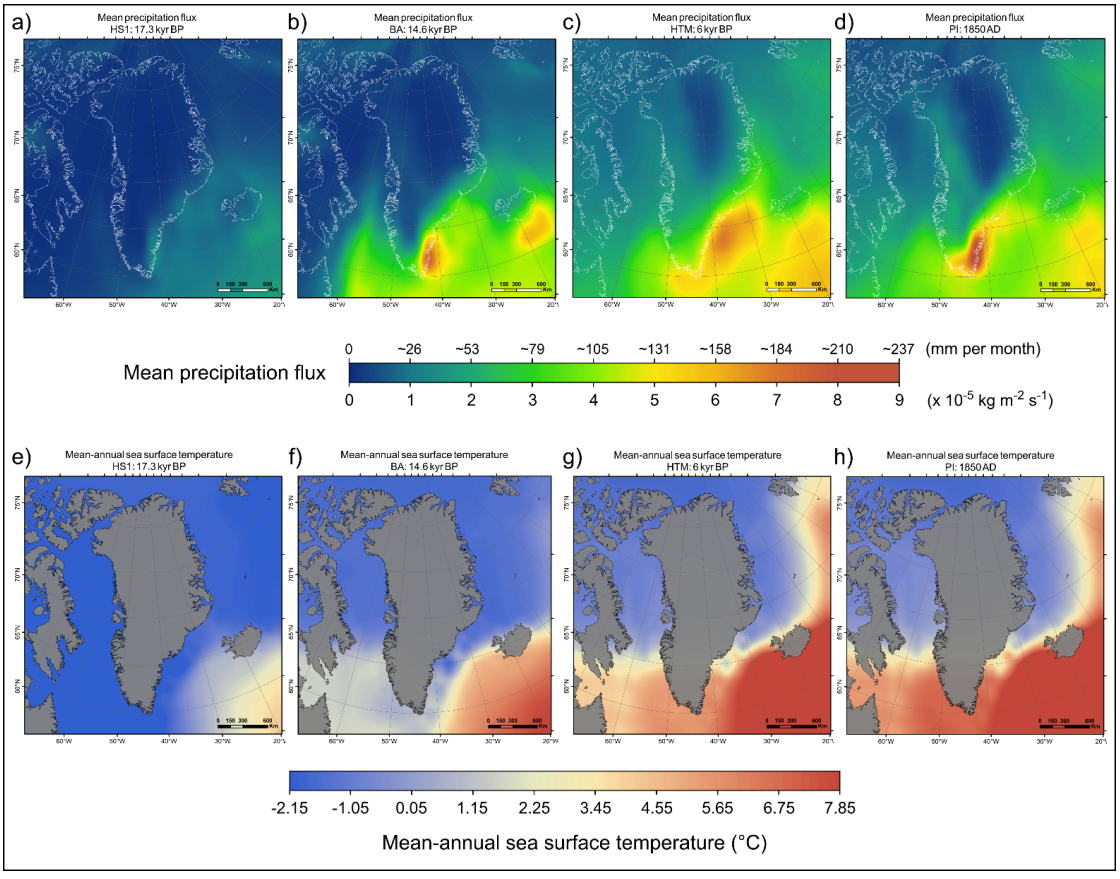

Figure 6. Two-dimensional fields of mean annual precipitation flux (iCESM-derived; panels a-d) and sea-surface temperature (panels e-h) (Osman et al., 2021**) input data used as forcings in our transient ensemble simulations. These data are shown as snapshots for the HS 1 cooling event (panels a, e), the BA warming event (panels b, f), the HTM warming event (panels c, g), and the PI (1850 AD; panels d, h). All climate and ocean input data fields are re-projected to EPSG:3413 and resampled to a 5 x 5 km resolution using cubic convolution.**

https://doi.org/10.5194/egusphere-2025-1616
Preprint. Discussion started: 10 April 2025

2.2 Model initialisation procedure

For model initialisation, we simulate a GrIS in balance with boundary conditions at 24 kyr BP, *i.e.* the starting year of our transient simulations, chosen to be significantly earlier (up to 9 kyr) than the local LGM (17.5-15 kyr BP; Lecavalier et al., 2014). To do so, we use present-day GrIS thickness (see section 2.1.2) and run a 30 kyr-long simulation using parameterisations described above. Ensemble-varying parameters are set to their mid-range values (Table 1). After 30 kyr of simulation with a static climate (from 24 kyr BP), modelled surface and basal ice velocities are stable across the domain, while mass flux rates in glacierised areas are near zero. Basal mass flux for grounded and sub-shelf ice as well as surface melt, accumulation and runoff rates all reach steady state. The spun-up grounded GrIS area reaches 2.27 10^6 km^2, while grounded-ice volume approximates 8.22 m sea-level-equivalent (SLE), ~0.8 m above the present-day GrIS volume (7.42 ± 0.05 m SLE; Morlighem et al., 2017). In this study, grounded GrIS volume calculations (in m SLE) exclude ice under floatation, computed using the PISM-derived time-dependent floatation criterion. The calculation also excludes the ISS, periphery glaciers and icecaps, and any ice thinner than 10 m (after Albrecht et al., 2020). We use ice density, sea water density, and static ocean surface area values of 910 kg m^{-3}, 1027 kg m^{-3}, and 3.618 x 10^8 km^2 (Menard and Smith, 1966), respectively. This spun up GrIS is used as the initial condition for all ensemble transient simulations.

2.3 Ensemble design

Numerical ice-sheet modelling is governed by a plethora of parameters, many of which are poorly constrained by physical processes or empirical data. Uncertainties associated with subjective parameter configurations are large, and generally greater in paleo simulations, due to a lack of observational data (Tarasov et al., 2012). To minimise biases in parameter choices and to assess model-data fit (see section 2.4) using a wide range of parameter configurations, we perturbate an ensemble of 100 simulations with 10 varying parameters (Table 1). We use the Latin hypercube sampling technique (Iman, 2008; Stein, 1987) with the maximin criterion (van Dam et al., 2007) to ensure homogeneous sampling of the high-dimensionality parameter space, while minimising potential redundancies. The 10 ensemble-varying parameters were drawn from five main groups:

-Ice dynamics: we alter the flow law (Eq. 1) enhancement factor (E) uniformly for both the SIA and SSA using a range (0.5 - 3) bracketing the value E = 1.25 found to produce best fit with contemporary GrIS flow speeds (Aschwanden et al., 2016). We vary the sliding law exponent q (Eq. 3) between 0.01 and 1, permitting to continuously alter the dependency of basal shear stress on sliding velocity from nearly purely-plastic to linear.

https://doi.org/10.5194/egusphere-2025-1616
Preprint. Discussion started: 10 April 2025

-Basal yield stress: to alter the impact of bed elevation (and bed strength) on basal yield stress between simulations, we vary ϕ_{min} and ϕ_{max} (Eq. 4) between 4 - 15° and 20 - 45°, respectively, which bracket values obtained by Aschwanden et al. (2016) for present-day GrIS hindcasting.

-SMB: Based on present-day GrIS surface melt, PDD snow and ice melt factors vary between 2 - 5 and 5 - 12 mm *we* d^{-1} $°C^{-1}$, respectively (Braithwaite, 1995; Fausto et al., 2009; Aschwanden et al., 2019). We also vary coefficient a in Eq. 5 between -0.25 and -0.1, thus modifying the impact of temperature change on the standard deviation of daily temperature variability (σ), following the relationship established by Seguinot and Rogozhina (2014).

-Calving: preliminary testing revealed that varying the minimum thickness threshold of ice shelf fronts had a greater impact on modelled GrIS extent than modifying the eigen calving law constant, K (Eq. 6). The thickness threshold was thus retained as an ensemble parameter and is varied between 25 and 200 m, based on observations (Motyka et al., 2011; Morlighem et al., 2014).

-Climate forcing: paleo-climate data from earth-system models can have biases, for instance due to their own paleo-ice-sheet forcings displaying inaccurate geometries (Buizert et al., 2014; Erb et al., 2022; He et al., 2021a). To account for potential biases, we apply variations in input climate fields using space-independent temperature and precipitation offsets as ensemble-varying parameters (Table 1). Based on surface air temperature variability over Greenland (1 stdev) in Osman et al. (2021)'s ensemble, we vary temperature fields by -3.5 to +3.5 °C (Table 1). Furthermore, preliminary simulations showed a high sensitivity of modelled GrIS extent and volume to precipitation changes. We thus vary precipitation between simulations and choose a wide range of offsets, *i.e.* between 20 and 200 % input precipitation.

https://doi.org/10.5194/egusphere-2025-1616
Preprint. Discussion started: 10 April 2025

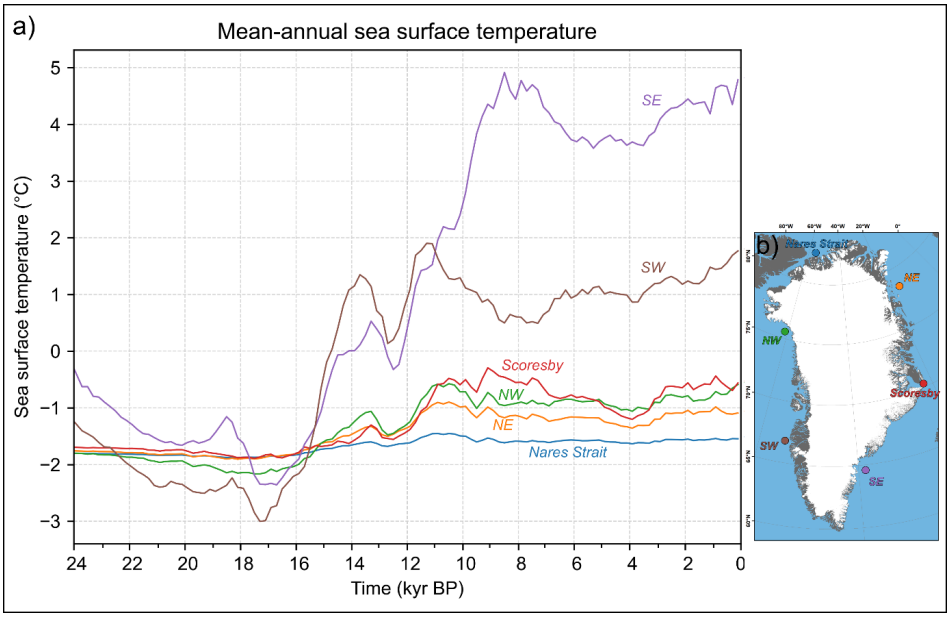

Figure 7. Time series of mean annual sea-surface temperature input data (panel a) (Osman et al., 2021) **extracted from our two-dimensional input forcing fields, for five distinct locations taken from different ocean basins offshore the present-day GrIS (as shown by the inset: panel b).**

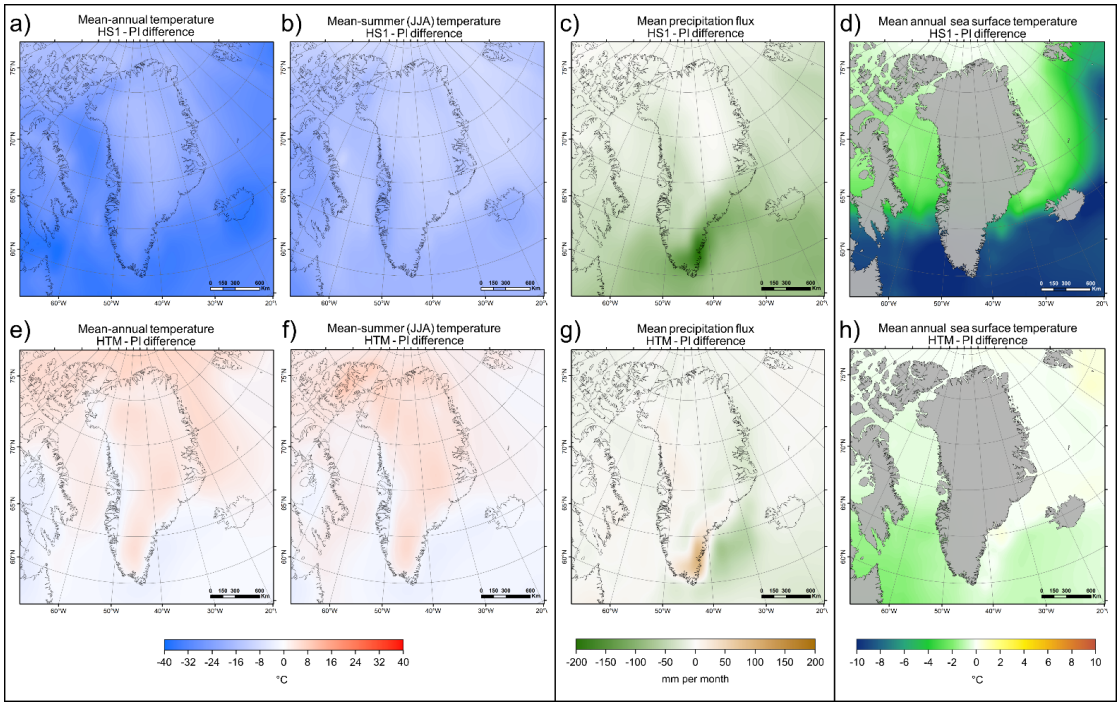

Figure 8. Fields of differences in input reference height mean annual (panels a, e) and mean summer (JJA-mean; panels b, f) air temperature, precipitation rate (panels c, g), and sea-surface temperature (panels d, h) between Heinrich Stadial 1 (17.5 kyr BP: peak cooling during our simulations) and the PI era (1850 AD) for panels a-d, and between the Holocene Thermal Maximum (6 kyr BP: peak warming during our simulations) and the PI for panels e-h.

https://doi.org/10.5194/egusphere-2025-1616
Preprint. Discussion started: 10 April 2025

2.4 Model-data comparison scheme

Isolating ensemble best-fit simulations requires a quantitative assessment of model agreement with data on past GrIS behaviour. Here, each ensemble simulation is scored based on three chronologically-distinct tests, described below. Prior to conducting these tests, floating ice, the IIS, ice thinner than 10 m, and modelled peripheral icecaps and glaciers are removed from modelled ice-thickness fields.

-**The *local-LGM extent* test**; assesses the fit between simulations and grounded GrIS extent during the local LGM, reached between ~21 and ~15 kyr BP depending on regions (*e.g.* Funder et al., 2011; Hogan et al., 2016; Jennings et al., 2017; Ó Cofaigh et al., 2013; Sbarra et al., 2022). As the GrIS was then fully marine-terminating, data constraining past ice extent are challenging to obtain and rare (Sbarra et al., 2022a). Given this uncertainty, we produce a conservative local LGM extent mask covering the area between the outermost PaleoGrIS 1.0 isochrone (~14-13 kyr BP) (Leger et al., 2024), reconstructing GrIS margins following initial deglaciation, and the continental shelf break, a likely maximum extent constraint (Fig. 9). Due to numerous challenges in dating the GrIS's local LGM (Jennings et al., 2017), no chronology is considered in this test, rather only absolute extent. For each simulation, we compute the percentage of mask pixels covered by modelled grounded ice at any point in time. These percentages are then normalised to compute a score per simulation (0-1) (Fig. 10). High-scoring simulations model an extensive grounded GrIS covering more of the mid- to outer continental shelves, thus reconstructing a more accurate local LGM geometry (Fig. 10).

-**The *deglaciation extent* test**; assesses the simulations' ability to fit an empirical reconstruction of GrIS retreat during the last deglaciation (~15 - 5 kyr BP). To do so, we use ATAT v1.1 (Ely et al., 2019) to score simulations against the PaleoGrIS 1.0 isochrone reconstruction (Leger et al., 2024), which spans 13 ± 1 kyr BP to 7 ± 0.5 kyr BP. We use the 'isochrone buffer' product, a mask-based version of the margin reconstruction designed for comparison with >1 km-resolution models (see Fig. 15 in Leger et al., 2024). Here, three ATAT output statistics are equally weighted in a final normalised score (0-1): i) the percentage of pixels from PaleoGrIS 1.0 buffers covered by modelled grounded ice, ii) the percentage of these pixels that agree within chronological error, and iii) the Root-Mean Squared Error in timing for the latter (see Table 4 in Ely et al., 2019). Consequently, this test assesses whether modelled GrIS margins retreat over the correct regions, and at both the correct time and rate (Figs. 9, 10).

-**The *Pre-Industrial extent* test**; assesses the simulations' ability to reproduce the PI (1850 AD) GrIS extent. To do so, we compute the difference in grounded ice extent between the present-day GrIS (BedMachine v4 re-sampled to 5 km, periphery glaciers removed) and our simulations' last frame (1850 AD). While these two products represent GrIS states at times differing by ~150 years, we consider this difference to be

https://doi.org/10.5194/egusphere-2025-1616
Preprint. Discussion started: 10 April 2025

negligible given our 24 kyr-long simulations and the 5 x 5 km spatial uncertainty inherent to both products, which likely exceeds the offset between the two extents. We thus integrate the number of pixels over which modelled PI grounded GrIS margins are both more and less extensive than the present-day margin (Figs. 9, 10). The total number of misfit pixels is then normalised to produce a final relative score (0 - 1).

To isolate overall best-fit simulations, we follow a chronologically-ordered sieving approach and sequentially remove simulations that do not meet threshold values at each test. Starting with the *local-LGM extent* test, only simulations with mask pixel-cover percentages >40% are retained. Of those, only simulations yielding normalized scores >0.8 (out of 1) at the *deglaciation extent* test are retained. Of those, only simulations presenting a total number of misfit pixels <19800 at the *Pre-Industrial extent* test are retained. These thresholds were selected such that 60 - 70% of simulations are removed by each sieve while keeping five overall best-fit simulations (upper 95th percentile of model-data comparison scores). This sequential sieving strategy enables us to avoid retaining simulations which may model the most recent ice-sheet state more accurately (*i.e.* present-day GrIS) but for the wrong reasons, *e.g.* when their previous paleo evolution strongly disagrees with empirical data.

Table 1. List of ensemble-varying parameters (n = 10) and ranges sampled with the Latin Hypercube technique. Note the references cited here did not necessarily employ the same parameter values. They were used as primary source of knowledge for making a final decision on the chosen parameter ranges to sample from in this study. For more justification and details, the reader is referred to the methods section.

Model parameter *(PISM parameter name)*	**Range**	**Unit**	**Source**
Flow law enhancement factor (*sia_e* and *ssa_e*)	[0.5 - 3]	n/a	Aschwanden (2016)
Regularized Coulomb sliding law exponent (*q*)	[0.01 - 1]	n/a	Zoet and Iverson (2020)
Topographic control on Yield Stress: lower ϕ treshold (ϕ_{min})	[4 - 15]	angle degree	Aschwanden (2016)
Topographic control on Yield Stress: upper ϕ treshold (ϕ_{max})	[20 - 45]	angle degree	Aschwanden (2016)
PDD melt factor for ice (*surface.pdd.factor_ice*)	[5 - 12]	mm *we* .d^{-1} .°C^{-1}	Braithwaite (1995); Fausto *et al*. (2009)
PDD melt factor for snow (*surface.pdd.factor_snow*)	[2 - 5]	mm *we* .d^{-1} .°C^{-1}	Braithwaite (1995); Fausto *et al*. (2009)
Rate of change in Stdev of daily temperature variability as function of elevation (*param_a*)	[-0.25 - -0.1]	n/a	ERA 40 re-analysis: Seguinot & Rogozhina (2014)
Minimum thickness of terminal floating ice shelf (*thickness_calving_threshold*)	[25 - 200]	m	Albrecht *et al*. (2021); Pittard *et al*. (2022)
Input temperature forcing: Temperature scalar offset (*delta_T*)	[-3.5 - 3.5]	°C	Osman *et al*. (2021)
Input precipitation forcing: % precipitation scaling (*frac_P*)	[0.2 - 2.0]	scalar multiplier	Initial sensitivity tests

https://doi.org/10.5194/egusphere-2025-1616
Preprint. Discussion started: 10 April 2025

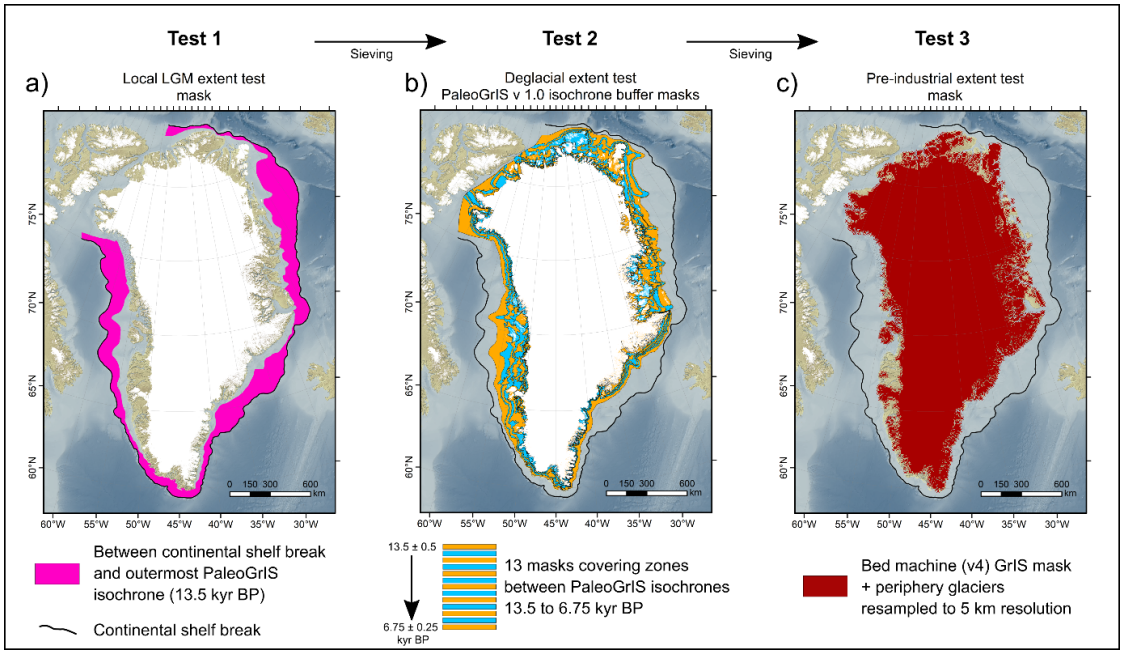

Figure 9. Maps highlighting the spatial coverage of masks derived from empirical datasets (Morlighem et al., 2017**; **Leger et al., 2024**) and used for our three distinct quantitative model-data comparisons tests: *i.e.* the *local-LGM extent test* (panel a), the *deglacial extent test* (panel b), and the *pre-industrial extent test* (panel c). Bathymetry data shown in these maps is from the 15 arc-second resolution General Bathymetric Chart of the Oceans (GEBCO Bathymetric Compilation Group 2022, 2022). The white masks highlight all present-day ice cover.**

https://doi.org/10.5194/egusphere-2025-1616
Preprint. Discussion started: 10 April 2025

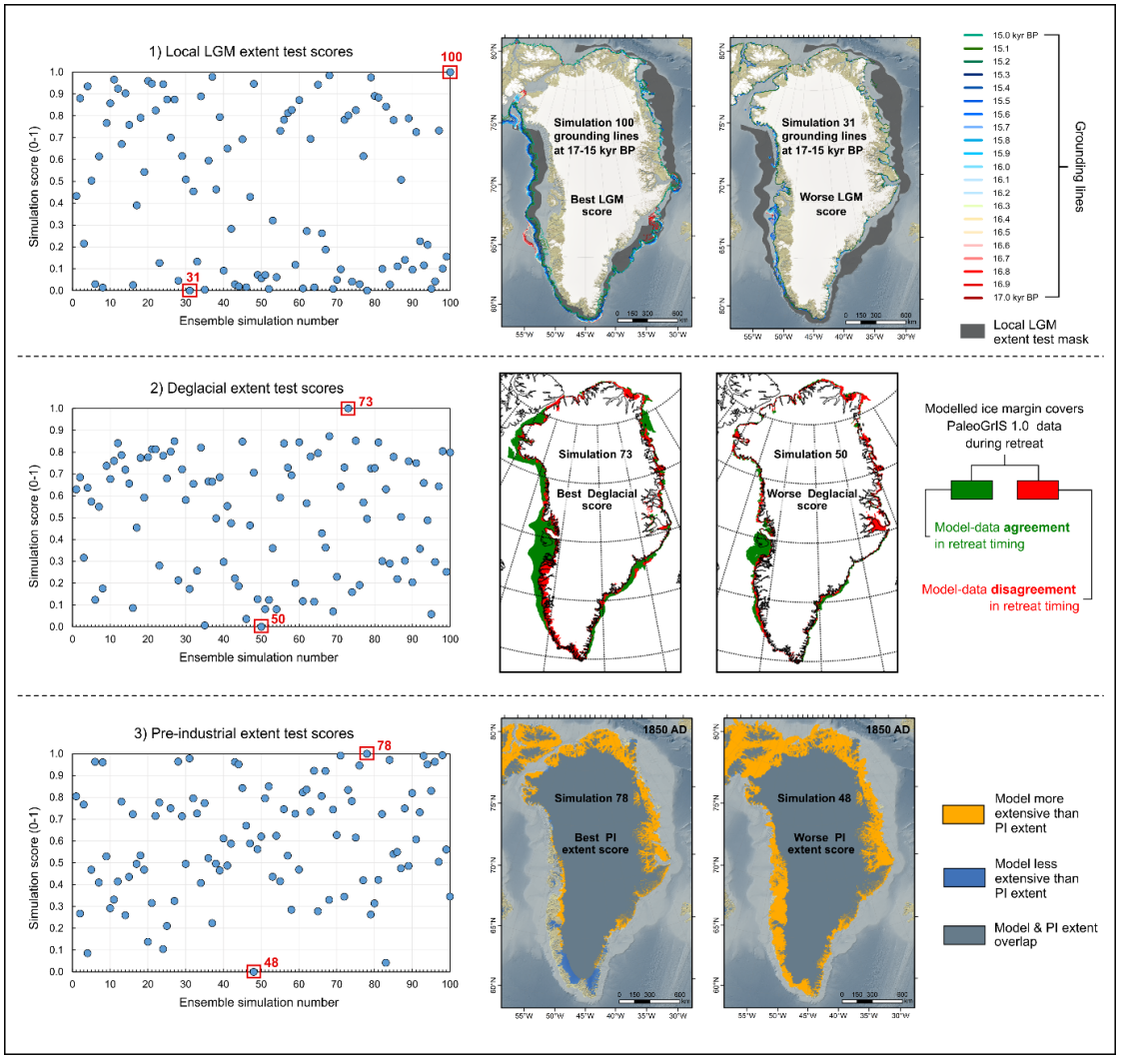

Figure 10. Ensemble simulation scores at our three model-data comparison tests (*local-LGM extent test*, *deglacial extent*, and *PI extent test*) and example results illustrated for both the best-scoring and worse-scoring ensemble simulations, at each test. Note that for the *PI-extent test*, the 2D mask used as empirical data and described in this figure as the "PI extent" is the grounded ice extent of the present-day GrIS mask from BedMachine v4 (Morlighem et al., 2017**) re-sampled to 5 km resolution, with periphery glaciers removed. While the true PI and present-day extents represent GrIS states that differ by ~150 years, we here consider this difference to be negligible given our 24 kyr-long simulations and the 5 x 5 km spatial uncertainty inherent to both products. That uncertainty, once propagated, likely exceeds the extent offset between the two states. Bathymetry and topography data shown in these maps are from the 15 arc-second resolution General Bathymetric Chart of the Oceans (GEBCO Bathymetric Compilation Group 2022, 2022).**

https://doi.org/10.5194/egusphere-2025-1616
Preprint. Discussion started: 10 April 2025

3 Insights on past Greenland-Ice-Sheet history

3.1 Modelled Greenland Ice Sheet during the local LGM

3.1.1 Ensemble-wide trends

All ensemble simulations (n=100) model an increase (of up to ~23%) in grounded GrIS extent between the global LGM (*i.e.* 24 - 21 kyr BP) and the GrIS-wide local LGM, here modelled between 17.5 and 16 kyr BP (Fig. 11). This is consistent with the timing of maximum GrIS volume and extent in other recent modelling studies (*e.g.* 16.5 kyr BP in Lecavalier et al., 2014; 17 - 17.5 kyr BP in Yang et al., 2022). Here, modelled GrIS maximum expansion is synchronous with the Heinrich Stadial 1 (HS1: ~18 - 14.7 kyr BP: He et al., 2021) cooling event. In our prescribed climate forcing (iCESM-derived), HS1 is associated with decreases in mean annual air temperatures of between 5 °C and 7 °C over the GrIS (Figs. 4, 5), and reductions in sea surface temperatures of up to 1 °C in ocean basins surrounding Greenland (Figs. 6, 7). In nearly all ensemble simulations, HS1 cooling forces modelled surface accumulation rates to increase between 24 and 16 kyr BP (by up to 200% for certain simulations) and causes reduced sub-shelf melt (by up to 350%), between 18 and 16 kyr BP (Fig. 12).

3.1.2 Insights from local LGM best-fit simulations

In this section, we refer to 'lLGM best-fit simulations' as the five best-scoring ensemble simulations at the *local-LGM extent* test (Figs. 13, 14, 15-17).

Grounded GrIS extent during local LGM

Our lLGM best-fit simulations yield maximum total grounded GrIS areas that range between 2.80 and 2.85 million km^2 (excluding the IIS) (Fig. 13), an extent ~1.65 times greater than the present-day ice sheet (1.71 million km^2; Morlighem et al., 2017). For these simulations, agreement with empirical data on the local LGM ice extent is relatively good. Our lLGM best-fit simulations are 4 ± 0.7% and 10 ± 0.6% less extensive than the minimum and maximum GrIS extents reconstructed by the PaleoGrIS 1.0 database for the local LGM, respectively (Leger et al., 2024)(Figs. 14, 17). The remaining misfits are mainly located in NE Greenland, where no ensemble simulation produces grounded ice reaching the mid-to-outer continental shelf during the local LGM (Figs. 14, 17, 18), contrary to recent empirical data (*e.g.* Hansen et al., 2022; Davies et al., 2022; Roberts et al., 2024). Indeed, these studies suggest local LGM grounded ice margins reached between ~100 and ~200 km further East than our most extensive simulations. This implies the true local LGM (~17 - 16.5 kyr BP) areal extent of the grounded GrIS was likely closer to 2.9 - 3.1 million km^2, consistent with the Huy3 model (Lecavalier et al., 2014).

https://doi.org/10.5194/egusphere-2025-1616
Preprint. Discussion started: 10 April 2025

Along the Western GrIS margin, from offshore Uummannarsuaq in the South (Cape Farewell) to offshore Kangaarasuk in the North (Cape Atholl), all lLGM best-fit simulations (and a large proportion of our ensemble) model a grounded GrIS margin that reaches the continental shelf edge during the local LGM (Figs. 14, 15, 17). This is consistent with empirical constraints on the Western GrIS local LGM extent (*e.g.* Ó Cofaigh et al., 2013; Rinterknecht et al., 2014; Sbarra et al., 2022). Therefore, both empirical and modelling studies increasingly suggest the grounded GrIS likely reached the continental shelf edge along its entire Western margin during the local LGM. Furthermore, our lLGM best-fit simulations produce extensive ice shelves extending across Baffin Bay during that time. As the LIS was also contributing significant ice flux into Baffin Bay from the West around that time (Dalton et al., 2023), it seems possible for Baffin Bay to be fully covered by ice shelves during the local LGM, between 18 and 16 kyr BP. We also note that towards the relatively shallow (500 - 600 m below present-day sea level) Davis strait saddle, offshore CW Greenland, four out of five lLGM best-fit simulations model grounded ice that extends beyond the continental shelf break and onto the saddle, during the local LGM (Fig. 14). Assuming the LIS flowing eastwards from Baffin Island was able to extend over the saddle by a similar extent, it seems possible that grounded ice from the two ice sheets was able to coalesce over Davis Strait, as modelled in some previous studies (*e.g.* Patterson et al., 2024; Gandy et al., 2023).

We find modelled ice streams along the Western GrIS margin (ice flow > ~800 m yr^{-1}: *e.g.* Jacobshavn, Uummanaq) vary little in flow velocity, shape, and flow trajectory between lLGM best-fit simulations. In SE and CE Greenland, contrastingly, we find more inter-simulation variability in ice dynamics. The modelled Helheim, Kangerlussuaq and Scoresby ice streams show greater variations in flow velocity, trajectories, and shapes (*e.g.* width and length of fast-flow corridors), thus indicating a greater sensitivity to ensemble-varying parameters and making modelled local LGM ice velocities more uncertain in these regions (Fig. 17). In all five lLGM best-fit simulations, grounded ice from these three eastern ice streams reaches the continental shelf edge during maximum expansion (Figs. 14, 17). However, no simulation produces a margin that extends onto the continental shelf between the Kangerlussuaq and Scoresby ice streams, offshore the Geikie Plateau peninsula (Figs. 14, 17). This specific section of the continental shelf lacks geochronological constraints (Leger et al., 2024), making it challenging to assess the accuracy of our models' reconstructions in this region.

https://doi.org/10.5194/egusphere-2025-1616
Preprint. Discussion started: 10 April 2025

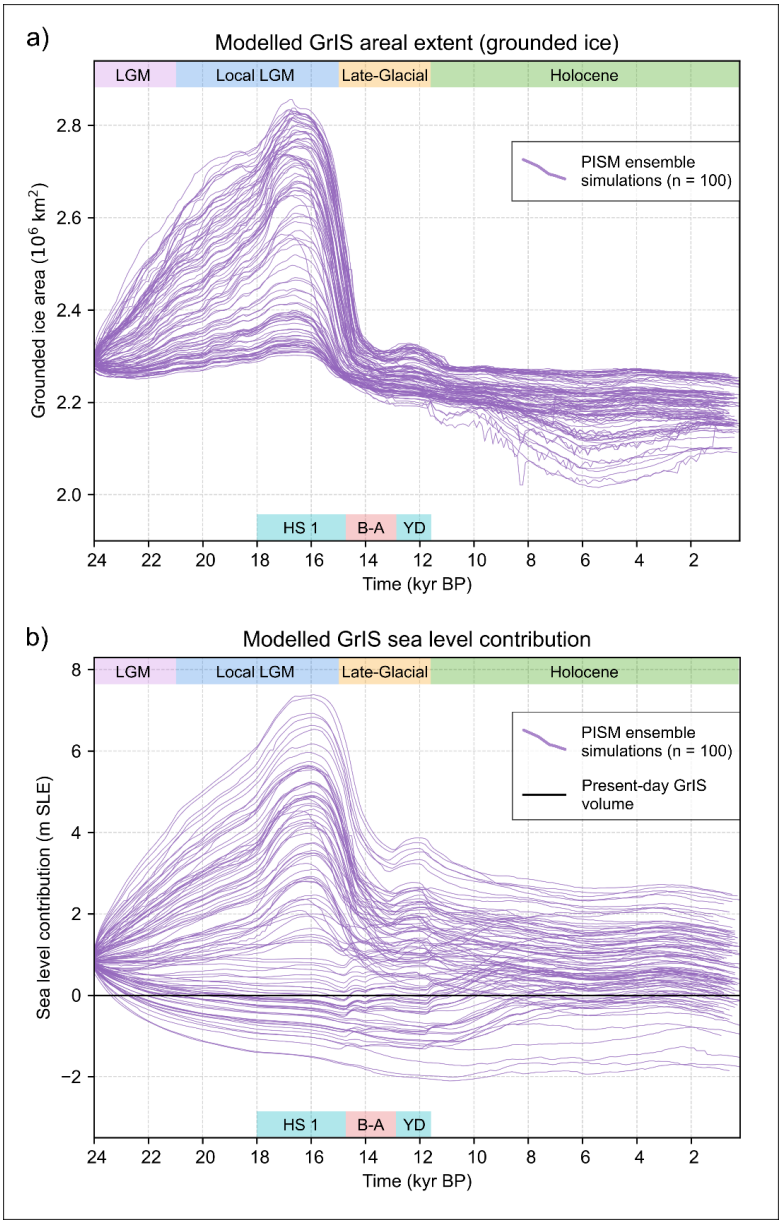

Figure 11. Modelled grounded ice area (panel a) and ice volume (panel b) for the 100 transient PISM ensemble simulations of the GrIS from 24 kyr BP to the PI era (1850 AD). Here, the modelled grounded GrIS volume (in m SLE) is expressed in 'sea level contribution' by subtracting the estimated present-day GrIS volume from our results (7.42 m SLE; Morlighem et al., 2017**). GrIS volume calculations moreover exclude ice under floatation computed using the PISM-derived time-dependent floatation criterion. The calculation also excludes the Innuitian ice sheet (IIS), periphery glaciers and icecaps, and any ice thinner than 10 m (after** Albrecht et al., 2020**). We use ice density, sea water density, and static ocean surface area values of 910 kg m^{-3}, 1027 kg m^{-3}, and 3.618 x 10^{8} km^{2}, respectively.**

https://doi.org/10.5194/egusphere-2025-1616
Preprint. Discussion started: 10 April 2025

GrIS volume and thickness during the local LGM

lLGM best-fit simulations produce maximum grounded GrIS volumes (ice above floatation, excluding the IIS and peripheral glaciers) that are between 6 and 7.5 m SLE greater than the present-day volume (~7.42 m, Morlighem et al., 2017) (Fig. 13d). These lLGM volumes are distinctly higher than previous estimates from the literature, generally comprised between 2 and 5.5 m SLE (Bradley et al., 2018; Yang et al., 2022; Simpson et al., 2009; Clark and Mix, 2002; Huybrechts, 2002; Niu et al., 2019; Fleming & Lambeck, 2004; Quiquet et al., 2021; Buizert et al., 2018; Tabone et al., 2018; Khan et al., 2016) (Fig. 19). We however note that published volume estimates display an increasing trend in time, with more recent studies more often reporting values between 4 and 5.5 m SLE. Moreover, reported GrIS LGM volume estimates are negatively correlated with model resolution (power regression $R^2 = 0.5$), suggesting models using a higher-resolution grid tend to produce a thicker GrIS during the local LGM (Fig. 19). All previous studies producing an ensemble of GrIS LGM-to-present model simulations with model-data comparison (Lecavalier et al., 2014; Simpson et al., 2009) used substantially coarser grid resolutions (15-20 km) than this study (5 km). Of these modelling studies, moreover, few include floating ice shelves in their models, which are known to often provide a buttressing effect leading to ice-flux lowering and thus increases in grounded ice-sheet thickness (Pritchard et al., 2012). Together, these may help explain the higher volumes obtained in our results. Moreover, it can be challenging to directly compare previously reported GrIS LGM volume estimates as different methods are used to compute this number (Albrecht et al., 2020). Various studies use different present-day GrIS volume estimates, ice and ocean water densities, global ocean areas, and do not always exclude floating ice nor ice under floatation using a time-dependent relative sea-level output. However, we believe our workflow follows a method close to that of Lecavalier et al. (2014) when reporting the modelled local LGM volume of the Huy3 model (in m SLE). Computing the ratio of modelled GrIS-wide grounded ice volume (in 10^{15} m^3 unit) to areal extent (in 10^{12} m^2 unit) reveals that, during the local LGM (~16.5 kyr BP), the Huy3 model features a ratio of ~1.73 (see Fig. 15 in Lecavalier et al., 2014). In comparison, our five overall best-fit simulations (which pass all sieves) display volume/area ratios of between 2.10 and 2.25, thus 20 - 30% greater than the Huy3 model. Our best-fit simulations thus produce a much thicker GrIS than the Huy3 model during the local LGM, despite our results producing GrIS summit elevations that are comparable to the present-day ice sheet (Fig. 15). We thus hypothesise that previous modelling studies may have underestimated the thickness, mean surface slope, and volume of the grounded GrIS during the local LGM, although we acknowledge this hypothesis will require more testing in future work.

https://doi.org/10.5194/egusphere-2025-1616
Preprint. Discussion started: 10 April 2025

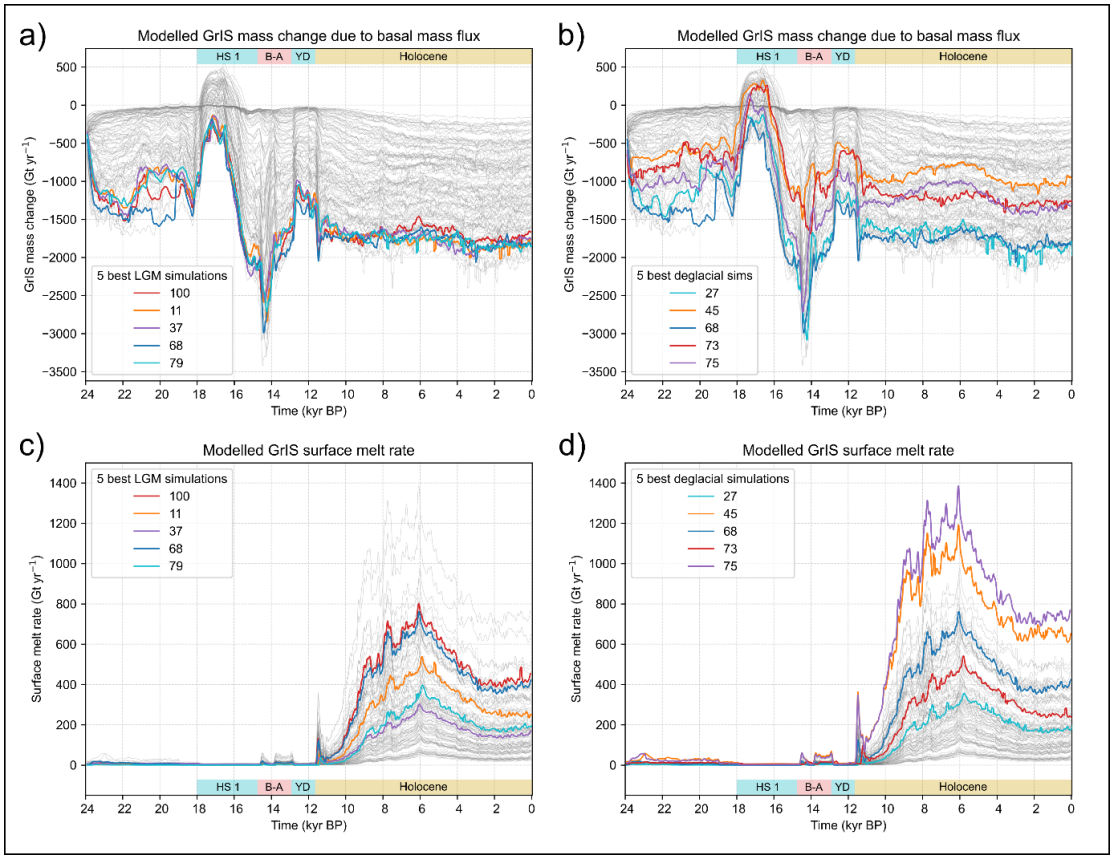

Figure 12. Time series of modelled annual rates of GrIS mass change due to basal mass flux (panels a, b), and of modelled GrIS-wide surface melt rate (panels c, d), for our five best-scoring ensemble simulations at both the *local-LGM extent* test (panels a, c) and the *deglacial extent* test (panels b, d), highlighted by thicker coloured lines. Data from all other ensemble simulations are shown with thin, light grey lines.

https://doi.org/10.5194/egusphere-2025-1616
Preprint. Discussion started: 10 April 2025

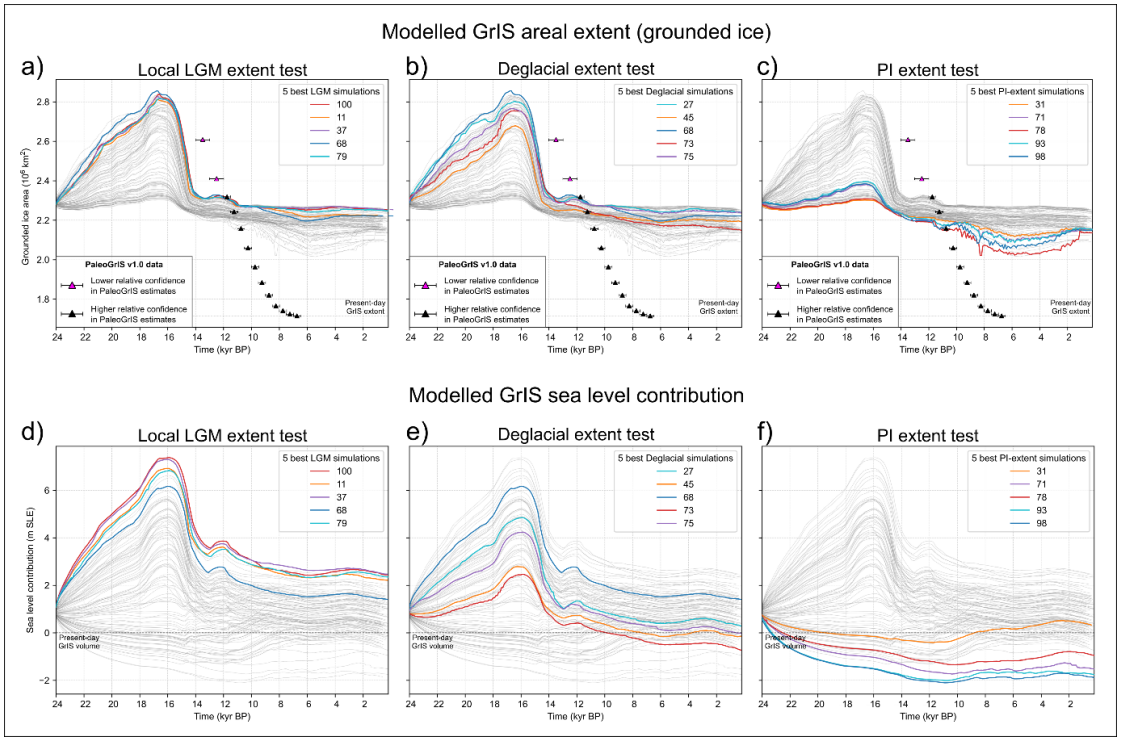

Figure 13. Modelled grounded ice area (panels a-c) and volume (in m SLE, expressed as sea level contribution; panels d-f) for the 100 ensemble simulations (light grey time series). The five best-scoring simulations at each of our three model-data comparison tests are highlighted by thicker coloured time series : panels a, d for the *local LGM extent* test, panels b, e for the *deglacial extent* test, and panels c, f for the *PI extent* test. Data from the PaleoGrIS v1.0 isochrone reconstruction of GrIS former grounded ice extent (Leger et al., 2024**) are shown with triangle symbols. Note the GrIS-wide model-data misfit in ice extent apparent here can be misleading as it is spatially heterogeneous and heavily influenced by a few regions concentrating most of the misfit (*i.e.* NO, NE, and CE Greenland): see Fig. 22.**

https://doi.org/10.5194/egusphere-2025-1616
Preprint. Discussion started: 10 April 2025

In our lLGM best-fit simulations, maximum GrIS volume is associated with spatially-heterogeneous magnitudes of GIA-induced bed subsidence during the local LGM (Supplementary Fig. 1). Highest modelled bed subsidence values reach ~500 m below the present-day topography, and occur systematically towards CW Greenland, around the Disko Bay and Sisimiut regions. Three secondary regions of high GIA-induced bed subsidence are also modelled, reaching values of ~400 m below the present-day bed. These are located in CE Greenland (the inner Scoresby Sund region), upper NE Greenland (The Danmark Fjord region), and central Ellesmere Island (Supplementary Fig. 1). The resulting pattern of total glacial isostatic loading (non-local and local components combined) during the local LGM is broadly consistent with previous modelling efforts focusing on GIA signals and model-data comparison using relative sea level indicators (*e.g.* Simpson et al., 2009; Lecavalier et al., 2014; Bradley et al., 2018).

LGM ice geometry at the locations of ice cores

In Southern Greenland, and following modelled flowlines from the location of the DYE-3 ice core, lLGM best-fit simulations produce a notably different ice-sheet geometry during the local LGM than today (Fig. 15). Modelled ice surface elevations are greater by ~300 - 500 m at the local summit, despite increased isostatic loading and bed subsidence (of ~400 m) relative to today. In this region, maximum ice thickness is thus modelled to be ~700 - 900 m greater during the local LGM than is estimated for the present-day (Morlighem et al., 2017a). Furthermore, towards DYE-3, our lLGM best-fit simulations suggest a notable shift of the main East/West ice divide, here modelled to be located further West than the present-day's by approximately 100 km (Figs. 15, 16). Such a glacial-interglacial ice-divide migration, if further validated, could have implications for the DYE-3 ice core record (Dansgaard et al., 1982), which may not have remained as close to the local GrIS summit during Quaternary glacial maxima as previously thought. Instead, ice from the drill site may have been located further East and well within the Helheim glacier catchment during glacial maxima, where higher flow velocities and layer deformation could produce irregularities in the ice core profile and complicate chronological interpretations (Rasmussen et al., 2023).

In Northwestern Greenland, and towards the location of the NEEM ice core (Rasmussen et al., 2013), our lLGM best-fit simulations model both maximum ice thickness and ice surface elevations to be ~200 - 400 m greater than the present-day GrIS (Fig. 15). However, no major migration of the main ice divide is modelled in that region (Fig. 16). Towards central Greenland and the locations of the GISP2 and GRIP ice cores (Grootes et al., 1993), our best-fit simulations produce similar ice surface elevations during the local LGM than observed for the present-day GrIS (Fig. 15). There, a complex system of multiple ice divide is modelled during the local LGM, with the main East/West ice divide being modelled further East than the present-day's, by up to 150 km (Fig. 16). In Northern Greenland and towards the location of the NGRIP ice core (North Greenland Ice Core Project Members, 2004), both the location of the main East/West ice divide and ice

https://doi.org/10.5194/egusphere-2025-1616
Preprint. Discussion started: 10 April 2025

surface elevation are modelled to remain close to the present-day's during the local LGM. Therefore, towards both central (GISP2, GRIP) and northern (NGRIP) GrIS summits, our model results suggest that the local LGM GrIS was not necessarily thicker than today (Fig. 16).

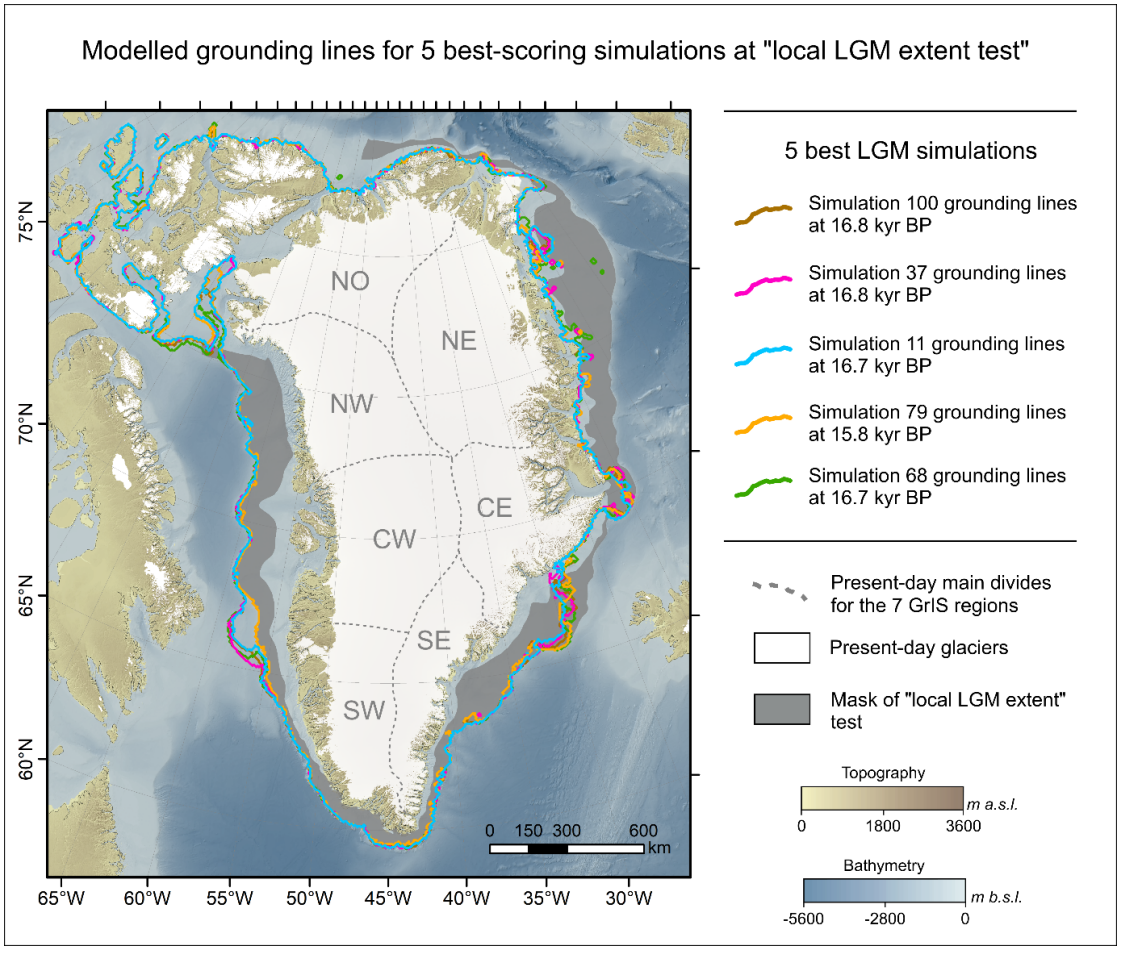

Figure 14. Modelled grounding lines during the GrIS-wide local LGM (maximum ice extent, whose timing is simulation-dependent) for the five best-scoring simulations at the *local-LGM extent* test. Our division scheme of the GrIS in seven major catchments/regions, used and referred to throughout the text for inter-regional comparisons, is shown with dashed grey lines. Bathymetry and topography data shown in this map are from the 15 arc-second resolution General Bathymetric Chart of the Oceans (GEBCO Bathymetric Compilation Group 2022, 2022). The white mask highlights all present-day ice cover.

https://doi.org/10.5194/egusphere-2025-1616
Preprint. Discussion started: 10 April 2025

GrIS discharge during the local LGM

Our lLGM best-fit simulations produce a faster-flowing GrIS during the local LGM than today. In these simulations, the glaciated areas covered by ice streams (>800 m yr^{-1} surface velocities: Bennett, 2003) are between 6.8 and 10.7 times greater during the local LGM, relative to today (Joughin et al., 2018a) (Fig. 17). Such an increase in flow velocities combined with the greater ice extent necessarily increases the magnitude and rate of ice discharge, relative to today. During the local LGM, our best-fit simulations model GrIS-wide discharge rates that reach between 1500 and 1900 Gt yr^{-1} (Fig. 20). Such discharge rates are between ~2.8 and ~4.3 times greater than those estimated for the present-day (487 ± 50 Gt yr^{-1} between 2010 and 2019 AD; Mankoff et al., 2020). This has implications for discussing past iceberg production volumes, the contribution of the GrIS to past Heinrich events, and its potential role in former and future AMOC slowdowns (Ma et al., 2024). However, there are exceptions to modelled localised LGM speedups. In northern Greenland, our lLGM best-fit simulations produce Peterman and Humboldt outlet glaciers that flow slower during the local LGM than current observations. This is likely caused by the GrIS and IIS coalescing during the local LGM, creating an ice dome over Nares strait with low surface slopes and local flow divergence buttressing and decreasing ice flux rates from upflow regions of the ice sheet.

https://doi.org/10.5194/egusphere-2025-1616
Preprint. Discussion started: 10 April 2025

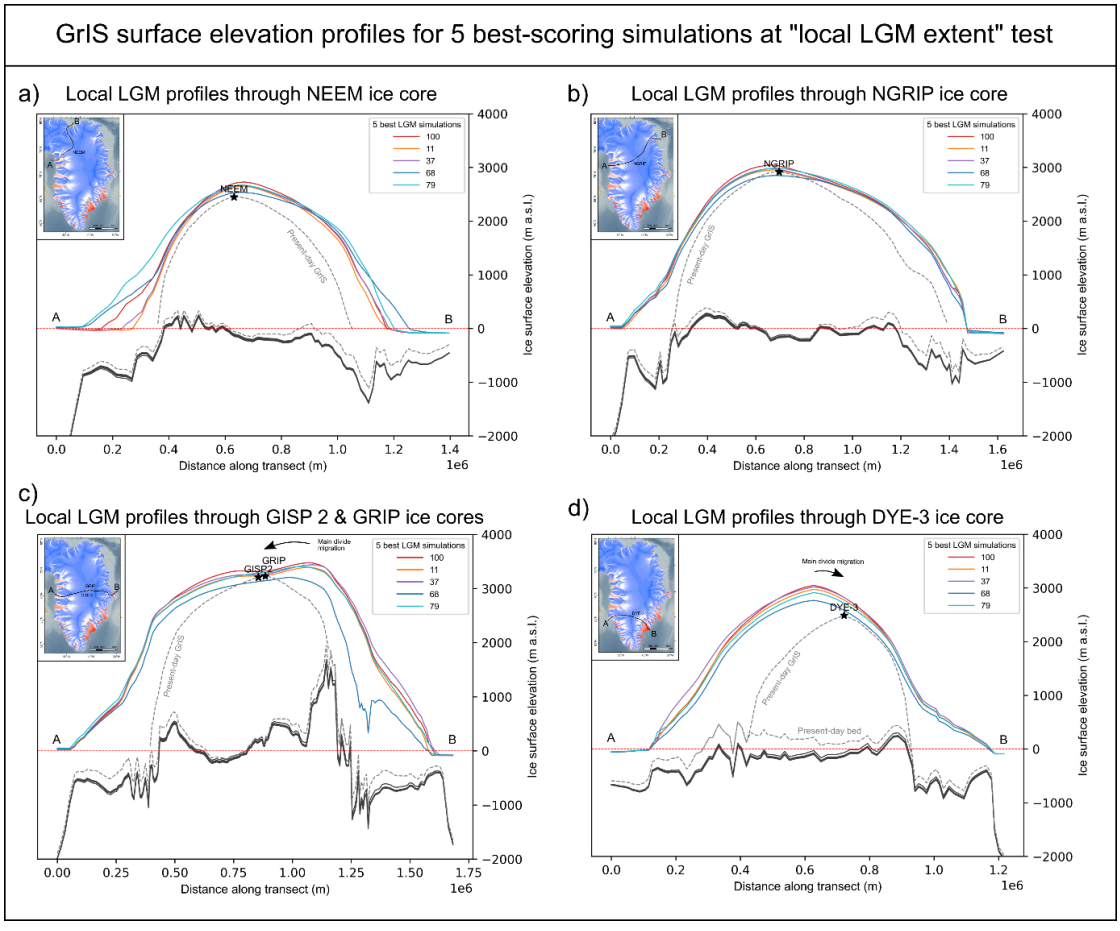

Figure 15. Modelled ice surface and bed elevations during the local LGM extracted across four different transects for our five best-scoring simulations at the *local-LGM extent* test (thicker coloured lines), and for the present-day GrIS (dashed grey lines). The four transects were drawn following modelled ice flow lines while ensuring to cross the NEEM (panel a), NGRIP (panel b), GISP 2 and GRIP (panel c), and the DYE-3 (panel d) ice core locations, as shown by the black lines in the inset maps.

https://doi.org/10.5194/egusphere-2025-1616
Preprint. Discussion started: 10 April 2025

3.2 Modelled Greenland Ice Sheet during the Late-Glacial

3.2.1 Ensemble-wide trends

Following the local LGM, nearly all ensemble simulations produce rapid and high-magnitude retreat of GrIS margins between 16 and 14 kyr BP, during the late HS1 and the *Bølling–Allerød* warming event (B-A; ~14.7-12.9 kyr BP; He et al., 2021) (Fig. 11). Depending on regions, this sudden warming is associated with increases in mean annual and mean summer temperatures of between 5 and 12 °C in our forcing data (Fig. 5), while our input sea surface temperatures increase by between 0.2 and 3.8 °C (Fig. 7). For simulations that model an expansion of the grounded GrIS over continental shelves between 24 and 16 kyr BP, subsequent retreat during the B-A causes a near complete deglaciation of continental shelf covers. During the late HS1 and B-A warming (16-14 kyr BP), we find nearly no modelled surface melt across any simulations, and until ~12 kyr BP (Fig. 12). Modelled margin retreat and mass losses between 16 and 14 kyr BP are instead associated with more negative (up to tenfold) basal mass fluxes, caused by ocean warming increasing sub-shelf melt rates (Fig. 12). A ~30% decrease in modelled ice accumulation rates during that time also plays a smaller role. These mechanisms lead to substantial ice sheet thinning of up to 800 m in 2 kyr during that period (Supplementary Fig. 2). Our ensemble thus suggests that during the late HS1 and B-A warming, between 16 and 14 kyr BP, ocean forcing likely caused the GrIS to retreat rapidly and lose most of its glaciated continental-shelf areas, despite air temperatures remaining too cold to produce any surface melt (Fig. 12).

At the ice-sheet scale, ensemble simulations produce little or no GrIS margin re-advance during the Younger Dryas stadial (YD: ~12.9 - 11.7 kyr BP). For the few simulations that demonstrate some grounded margin re-advance during the YD, they recover less than ~3% of the area lost during deglaciation just prior (~16 - 14 kyr BP). Towards the north Atlantic region, the YD was a high magnitude but relatively short-lived (~1.2 kyr) cooling event, with our input climate forcing suggesting mean annual temperatures over the GrIS decreasing by ~7 °C, relative to 13 kyr BP (Fig. 5). In our simulations, the modelled GrIS is likely still adjusting to the substantial mass and extent loss experienced just prior, during B-A warming. We find that despite large parameter and climate perturbations between simulations (Table 1), the inertia and memory from the B-A warming phase combined with the relatively short-lived nature of the YD event prevented any simulation from producing substantial margin re-advances in most regions. Modelled GrIS volume, however, responds more dynamically to YD cooling than extent, with some simulations recovering up to 8% of the mass loss experienced just prior (16 - 13 kyr BP) (Figs. 11, 13). During the YD, these simulations display highly spatially heterogeneous variations in ice thickness with some thickening of up to ~200 m mainly modelled in CE and Southern GrIS regions, while other regions display continued thinning (Supplementary Fig. 2). Nevertheless, despite the high magnitude of cooling, our ensemble suggests large re-advances of

https://doi.org/10.5194/egusphere-2025-1616
Preprint. Discussion started: 10 April 2025

GrIS margins during the YD are unlikely and would have required a more sustained cooling event. This finding is consistent with a general lack of geomorphological and geochronological evidence for GrIS margin readvances during the YD (Leger et al., 2024), and confirms that the ice-sheet's inertia following millennial-scale warming and retreat can be substantial. Contrastingly, numerous periphery Greenland icecaps and glaciers, subject to less inertia due to lower ice volumes and extent, were found to be more sensitive and to have re-advanced during the YD (*e.g.* Larsen et al., 2016; Biette et al., 2020).

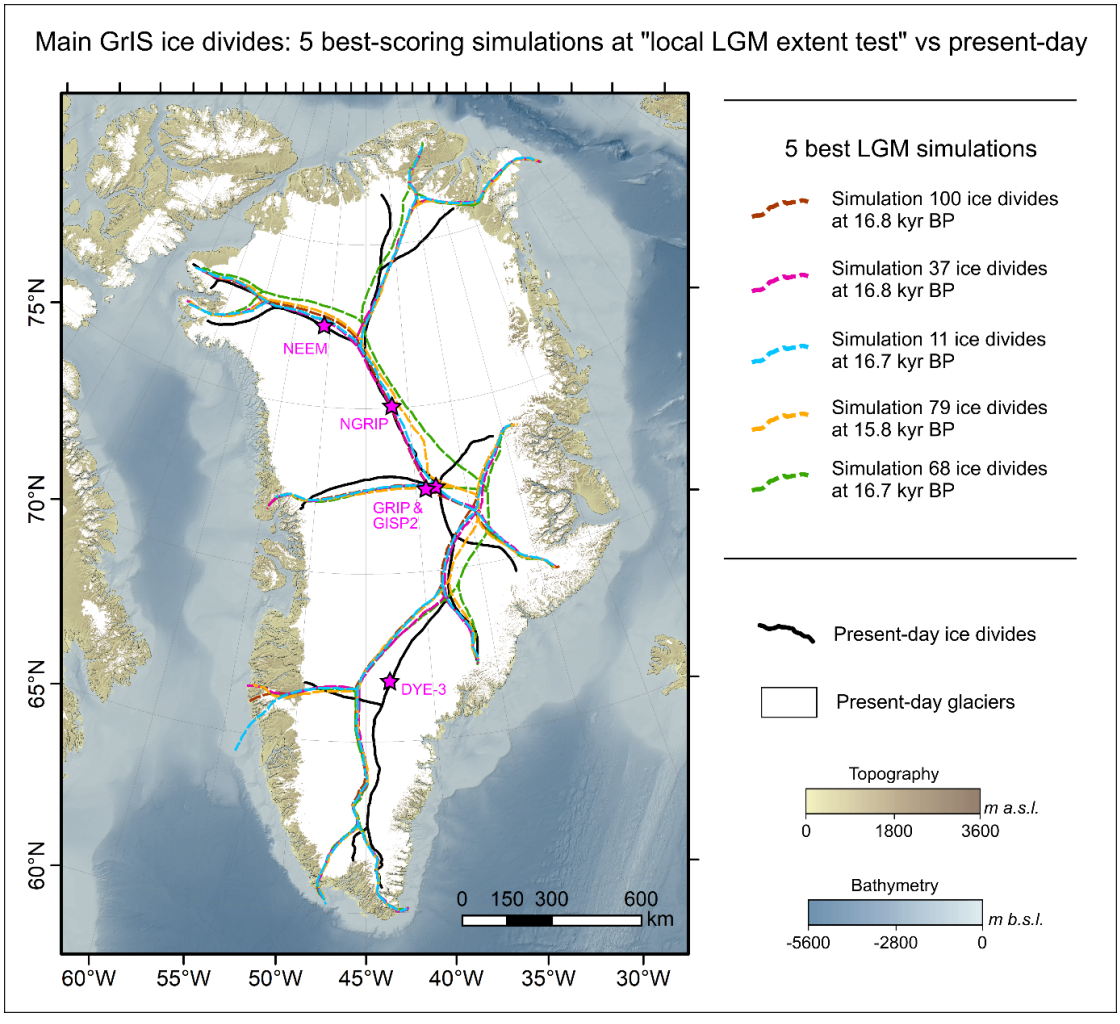

Figure 16. Main GrIS ice divides modelled during the local LGM (maximum GrIS extent, whose timing is simulation-dependent) for our five best-scoring ensemble simulations at the *local-LGM extent* test (dashed coloured lines). These are compared against the present-day GrIS main ice divides (continuous black line) extracted from surface ice velocity observations (Joughin et al., 2018)**. The locations of main Greenland ice cores discussed in this study are highlighted by the pink stars. Note the potent offset between the location of the DYE-3 ice core and modelled ice divides during the local LGM (more details in section 3.1.2.). Bathymetry and topography data shown in this map are from the 15 arc-second resolution General Bathymetric Chart of the Oceans (GEBCO Bathymetric Compilation Group 2022, 2022).**

https://doi.org/10.5194/egusphere-2025-1616
Preprint. Discussion started: 10 April 2025

3.2.2 Insights from deglacial best-fit simulations

In this section, we refer to our 'deglacial best-fit simulations' as the five best-scoring ensemble simulations at the *Deglacial extent* test (Figs. 10, 13).

Deglacial best-fit simulations produce spatially heterogeneous patterns of mass change during the last deglaciation (16 - 8 kyr BP) (Supplementary Fig. 2). For instance, during the YD stadial (13 - 12 kyr BP), only small peripheral regions of CE, SE, and SW Greenland experience mass gain, while other regions of the modelled ice sheet experience either no mass change, or instead mass loss. During peak B-A warming (16 - 14 kyr BP), we find modelled mass loss is most prominent in NW, CW, SW, and SE Greenland (Supplementary Fig. 2). At the ice-sheet scale, our deglacial best-fit simulations generate mass loss rates during the late HS1 and B-A warming periods (16-14 kyr BP) that reach maximum values of between ~500 and ~1400 Gt yr^{-1}, equivalent to between ~1 and ~3 mm SLE yr^{-1}, at around 14.5 kyr BP (Fig. 21). Comparatively, between 2003 and 2020 AD, the GrIS is estimated to have lost 200 to 300 Gt yr^{-1}, equivalent to approximately 0.57 mm SLE yr^{-1} (Simonsen et al., 2021). Therefore, our deglacial best-fit simulations model between 2.5 and 7 times greater mass loss rates during peak deglaciation (~14.5 kyr BP), than is estimated for the last two decades (Fig. 21). Such mechanisms lead to substantial ice-sheet thinning between 16 and 14 kyr BP in these simulations, especially-pronounced over the CW GrIS (Supplementary Fig. 2). During this event, moreover, the modelled rates of areal-extent loss reach maximum values of between 300 and 450 km^2 yr^{-1} (Supplementary Fig. 3). We note that these modelled area loss rates during peak B-A warming, here mostly related to ocean-forcing, notably exceed the near-constant rate of 170 ± 27 km^2 yr^{-1} estimated by the landform-derived PaleoGrIS 1.0 reconstruction for the ~14 - 8.5 kyr BP period (Leger et al., 2024). This may suggest that grounded GrIS retreat rates during B-A warming were greater than during the YD-to-early Holocene transition, the period covered by most data compiled in PaleoGrIS 1.0, when a higher proportion of the deglaciating GrIS was land-terminating.

Including Ellesmere Island in our model domain enables to potentially reconstruct and better understand the important mechanisms of coalescence during advance and the subsequent unzipping of the Greenland and Innuitian ice sheets over Nares Strait, during deglaciation. Here, we find that some of our deglacial best-fit simulations (*e.g.* simulation 73) do capture this behaviour (Fig. 23). In these simulations, the majority of grounded ice over Nares Strait is deglaciated between 10 and 8 kyr BP, approximately in line with geochronological empirical evidence (Jennings et al., 2011) (Fig. 23). We note that for simulations successfully modelling the full grounded-ice unzipping of the two ice sheets, final separation (although modelled too late) occurs consistently offshore Peterman glacier, towards Hall basin, while the Kane Basin further Southwest (offshore Humboldt glacier) deglaciates earlier (*e.g.* Fig. 23).

https://doi.org/10.5194/egusphere-2025-1616
Preprint. Discussion started: 10 April 2025

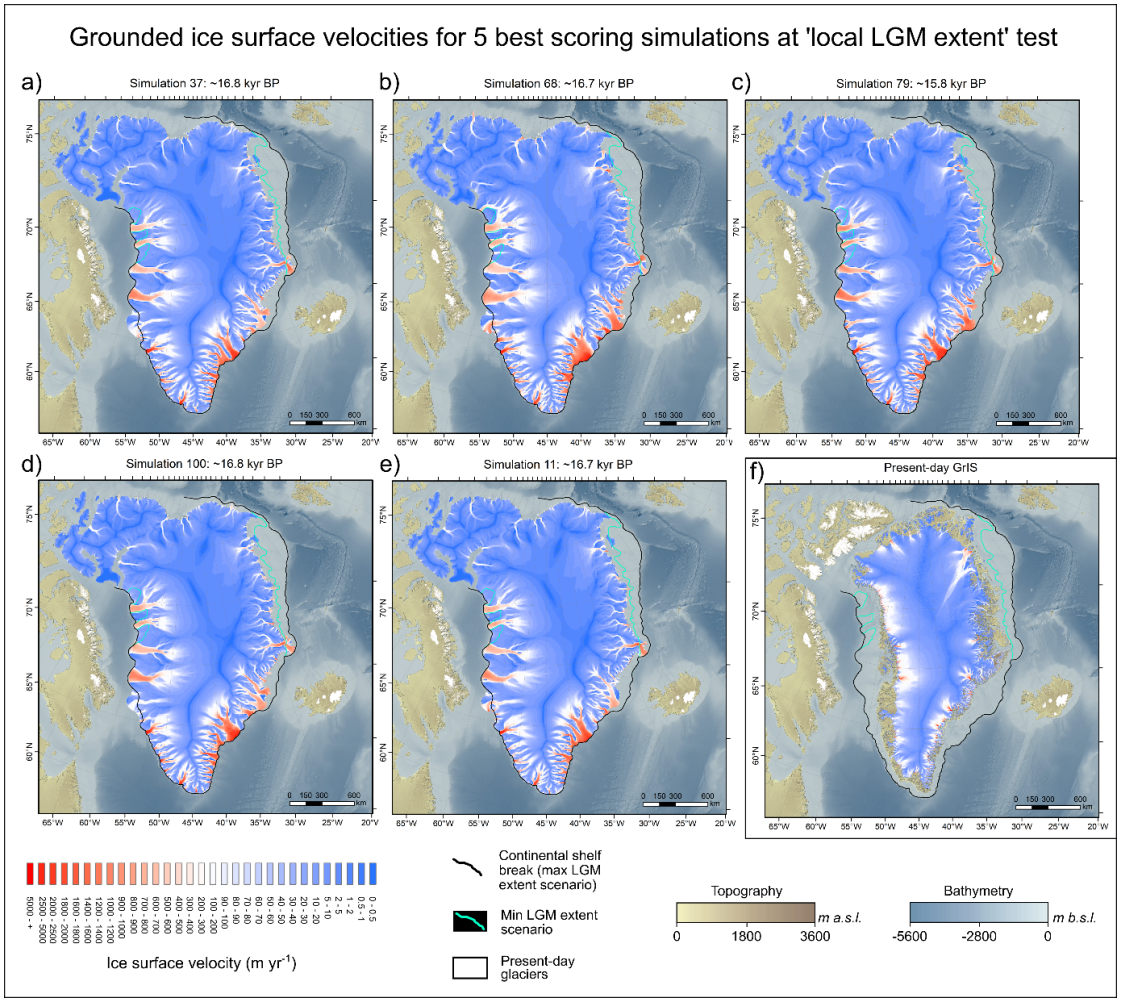

Figure 17. Modelled grounded ice surface velocities during the local LGM (maximum Gris-wide ice extent, whose timing is simulation-dependent) for our five best-scoring ensemble simulations at the *local-LGM extent* test (panels a-e), compared with observed present-day GrIS ice surface velocities (panel f; Joughin et al., 2018**). Bathymetry and topography data shown in this map are from the 15 arc-second resolution General Bathymetric Chart of the Oceans (GEBCO Bathymetric Compilation Group 2022, 2022).**

https://doi.org/10.5194/egusphere-2025-1616
Preprint. Discussion started: 10 April 2025

3.3 Modelled Greenland Ice Sheet during the Holocene

3.3.1 Ensemble-wide trends

The majority of our ensemble simulations produce a minimum in GrIS areal extent during the mid-Holocene, between 6 and 5 kyr BP, prior to modelling margin re-advances during the late-Holocene and Neoglacial periods (5 kyr BP - 1850 AD). This is consistent with empirical reconstructions of Holocene GrIS margin evolution (Funder et al., 2011; Sinclair et al., 2016; Leger et al., 2024). The modelled mid-Holocene minimum in grounded GrIS extent occurs in response to the Holocene Thermal Maximum (HTM), characterised by mean annual and mean summer surface air temperatures that were up to 7 - 5 °C warmer relative to the PI era (1850 AD), over the GrIS (Figs. 4, 5). In our climate forcing, the HTM occurs towards ~6 kyr BP for mean annual air temperatures, and between ~9 and ~6 kyr BP for mean summer temperatures (JJA-mean), depending on the region. In agreement with findings of the PaleoGrIS 1.0 reconstruction, our simulations thus capture a degree of ice-sheet inertia causing the ice extent response to lag the cessation of warming and ice-thickness adjustment by a few centuries, and up to a millennium, during the early-to-mid Holocene. Furthermore, we find all ensemble simulations model a notable increase in ice-sheet volume during the late Holocene (3-2 kyr BP) and produce widespread thinning during the neoglacial period (Fig. 11), thus following opposite trends relative to ice extent.

During most of the Holocene, between 8 kyr BP and 1850 AD, all ensemble simulations produce GrIS mass change rates that remain below 100 Gt yr^{-1}, despite important variations in climate and SMB parameters between simulations (Fig. 21). Such rates remain below present-day estimated mass loss rates of 200 - 300 Gt yr^{-1} (2003 - 2020 period; Simonsen et al., 2021). This observation is coherent with other GrIS modelling and reconstruction efforts suggesting the speed of contemporary and future GrIS mass loss is likely unprecedented throughout much of the Holocene (Briner et al., 2020). Similarly for GrIS-wide ice discharge rates, our ensemble suggests the estimated present-day rate of 487 ± 50 Gt yr^{-1} (Mankoff et al., 2020) is likely unprecedented for the past five thousand years (Fig. 20).

3.3.2 Insights from Pre-Industrial best-fit simulations

In this section, we refer to our 'PI best-fit simulations' as the five best-scoring ensemble simulations at the *PI extent* test (Figs. 10, 13).

We find that PI best-fit simulations (*e.g.* simulation 31) tend to produce a closer fit with the youngest PaleoGrIS 1.0 isochrones (during the mid-Holocene), relative to other ensemble simulations (Fig. 13). They model both a pronounced minimum in grounded GrIS extent at ~5 kyr BP, and a notable margin re-advance between ~5 kyr BP and the PI (1850 AD). During the Holocene minimum in ice extent, our PI best-fit

https://doi.org/10.5194/egusphere-2025-1616
Preprint. Discussion started: 10 April 2025

simulations model some retreat behind the present-day GrIS margin, as is suggested by empirical evidence (*e.g.* Briner et al., 2014). However, this is exclusively the case in SE and SW Greenland regions. No GrIS retreat behind present-day margins is modelled north of 68 °N, with the exception of the Humboldt glacier front (Supplementary Fig. 4). In all other GrIS regions, the modelled ice-sheet margin remains close to - or more extensive than - the present-day margin throughout the mid-to-late-Holocene, between 5 kyr BP and 1850 AD. It is worth noting that ensemble simulations with the lowest areal extent during the HTM (*e.g.* simulation 78; Fig. 13c) produce up to ~100 km of retreat behind the present-day GrIS margin in southernmost Greenland (north of Narsarsuaq), prior to re-advancing and reaching present-day margins by the end of the simulation (1850 AD). Although this result may well be an overestimation and should be interpreted with caution, our modelling suggests such a magnitude of retreat behind present-day margins (~100 km) in response to the HTM cannot be fully ruled out, in certain regions.

Within our PI best-fit simulations, simulation 31 yields a better match in ice thickness (Morlighem et al., 2017a) and ice surface velocity (Joughin et al., 2018) with the present-day GrIS (Supplementary Figs. 5, 6). The remaining four best-fit simulations underestimate PI GrIS volume (Fig. 13). Nonetheless, in simulation 31, PI ice thickness is still underestimated towards the GrIS interior (by up to ~600 m), and overestimated towards the ice-sheet's margins. We find our simulations produce lower ice surface velocities at the PI than present-day observations in most regions (Joughin et al., 2018). This is likely caused by the underestimated PI GrIS thickness towards its interior, resulting in lower ice surface slopes and thus underestimated driving stresses (Supplementary Figs. 5, 6, 12). The most notable examples are NEGIS and Jacobshavn Isbrae, where the present-day GrIS is flowing more than 200 m yr^{-1} faster than simulation 31 during the PI. Therefore, our PI best-fit simulations fail at reproducing the particular dynamics of NEGIS. In SE Greenland, however, there seems to be a higher concentration of regions where simulation 31 produces faster-flowing ice instead (by more than 200 m yr^{-1}). Interestingly, that is also the case for the terminus of Humboldt glacier (Supplementary Fig. 6).

https://doi.org/10.5194/egusphere-2025-1616
Preprint. Discussion started: 10 April 2025

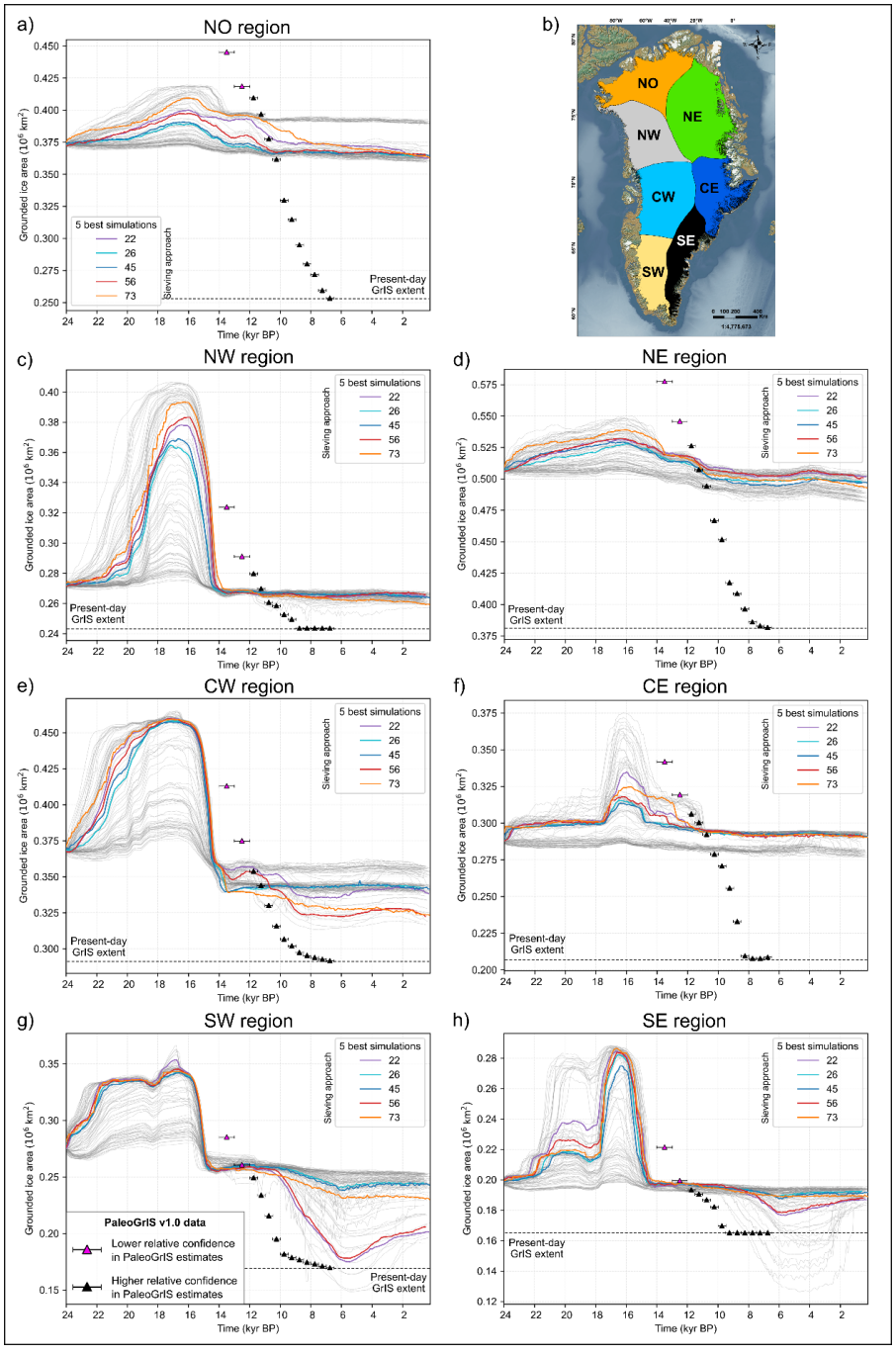

Figure 18. Time series of modelled grounded GrIS extent for our five overall best-fit simulations (which pass all sieves, highlighted by thicker coloured lines) for each of the seven main GrIS regions (panels a, c-h) whose locations are shown by the inset map on panel b. Data from the PaleoGrIS 1.0 ice-extent reconstruction (Leger et al., 2024) **are shown with triangle symbols. Data from all other ensemble simulations are shown with thin, light grey lines.**

https://doi.org/10.5194/egusphere-2025-1616
Preprint. Discussion started: 10 April 2025

4 Insights from model-data comparison

4.1 Model agreement with empirical data

When compared against the PaleoGrIS 1.0 ice extent reconstruction (Leger et al., 2024), all ensemble simulations underestimate the magnitude of grounded GrIS retreat during the last deglaciation, with at least 30% (~0.5 million km^2) of the ice-sheet-wide retreat signal missing (Figs. 13, 22). While more consistent with the PaleoGrIS 1.0 reconstruction during the late HS1 and B-A warming events (16 - 14 kyr BP), both rates and magnitudes of modelled margin retreat are too low during the early-to-mid Holocene (12-8 kyr BP). This remaining model-data misfit is apparent in all ensemble simulations despite our parameter and climate perturbations (Fig. 13, 22). In all simulations, the onset of modelled GrIS retreat also occurs earlier than is suggested by PaleoGrIS 1.0, with an offset of nearly 2 kyr (Fig. 22). However, the 14 - 12 kyr BP PaleoGrIS 1.0 isochrones are characterised by significant data scarcity and timing uncertainties associated with offshore samples, whose radiocarbon dating is challenged by high-latitude marine reservoir effects (Leger et al., 2024). The time ranges and error ranges of oldest PaleoGrIS 1.0 isochrones should thus be interpreted with caution.

When analysing model-data agreement at the regional scale, however, we find that model misfits with the PaleoGrIS 1.0 reconstruction are spatially heterogeneous (Figs. 18, 23, 24). Overall best-fit simulations (which pass all sieves) generally display a better fit with the PaleoGrIS 1.0 reconstruction during both the local LGM extent and the Lateglacial-to-mid-Holocene deglaciation in NW, CW, SW, SE Greenland, and towards the Kangerlussaq outlet glacier sub-region (CE Greenland south of Scoresby Sund), relative to other regions (Fig. 18). In these better-fitting regions, our best-fit simulations still underestimate the reconstructed magnitudes of grounded GrIS retreat, but often by less than 50 km. There are some smaller-scale exceptions such as the Nuuk fjord and Sisimiut regions where the ice-extent misfit is closer to 70 - 90 km, depending on the simulation and time slice analysed (Figs. 23, 24).

In NO, NE, and CE Greenland (north of 70 °N only), we find larger model-data misfits in GrIS margin extent and retreat rates (Fig. 18). While simulations passing all sieves display a good fit with PaleoGrIS isochrones during the 12 - 11 kyr BP interval in these regions, they underestimate both grounded ice extent during the local LGM, and rates and magnitudes of retreat during the Late-Glacial and early-to-mid Holocene periods (Figs. 18, 23, 24). In J.C. Christensen Land and Knud Rasmussen Land (NO Greenland, >80 °N), for instance, overall best-fit simulations model grounded margins that are typically around 200 km too extensive. The Scoresby Sund fjord system (CE Greenland, 70°N) is the region displaying the greatest extent misfit, with an underestimation of margin retreat that is closer to ~230 km, at maximum. Moreover, such underestimation remains relatively high (between ~90 and ~160 km) along the entire NE Greenland coast, with the exception of the Nioghalvfjerdsbrae (‘79N glacier’) and Zachariæ Isstrøm glaciers, where our modelled grounded ice

https://doi.org/10.5194/egusphere-2025-1616
Preprint. Discussion started: 10 April 2025

margins fit the PaleoGrIS 1.0 isochrones well throughout the early-to-mid Holocene (~11-6.5 kyr BP) (Figs. 23, 24).

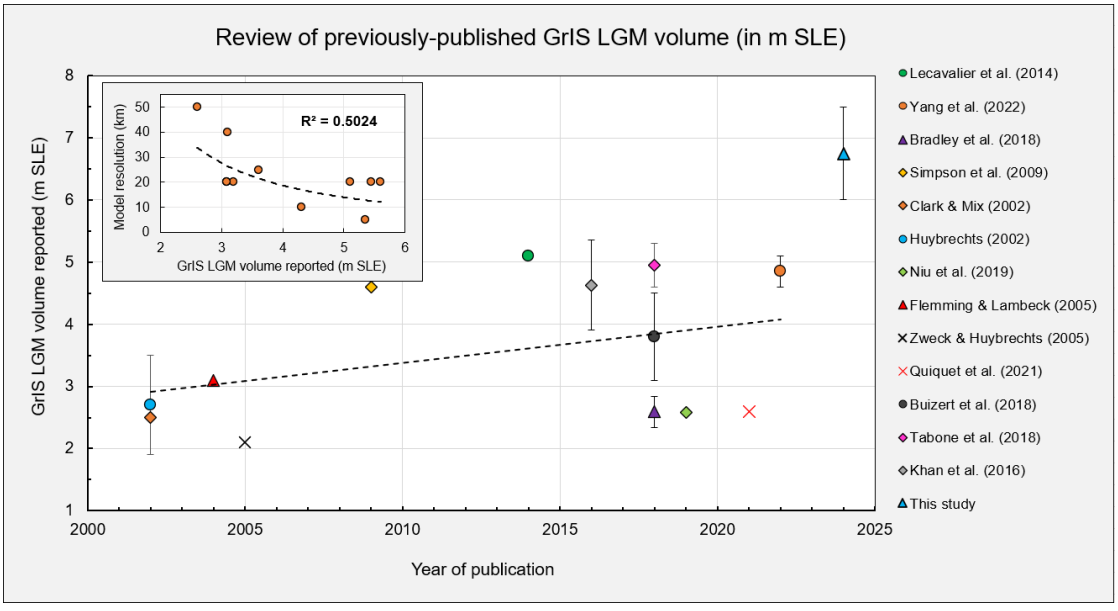

Figure 19. Review of previously modelled and/or reported GrIS volumes during the local LGM (in m SLE, expressed as 'sea level contribution'), and compared against this study's estimates. An increasing trend of reported values through time can be observed, along with a negative correlation between model horizontal grid resolution and reported modelled LGM volumes.

Table 2: Ensemble-varying parameter values for the five overall best-fit simulations (which pass all sieves).

Ensemble-varying model parameter	Simulation 22	Simulation 26	Simulation 45	Simulation 56	Simulation 73	Unit
Flow law enhancement factor (*-sia_e and -ssa_e*)	0,554	1,787	3,000	1,174	2,650	n/a
Regularized Coulomb sliding law exponent (*q*)	0,719	0,325	0,222	0,280	0,985	n/a
Topographic control on Yield Stress: lower ϕ treshold (ϕ_{min})	7,046	6,491	6,731	14,466	4,631	angle degree
Topographic control on Yield Stress: upper ϕ treshold (ϕ_{max})	36,100	22,427	20,000	31,905	41,246	angle degree
PDD melt factor for ice (*surface.pdd.factor_ice*)	10,241	7,665	12,000	10,946	10,078	mm *we* $.d^{-1}.°C^{-1}$
PDD melt factor for snow (*surface.pdd.factor_snow*)	4,485	2,491	4,945	4,500	3,444	mm *we* $.d^{-1}.°C^{-1}$
Rate of change in daily temperature variability Stdev as function of elevation (*param_a*)	-0,148	-0,225	-0,235	-0,112	-0,240	n/a
Minimum thickness of terminal floating ice shelf (*-thickness_calving_threshold*)	84,250	125,393	74,242	190,606	176,156	m
Input temperature forcing: Temperature scalar offset (*delta_T*)	2,736	3,172	3,500	2,595	1,609	°C
Input precipitation forcing: % precipitation scaling (*frac_P*)	1,446	1,289	1,305	1,471	1,397	scalar multiplier

https://doi.org/10.5194/egusphere-2025-1616
Preprint. Discussion started: 10 April 2025

Although we exclusively use data on former grounded ice extent for model-data comparison and simulation scoring, our results can also be compared against different empirical datasets used in previous studies. For instance, we here compare modelled surface ice elevation change between 8 kyr BP and 1850 AD at the location of four Greenland ice cores (GRIP, NGRIP, DYE-3, and Camp Century) against the δ^{18}O-derived Holocene thinning curves for these sites, originally produced by (Vinther et al., 2009) and improved by Lecavalier et al. (2013) (Fig. 25). Holocene thinning curves provide a mean to check whether modelled GrIS thinning rates are in general agreement with ice-core data. We find that, despite our five best-fit simulations (which pass all sieves) showing some differences in thinning magnitudes and trends, they all produce thinning signals that remain within the 1σ uncertainty bands of the ice core - derived data for more than 80% (100% for NGRIP) of the time period analysed here (8 - 0 kyr BP). One exception is simulation 22 which, at the location of the GRIP ice core, models a mid-Holocene surface elevation offset relative to PI that remains higher than the upper 1σ uncertainty limit, for approximately 2.2 kyrs (Fig. 25). Contrastingly, at the location of DYE-3, simulation 22 matches the thinning curve better than the remaining four best-fit simulations by producing a higher thinning rate between 8 and 6 kyr BP. All five best-fit simulations seem to slightly underestimate the higher thinning rate estimated at the Camp Century ice core, between 8 and 6.5 kyr BP, a misfit that has also been observed in previous paleo GrIS modelling efforts (e.g. Huy3 model; Lecavalier et al., 2014). Overall, despite not scoring our ensemble simulations using comparisons against Holocene thinning curves (Vinther et al., 2009; Lecavalier et al. 2013), our best-fit simulations produce thinning signals that generally remain within the uncertainty of the ice core - derived data (Fig. 25). This finding suggests that best-scoring simulations isolated by model-data comparison using detailed ice-extent reconstructions tend to also result in appropriate Holocene GrIS thinning signals. However, it must be noted that, although some ensemble simulations are clearly not in agreement with the ice core - derived thinning curves (Lecavalier et al., 2013), the majority of the ensemble remains close to, or within, the 1σ uncertainty bands of these data (Fig. 25).

We find simulations passing all sieves model temperate basal ice over the vast majority of the GrIS throughout the entire simulation time, from 24 kyr BP to 1850 AD (Supplementary Figs. 7, 8). However, persistent cold-based regions are modelled towards the ice-sheet's periphery in NO, NE, and CE Greenland. Although basal temperature is amongst the most uncertain model output variables, these results coincide with cosmogenic nuclide inheritance signals, found to be significantly higher for erratic and bedrock samples from NO and NE Greenland regions (Søndergaard et al., 2020; Larsen et al., 2020). These high nuclide inheritance signals observed in northern GrIS regions have often been attributed to a cold-based, non-erosive ice sheet during the local LGM and possibly throughout the last deglaciation (Søndergaard et al., 2020). Therefore, our model results are somewhat coherent with this hypothesis.

https://doi.org/10.5194/egusphere-2025-1616
Preprint. Discussion started: 10 April 2025

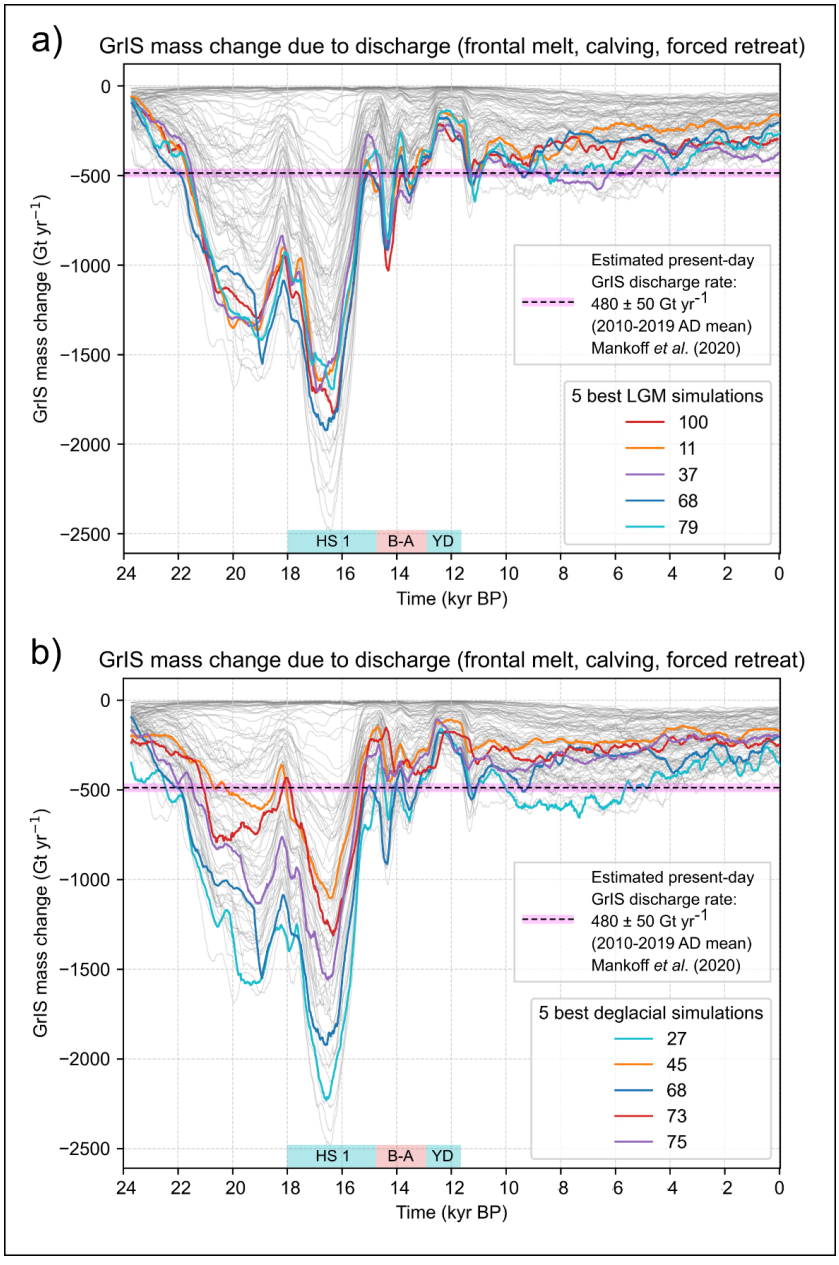

Figure 20. Time series of modelled GrIS mass change due to ice discharge for our five best-scoring ensemble simulations at both the *local-LGM extent* test (panel a) and the *deglacial extent* test (panel b), highlighted by thicker coloured lines, and compared with an estimated present-day GrIS ice discharge rate (Mankoff et al., 2020**). Data from all other ensemble simulations are shown with thin, light grey lines.**

https://doi.org/10.5194/egusphere-2025-1616
Preprint. Discussion started: 10 April 2025

4.2 No perfect ensemble simulation

Our model-data comparison scheme generates a different list of five best-fit simulations for each of our three tests, suggesting no single simulation matches empirical data better than others throughout the full modelled timeframe (24 - 0 kyr BP), and across all GrIS regions. (Fig. 13). Instead, specific ensemble simulations need to be selected and analysed to address research questions regarding certain time periods and/or certain Greenland regions. Consequently, producing a high-resolution (≤ 5 km) simulation of the LGM-to-present GrIS evolution that remains consistent with physics and that shows good and spatially/temporally homogeneous agreement with a detailed empirical dataset such as PaleoGrIS 1.0, remains a major challenge.

More specifically, we find that *deglacial extent* and *local-LGM extent* test scores are positively correlated (Supplementary Fig. 9). Thus, simulations showing a better relative match with data during the local LGM tend to also generate a better fit during the deglaciation, mostly because continental shelves need to first be ice-covered in order to deglaciate subsequently (Fig. 10). However, both the *deglacial extent* and *local LGM extent* test scores are negatively correlated with *PI extent* test scores. Ensemble simulations yielding higher scores during the local LGM and deglaciation tend to score worse at reproducing the PI extent, with a few exceptions (Supplementary Fig. 9). This is caused by a large proportion of simulations not successfully producing any significant GrIS advance nor retreat prior to the Holocene, but instead remaining closer to the present-day GrIS extent throughout the simulation (Fig. 13), and thus scoring better at the *PI extent* test. This finding highlights the importance of applying a chronologically-ordered sieving of an ensemble using multiple model-data comparison tests when isolating best-fit simulations. Indeed, this ordering of sieves helps to avoid overrating a simulation that produces a better PI (or present-day) ice-sheet state, but for the wrong reasons. More generally, this result highlights that a model initialisation successfully reproducing the GrIS PI geometry is not guaranteed to be an ideal initial state for forward modelling, as such parameterisation may not necessarily capture the transient longer-term ice-sheet behaviour, inertia, and memory inherited from the last glaciation and subsequent retreat.

4.3 Are certain parameter values better than others?

We here analysed ensemble-varying parameter values (n = 10) for the five best-scoring simulations at each of our three model-data comparisons tests (Figs. 10, 26, Table 1), and find the following:

Three out of 10 ensemble-varying parameters, *i.e.* the precipitation offset, the air temperature offset, and the flow law enhancement factor (Table 1), present some clustering in best-fit parameter values. For these three parameters, specific values may lead to better model-data fit (Table 2, Fig. 26). Here, a ‘cluster’ is defined as when parameter values of the five best-scoring simulations at each test (Table 2) cover a range that is less than 50% of the original sampled parameter range (Table 1). For two ensemble-varying parameters, *i.e.* the

https://doi.org/10.5194/egusphere-2025-1616
Preprint. Discussion started: 10 April 2025

precipitation offset and the flow law enhancement factor, values leading to better model-data fit appear to be test-specific and thus time-dependent. Parameter clusters suggest, for instance, that flow law enhancement factors lower than 1 lead to better relative model-data fit in GrIS extent during the local LGM (Table 2, Fig. 26). This may imply that better model-data fit during maximum expansion requires to model a GrIS with harder, less deformable, and more viscous ice (or with lower impurity contents), than is modelled with default flow law constants (E=1, n=3). Parameter clusters moreover suggest that better model-data fit may require between 1.3 to 2 times higher precipitation during the local LGM and deglacial periods, and instead between 2 to 5 times lower precipitation during the PI (1850 AD), than is obtained with our default climate forcing (Table 1, Figs. 6, 8, 26). However, we acknowledge that due to complex parameter interactions, and the simplicity of our SMB parameterisation (PDD), these trends may not necessarily help detect biases in input climate but may instead hide more impactful misrepresentations of ice dynamics and/or boundary conditions, thus precluding any definitive interpretations linked to individual model parameters.

For seven out of 10 ensemble-varying parameters (impacting SMB, yield stress, sliding, or calving), no best-fit clusters could be identified, suggesting better model-data fit can be achieved with highly variable parameter values covering more than 50% of the sampled ranges (Tables 1, 2, Fig. 26). This result either suggests that: **i**) these seven parameters may not significantly impact the transient evolution of grounded GrIS extent; and/or **ii**) the various interactions between these seven parameters may be more impactful than individual parameter perturbations; or **iii**) identifying best-fit clusters for some of these seven parameters may require a larger-than-100-simulation ensemble and a more comprehensive exploration of the parameter space. This result justifies the use of an ensemble approach when attempting to match a paleo-GrIS model reconstruction with empirical data, as we find highly variable parameter configurations can generate relatively better model-data fit.

https://doi.org/10.5194/egusphere-2025-1616
Preprint. Discussion started: 10 April 2025

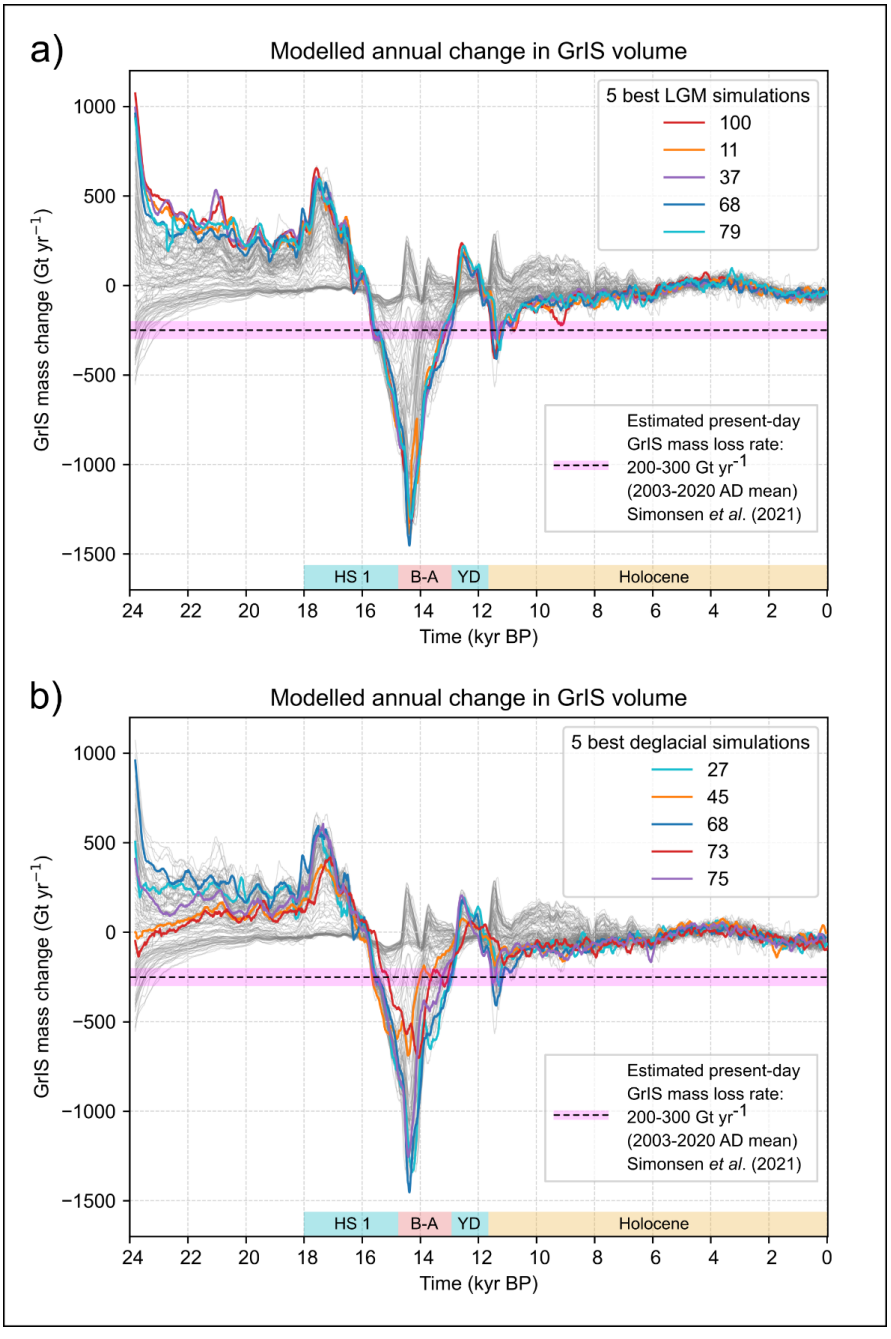

Figure 21. Time series of modelled annual rates of GrIS mass change for our five best-scoring ensemble simulations at both the *local-LGM extent* test (panel a) and the *deglacial extent* test (panel b) highlighted by thicker coloured lines. The time series are compared against an estimate of present-day GrIS mass loss rate (2003-2020 AD mean; Simonsen et al., 2021**). Data from all other ensemble simulations are shown with thin, light grey lines.**

https://doi.org/10.5194/egusphere-2025-1616
Preprint. Discussion started: 10 April 2025

5 Remaining misfits: possible causes

As mentioned above (see section 4.1.), we find model-data misfits in grounded ice extent display strong inter-regional heterogeneities, and are larger in the NO, NE, and CE Greenland regions (Figs. 18, 23, 24). Additionally, we find ensemble simulations passing all sieves (see Methods section) present the most dynamic responses in ice extent through time. They display both higher and lower grounded GrIS extents than ensemble-mean values during the local LGM and mid-Holocene periods, respectively (Fig. 22). This may suggest that remaining model-data misfits are related to our model not capturing certain mechanisms that would enable shorter response times to changes in boundary conditions and produce higher-amplitude transitional advance and retreat phases. In the following sections, we discuss and hypothesise in more detail the possible mechanisms leading to remaining misfits by dividing them into: **1**) Misfits in GrIS advance during the local-LGM; and **2**) Misfits in GrIS retreat during the Late-Glacial and Holocene periods.

5.1 Underestimated LGM advance in NE and NO Greenland

Along the NE Greenland coast (81-71°N), our simulations underestimate the magnitude of grounded ice advance during the local LGM (~17.5-16 kyr BP) (Figs. 10, 14, 17, 18). Empirical investigations producing new geomorphological and geochronological reconstructions of GrIS thinning histories (*e.g.* Roberts et al., 2024) and offshore ice extent (*e.g.* Arndt et al., 2017; Davies et al., 2022; Hansen et al., 2022) suggest that local-LGM grounded GrIS margins reached between ~100 and ~200 km further East than is modelled by our best-scoring simulations (Figs. 14, 17).

A possible cause of model-data misfit during the local LGM may be related to our model initialisation (spinup) procedure reaching a steady-state that does not produce an extensive and/or thick enough GrIS at 24 kyr BP (*i.e.* the starting time of our transient simulations). This could be due to an inappropriate model parameterisation (*e.g.* SMB), or to biases in our static input atmospheric or oceanic forcings at 24 kyr BP (see section 2.2.). In the NO and NE regions, the GrIS may require a longer cooling period than the 7.5 kyrs modelled in transient ensemble simulations (between 24 and 16.5 kyr BP) to fully re-adjust to the new parameterisation and switch from a margin location provided by the unique initial state (here close to the present-day GrIS margin) to a margin that needs to reach the mid-to-outer continental shelf. If this is the case, a bias in our model initialisation at 24 kyr BP may be responsible for the underestimated grounded ice advance during the local LGM in NO and NE Greenland.

https://doi.org/10.5194/egusphere-2025-1616
Preprint. Discussion started: 10 April 2025

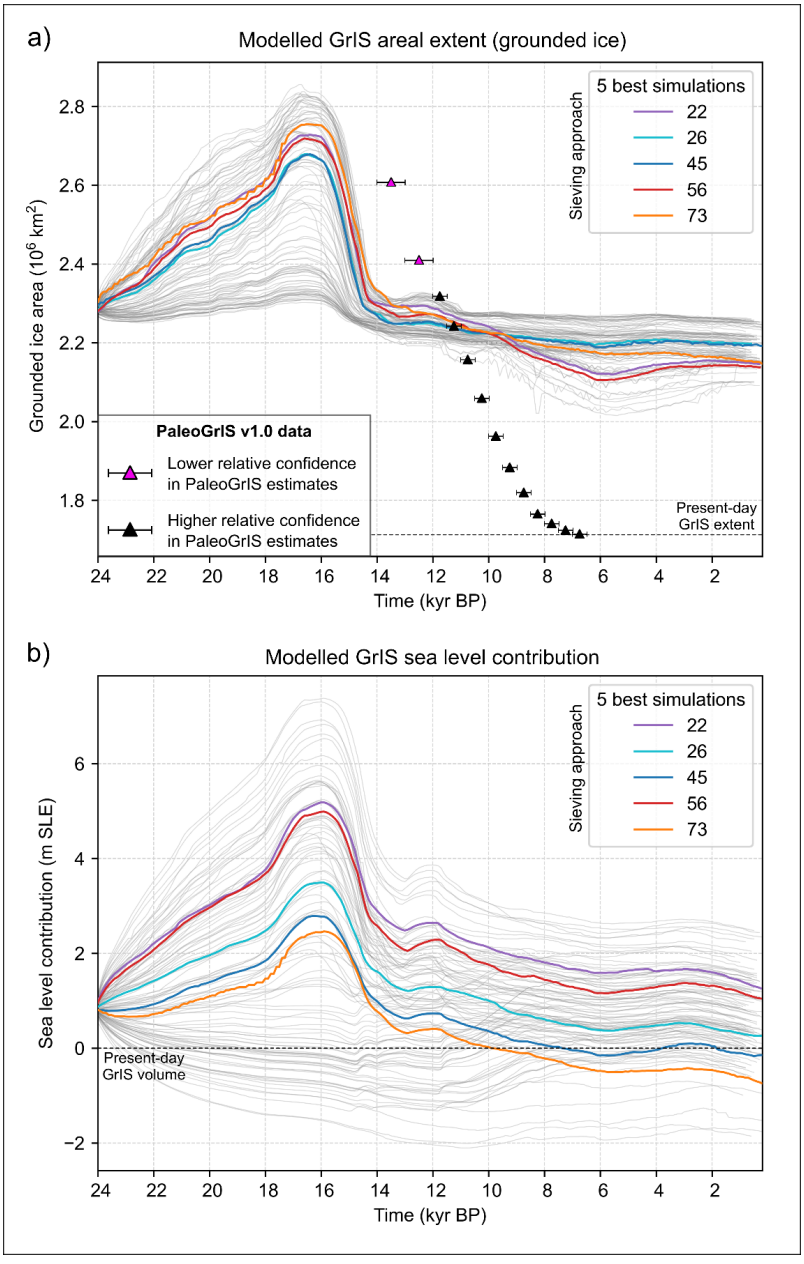

Figure 22: Modelled grounded ice area (panel a) and volume (panel b; in m SLE, expressed as sea level contribution) for the 100 ensemble simulations (light grey time series), with the five overall best-fit simulations (which pass all sieves) highlighted with thicker coloured time series. The PaleoGrIS v1.0 isochrones data reconstructing the GrIS's former grounded ice extent are shown with triangle symbols on panel a (Leger et al., 2024)**. Note the GrIS-wide model-data misfit in ice extent apparent here can be misleading as it is spatially heterogeneous and heavily influenced by a few regions concentrating most of the misfit (*i.e.* NO, NE, and CE Greenland): see Fig. 18. Note the five overall best-fit simulations highlighted here, while passing all sieves, are not the best-scoring simulations at each individual model-data comparison test (see Fig. 13), but rather they score better than other simulations when combining all tests. For instance, their volume during the local LGM (panel b: ~16 kyr BP) is lower and less realistic than values of best-scoring simulations at the *local LGM extent* test (see Fig. 13d).**

https://doi.org/10.5194/egusphere-2025-1616
Preprint. Discussion started: 10 April 2025

Another potential source of model-data misfit could be biases in our input climate forcing causing either too low precipitation rates, or too high sea-surface temperatures (SST) across NO and NE Greenland. We do not expect biases in input air temperature forcing to have a meaningful impact at this stage, as despite our conservative ensemble parameter perturbations, we find no PDD-derived surface melt is produced until 12 kyr BP, thus several millennia after the local LGM and initial deglaciation, due to mean annual and summer temperatures remaining below 0°C (Figs. 4, 5). We note that during HS1 cooling, input mean-annual SST drops to lower minimum values (-2 to -3 °C) offshore SE and SW Greenland than offshore NE Greenland (-1.5 to -2 °C) (Figs. 6, 7), which may highlight a possible overestimation of our sea-surface temperature forcing (from Osman et al., 2021) in NE Greenland during the local LGM. This 0.5-2°C drop in SST at around 18-17 kyr BP, which occurs in response to HS1, is a key driver of modelled GrIS expansion during the local LGM, as it is associated with sharp reductions in GrIS-wide sub-shelf melt rates and thus basal mass loss rates (Fig. 12). A small underestimation in HS1 sea-surface cooling offshore NE Greenland, in the order of 1-2°C for instance, may be enough to deter the modelled GrIS margins from advancing extensively. This hypothesis may also be reinforced by the general lack of spatial coverage of SST proxy records used in the data-assimilation scheme of Osman et al. (2021) north of 65°N, offshore Greenland coasts. Biases may also be introduced by our interpolation scheme used for resampling from the nominal 1° horizontal resolution of the original data (Osman et al., 2021), equivalent to a ~20 x 27 km grid offshore NE Greenland, to our 5 x 5 km model grid. This highlights that our experiment may be limited by a lack of variation in SST input fields between ensemble simulations. A future experiment using an ensemble-varying parameter introducing spatial and temporal perturbations to the input ocean forcing may help test this hypothesis and possibly increase model-data fit.

Our simulations may also underestimate grounded ice extent in the NO and NE due to too low accumulation rates, largely controlled by our input precipitation forcing. Throughout these regions, iCESM-derived forcing suggests precipitation rates below 20 mm per month during HS1 (Fig. 6). We note that although iTRACE represents an improvement from the former CESM-derived transient global simulation of the last deglaciation (TRACE-21, Liu et al., 2009), it may still be subject to CESM biases that can sometimes misrepresent present-day and former precipitation rates over certain GrIS regions (van Kampenhout et al., 2020; Lofverstrom et al., 2020). In the case of NO and NE Greenland, input precipitation biases in the iTRACE simulation can also originate from global ice-sheet reconstruction used as forcing within iCESM (ICE-6G: Peltier et al., 2015), which may provide slightly incorrect geometries in these regions, impacting the modelled climate used here as input (*e.g.* Bouttes et al., 2023). More specifically, the ICE-6G reconstruction does not produce a GrIS that extends much beyond the present-day Greenland coastlines, which likely introduces regional biases in CESM simulations due to missing feedbacks between the ice-sheet and the earth system (Bradley et al., 2024). Although we use an ensemble-varying parameter introducing

https://doi.org/10.5194/egusphere-2025-1616
Preprint. Discussion started: 10 April 2025

precipitation perturbations of up to +200% (Table 1), such an increase is not space-dependent and may still be too low over NE Greenland. This may be suggested by our lLGM best-fit simulations all displaying precipitation offset values that are clustered towards the upper parameter-range threshold, between 1.8 and 2.0 (Fig. 26). Thus, better model-data scores at the *local-LGM extent* test could potentially be achieved with precipitation offset values above +200%.

Alternatively, our ensemble may be too small to fully explore the full impacts of our climate correction parameters on grounded GrIS extent evolution. As a test, we conducted an additional simulation using default (mid-range) values for all ensemble-varying parameters excluding the precipitation scalar offset (Table 1), here set to 2.0 (+200% precipitation rate). This test simulation successfully produces an extensive HS1 advance of the grounded GrIS margin offshore NE Greenland, reaching a mid-shelf position. This modelled local LGM advance is more extensive than any of our ensemble simulations, and suggests a 100 simulation ensemble is too small to explore the parameter-space region that models this preferable GrIS behaviour. Therefore, although computationally unfeasible here, running a larger ensemble while keeping perturbed parameter ranges identical to our setup may likely produce simulations yielding a better model-data fits in ice extent, during the local LGM.

https://doi.org/10.5194/egusphere-2025-1616
Preprint. Discussion started: 10 April 2025

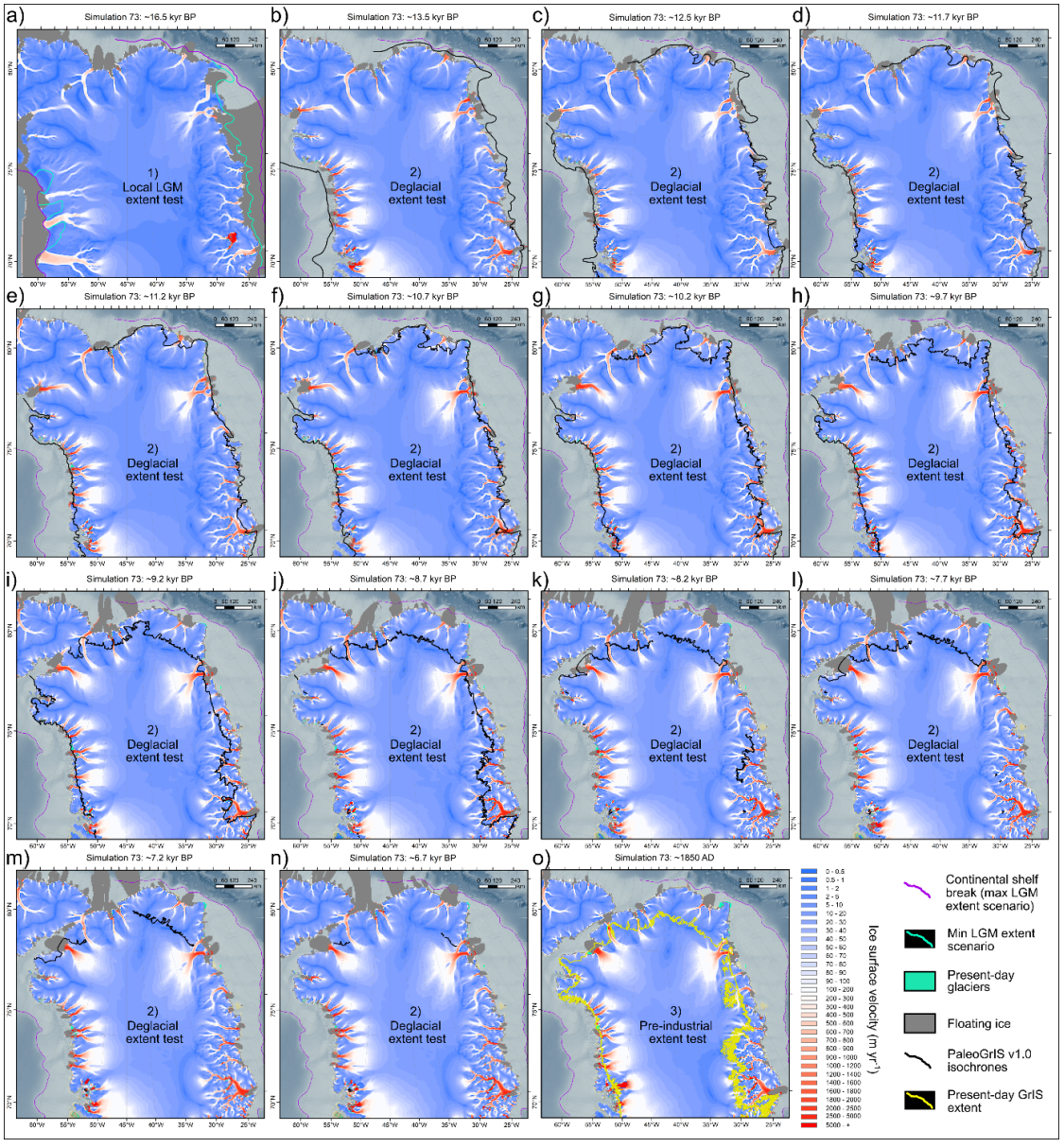

Figure 23. Modelled ice surface velocities of grounded ice for one of the five overall best-fit ensemble simulations (simulation number 73; which passes all sieves), during the local LGM (panel a), during each of the PaleoGrIS 1.0 isochrone time slices (panels b-n) (Leger et al., 2024)**, and during the PI (1850 AD; panel o). PaleoGrIS 1.0 isochrones for relevant time-slices are plotted with a thick black line. This figure only shows the northern half of the modelled ice sheet for ease of visualization. The southern half is shown in Figure 24. Bathymetry data shown in these maps is from the 15 arc-second resolution General Bathymetric Chart of the Oceans (GEBCO Bathymetric Compilation Group 2022, 2022).**

https://doi.org/10.5194/egusphere-2025-1616
Preprint. Discussion started: 10 April 2025

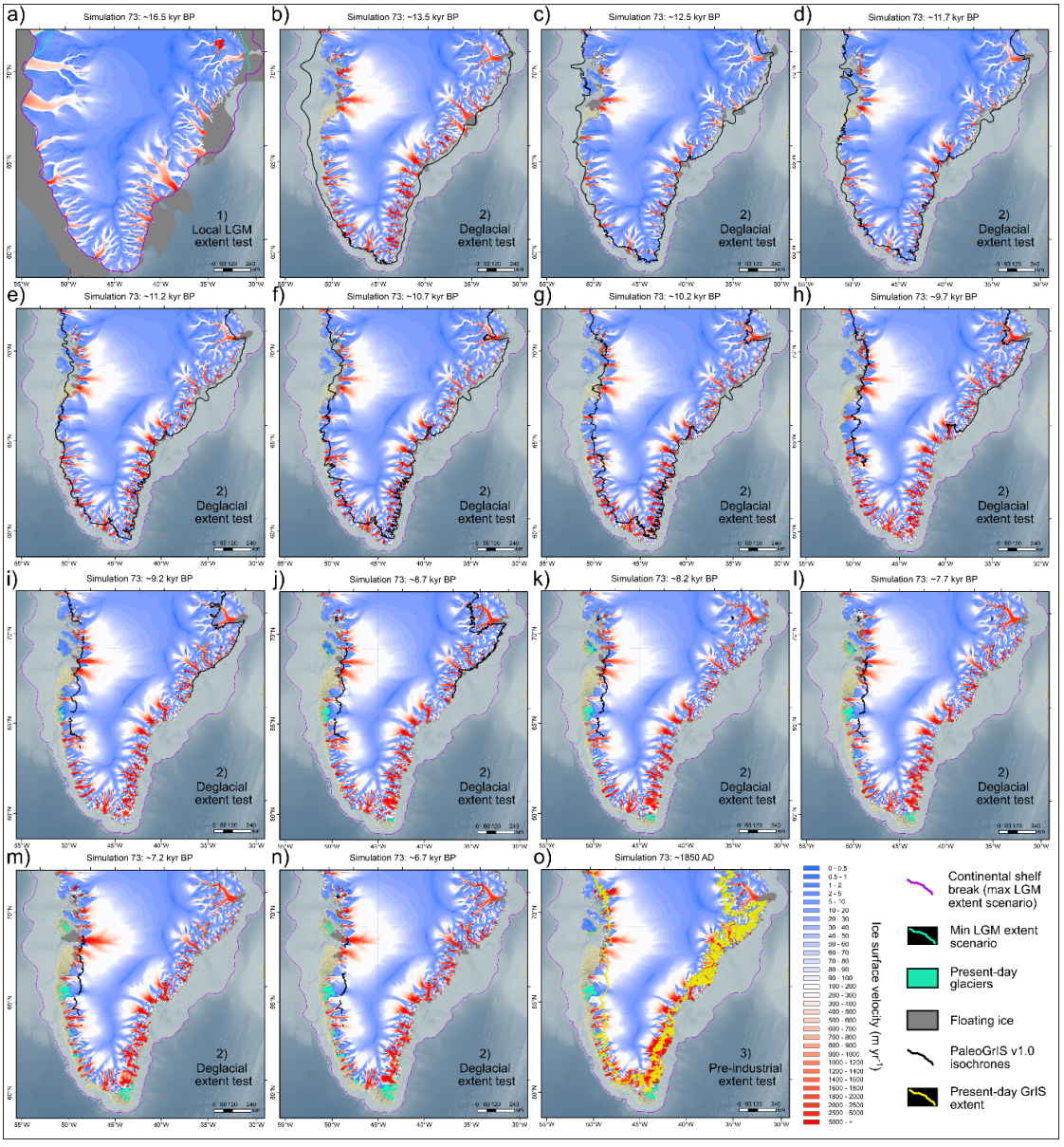

Figure 24. Modelled ice surface velocities of grounded ice for one of the five overall best-fit ensemble simulations (simulation number 73; which passes all sieves), during the local LGM (panel a), during each of the PaleoGrIS 1.0 isochrone time slices (panels b-n) (Leger et al., 2024)**, and during the PI era (1850 AD; panel o). PaleoGrIS 1.0 isochrones for relevant time-slices are plotted with a thick black line. This figure only shows the southern half of the ice sheet for ease of visualization. The northern half is shown in Figure 25. Bathymetry data shown in these maps is from the 15 arc-second resolution General Bathymetric Chart of the Oceans (GEBCO Bathymetric Compilation Group 2022, 2022).**

https://doi.org/10.5194/egusphere-2025-1616
Preprint. Discussion started: 10 April 2025

5.2 Underestimated deglacial retreat

We note that the CE and NE GrIS regions, where the greatest model-data misfits with PaleoGrIS 1.0 are found (Figs. 18, 23, 24), also present the highest concentration of high and steep topographies (1500 - 3000 m a.s.l.) in Greenland (Morlighem et al., 2017). We hypothesise that coarse model resolution may be a factor contributing to the higher relative ice-extent misfits observed in these regions during the Late-Glacial and Holocene deglaciation. Indeed, a large portion of the Eastern Greenland coast features the steepest and highest mountain ranges of the continent, stretching from 67 °N (Schweizerland Alps) to 77 °N (Halle range), and dissected by a complex network of overdeepened valleys. This topographic setting leads to the highest concentration of deglaciated and relatively long (>100 km), narrow (<15 km), deep and steep-sided fjords in Greenland (Swift et al., 2008). These major fjord systems include the Kangertittivaq (Scoresby Sund), Kangerluk Kong Oscar, Kangerluk Kejser Franz Joseph (Fig. 27), Gael Hamke Bay, Shannon Bay and Dove Bay (76°N) complexes. According to geochronological reconstructions, the retreat of GrIS outlet glaciers from the outer mouths of these CE and NE Greenland fjords to near their present-day positions occurred mainly between ~12 and ~8.5 kyr BP (*e.g.* Marienfeld, 1990; Bennike et al., 1999; Håkansson et al., 2007; Leger et al., 2024). However, the majority of this retreat is missing in our ensemble simulations. A 5 x 5 km horizontal resolution may not be fine enough to capture the complexity of GrIS margin retreat into the complex network of over-deepened fjords and steep valleys of these regions. By drawing topographic elevation profiles across one the region's main fjords (Kangerluk Kejser Franz Joseph, 73.2°N; 23.2°W), we find that even for one of the widest NE Greenland fjords (~20 km), formerly acting as the main topographic conduit for the Waltershausen Glacier, the topography is heavily flattened at 5 km resolution (Fig. 27). Across the profile, summit elevations of fjord-side mountains are underestimated by 30 - 50%, and average slope along the transect is 40% and 35% lower than for 150 m and 1 km resolution grids, respectively (Fig. 27). Thus, at 5 x 5 km resolution, the modelled GrIS is less topographically constrained than it should be during deglacial margin retreat and thinning (Fig. 27). A better resolved topography (*e.g.* 1 x 1 km or lower) would likely lead to both higher ice flux rates within narrow valleys, due to higher summits, steeper bed slopes, and greater ice flow convergence, but also to deeper fjords enabling more water ingress as modelled tidewater glaciers retreat. Both mechanisms, unlikely to be captured at 5 x 5 km, would together enhance modelled GrIS thinning and retreat rates during the Late-Glacial and early-to-mid Holocene in these regions. In such steep terrain, higher-resolution modelling may lead to better model-data fit for a given parameter configuration (Leger et al., 2025). This was in part shown by Aschwanden et al. (2016) who, using PISM, found that observed flow velocities of main present-day GrIS outlet glaciers (*e.g.* Nuussuup Sermia, Sermeq Kujalleq) were better matched using resolutions of 600 and 1500 m, relative to 3600 and 4500 m, with the latter causing maximum flow velocities to be underestimated by factors of 4 - 7. Therefore, while the inability to resolve fine topographies generates biases across the domain, we argue its negative impact on model-data fit is likely to be greater in CE and NE Greenland, relative to other regions, due to the greater concentration of steep and high-relief topographies.

https://doi.org/10.5194/egusphere-2025-1616
Preprint. Discussion started: 10 April 2025

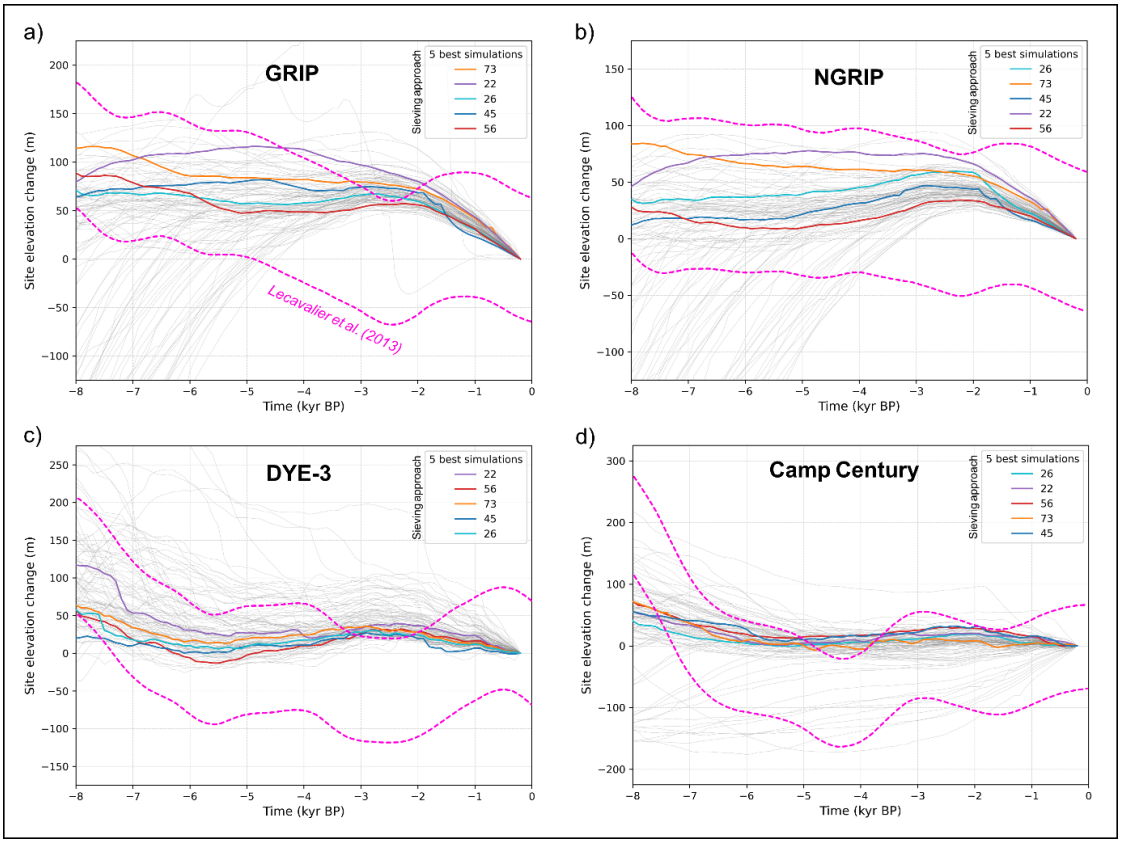

Figure 25. Comparison between ice elevation change modelled by our five overall best-fit simulations (which pass all sieves; thicker coloured lines) and the 1σ uncertainty band of the Holocene thinning curves (dashed pink lines), derived from ice core δ^{18}O records. Holocene thinning curves were produced by Lecavalier et al. (2013)**, improving from** Vinther et al. (2009) **following an elevation correction for thickness changes at the Agassiz and Renland ice caps. Data from all other ensemble simulations from this study are shown with thin, light grey lines.**

https://doi.org/10.5194/egusphere-2025-1616
Preprint. Discussion started: 10 April 2025

Larger model-data misfits in the magnitude and rates of GrIS retreat during the Late-Glacial and early-to-mid Holocene in NO, NE, and CE Greenland could also be associated with biases in our input climate forcing, including possible underestimations of sea-surface and atmospheric warming (~14 - 6 kyr BP). As mentioned above, biases in iTRACE-derived climate are possible, especially towards the margins of the former GrIS. For instance, an overestimation of the ice thickness and extent reconstruction used as forcing within iCESM (ICE-6G: Peltier et al., 2015) during the last deglaciation in NO, NE, and CE Greenland, would lead to unrealistically high albedo feedbacks impeding the atmospheric warming required to model appropriate GrIS thinning and retreat rates. Our experiment features an ensemble-varying temperature offset parameter (Table 1) with maximum space-independent warming of up to +3.5 °C, along with ensemble-varying snow and ice PDD melt factors that can reach 5 and 12 mm *w.e.* d^{-1} $°C^{-1}$, respectively. However, if significant input climate biases exist in the regions of concern, these perturbations may still underestimate the resulting surface melt during deglaciation. Alternatively, our ensemble (n=100) may be too small to explore the full impact of these temperature and PDD melt parameter perturbations on modelled GrIS retreat during deglaciation. Furthermore, our SMB parameterisation, based on on a simple PDD scheme (Calov and Greve, 2005), does not capture certain ablation mechanisms such as sublimation and wind-driven snow layer erosion, nor does it fully capture the elevation feedback between the modelled ice-sheet surface and climate forcing. These missing mechanisms may be important to model deglacial GrIS thinning and retreat accurately at high latitudes (>75°N), where mean summer air temperatures during the HTM remained close to or below 0°C (at least in our forcing data) (Fig. 5) (Plach et al., 2019). Alternatively, the underestimated modelled GrIS retreat in NO, NE, and CE Greenland could be associated with a lower-than-needed ocean temperature increase during the last deglaciation (Osman et al., 2021; Figs. 6-8) offshore the present-day GrIS. Importantly, we also note that our ice-ocean interaction model does not consider multiple ocean layers, which are important when poorly mixed sub-surface layers of higher temperatures increase sub-shelf melt at depth and towards the grounding line (Lloyd et al., 2023). It also does not consider a seasonal cycle of ocean water temperature change as forcing, which may be important to model the necessary magnitude of deglacial sub-shelf melt in these regions.

Today, up to ~16% of the GrIS is thought to be drained by NEGIS (Hvidberg et al., 2020), a singular ice stream that can prove challenging to model accurately (Smith-Johnsen et al., 2020). In our best-fit ensemble simulations, some ice streaming is modelled towards and upflow from both Nioghalvfjerdsbrae (79N glacier) and Zachariae Isstrom glaciers, throughout the full simulation timespan (*e.g.* Figs. 17, 23). However, a comparison between our best-fit simulations at the *PI extent* test and observed GrIS surface velocities (Joughin et al., 2018b) reveals that our model underestimates GrIS flow speeds towards NEGIS (Supplementary Fig. 6). Our simulations do not capture its singular shape featuring a relatively narrow (<100 km) and long (>500 km) band of high (> 50 m yr^{-1}) surface velocities nearly reaching the ice-sheet's central East/West divide (Supplementary Fig. 6). Although uncertainties remain regarding the timing of last NEGIS activation into its present-day configuration, recent evidence suggests it was active during much of the

https://doi.org/10.5194/egusphere-2025-1616
Preprint. Discussion started: 10 April 2025

Holocene (Franke et al., 2022). Due to its significant impact on ice flux of the entire NE GrIS region, modelling an accurate NEGIS configuration throughout the Late-Glacial and Holocene periods would produce higher regional-mean discharge and thinning rates. Over millennial timescales, this may help model greater and more data-consistent GrIS margin retreat rates during deglaciation. Therefore, it is possible that not fully reproducing NEGIS may contribute to increasing model-data misfits in NE Greenland relative to other GrIS regions, where ice streams are generally less challenging to model accurately.

https://doi.org/10.5194/egusphere-2025-1616
Preprint. Discussion started: 10 April 2025

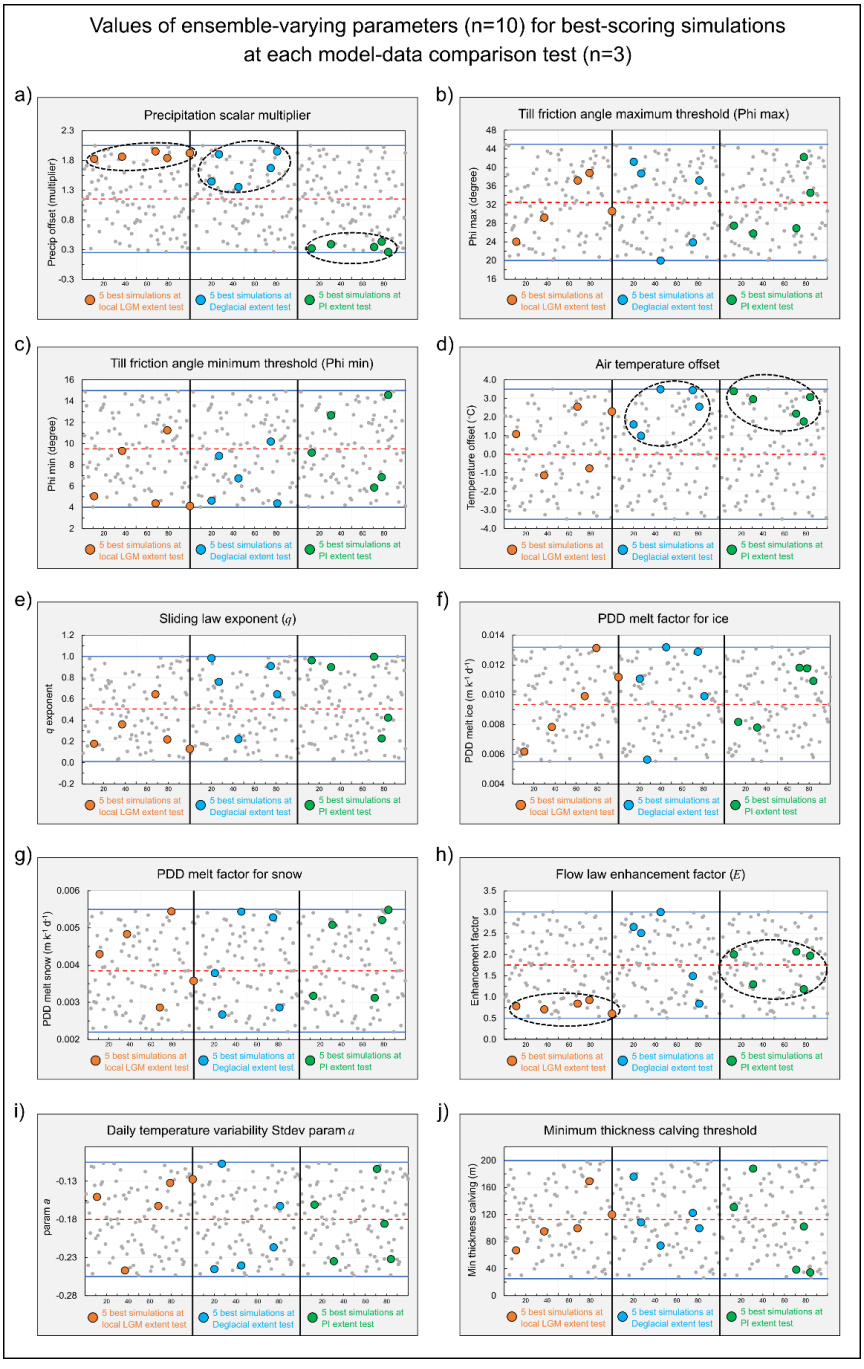

Figure 26. Values of the 10 ensemble-varying parameters for all simulations (n = 100, grey dots) and for the five best-scoring simulations (larger coloured dots) at each of the three model-data comparison tests (separated by vertical black lines). Dashed black ellipses (in panels a, d, and h) highlight best-fit parameter 'clusters', defined as such when the parameter values for the five best-fit simulations (coloured dots) cover a range < 50 % of the parameter value range (highlighted by horizontal blue lines) originally sampled with the Latin Hypercube technique (also see Table 1). All X axes represent ensemble simulation numbers (0 – 100).

https://doi.org/10.5194/egusphere-2025-1616
Preprint. Discussion started: 10 April 2025

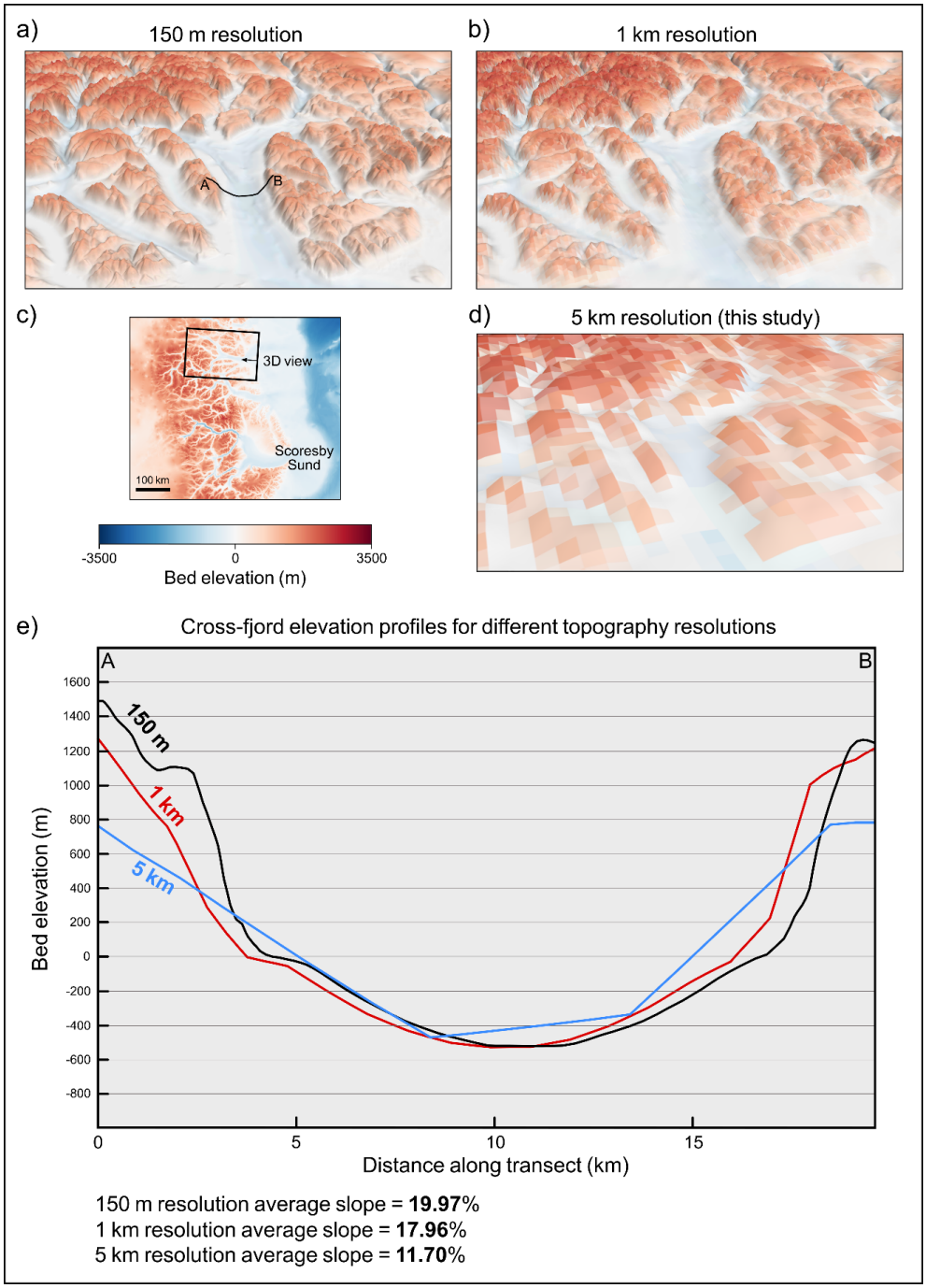

Figure 27. Three-dimensional views (panels a, b, and d) of bed topography (BedMachine v4 merged with GEBCO data) and cross elevation profiles (panel e) along a transect drawn across the Kangerluk Kejser Franz Joseph fjord (73.2°N; 23.2°W; black line in panel a). Elevation profiles are shown for three different grid resolutions (5 km, 1 km, and 150 m). While average slopes over such a terrain decreases by 10% between 150 m and 1 km resolution grids, it decreases by around 40% between 150 m and 5 km resolution grid, 5 km being the model resolution of this study. For more details regarding the bed topography used in this modelling study, the reader is referred to Figure 1 and its caption.

https://doi.org/10.5194/egusphere-2025-1616
Preprint. Discussion started: 10 April 2025

6 Conclusions

In this study, we conducted a perturbed-parameter ensemble of 100 PISM simulations of the entire Greenland-Ice-Sheet evolution from 24,000 years ago to the pre-industrial era (1850 AD) at a spatial resolution of 5 x 5 km. Each model simulation was quantitatively scored against ice-sheet-wide empirical data of former grounded ice extent and its timing. We here summarize the main results and findings from this model-data comparison experiment.

-The maximum grounded Greenland Ice Sheet extent, *i.e.* the local LGM, likely occurred between 17.5 and 16 kyr BP, during Heinrich Stadial 1. At that time, the grounded ice sheet reached an area of between 2.9 and 3.1 million km^2. During full glaciation, grounded ice likely reached the continental shelf break along the entire Western, Southern, and Southeastern Greenland coasts.

-Our results suggest that between the local LGM and today, the global mean sea level rise contribution of the Greenland Ice Sheet is between 6 and 7.5 meters, a number substantially higher than previous estimates (see section 3.1.2.). During the local LGM, the ice sheet was not necessarily thicker (nor higher-elevated) than today at its summits, towards the GISP2, GRIP, and NGRIP ice core locations. Contrastingly, in Southern and Northwestern Greenland (DYE-3 and NEEM ice cores), the ice sheet was likely up to ~1 km thicker than today, with an ice surface up to ~500 m higher in elevation, thus causing ice divide migrations between full glacial and interglacial periods. These migrations may have important implications for the chronological interpretation of the DYE-3 ice core. During maximum extent, the ice sheet was also flowing faster and was able to discharge up to 5.1 times more ice than today, thus contributing substantially more iceberg and freshwater delivery to the north Atlantic basin than today.

-The Greenland Ice Sheet likely retreated rapidly and extensively during the late Heinrich-stadial 1 and Bølling–Allerød warming events, between 16 and 14 kyr BP. During that time, the grounded ice sheet lost the majority of its continental shelf cover. This rapid demise was predominantly caused by ocean warming and increased sub-shelf melt, while air temperatures likely remained too cold to generate significant surface melt. During this phase of rapid retreat, the ice sheet may have experienced up to 7 times greater mass loss rates than are currently estimated for the present-day.

-At the Greenland Ice Sheet scale, margin stabilization and readvances during the Younger Dryas cooling event were likely limited and of low magnitude, as opposed to periphery glaciers which demonstrated a more dynamic response. We hypothesise this was caused by strong ice-sheet inertia and geometrical/thermal ice

https://doi.org/10.5194/egusphere-2025-1616
Preprint. Discussion started: 10 April 2025

memory feedbacks associated with the potent deglaciation experienced just prior, during Bølling–Allerød warming.

-The Greenland Ice Sheet likely reached a minimum in ice extent between 6 and 5 kyr BP, and thus lagged the cessation of Holocene Thermal Maximum warming by a few centuries, and up to a millennium, prior to experiencing late-Holocene and Neoglacial readvance. During the mid-Holocene, our simulations produce up to ~100 km of margin retreat behind the present-day Greenland Ice Sheet, but only south of 68 °N.

-While best-fit simulations present a reasonable agreement with the PaleoGrIS 1.0 grounded ice-extent reconstruction in Northwestern, Central-western, Southwestern, and Southeastern Greenland regions, we find larger model-data misfits remain in the Northern, Northeastern, and Central-eastern regions. There, the magnitudes and rates of modelled LGM advance and deglacial retreat are both underestimated, when compared to empirical data. Our results suggest these regions are significantly more challenging to model accurately. We hypothesise these misfits are possibly related to multiple causes including biases from: surface mass balance and ice-ocean interaction parameterisations, input climate, model resolution due to rougher local topographies, model initialisation, and the difficulty to reproduce the Northeast Greenland Ice Stream.

-No single ensemble simulation could achieve a better relative score at all three chronologically-distinct model-data comparison tests. Instead, we find different simulations, and thus different parameter configurations, are needed to better match empirical data in certain Greenland regions or during certain millennial-scale events (*e.g.* the early-Holocene). Thus, producing a physically-sound 3D model simulation that is data-consistent across all Greenland regions since the last glaciation, which would enable to accurately capture the ice-sheet's memory from this key period of environmental change, is still a major challenge. To achieve this, future work may need to employ larger ensembles, more appropriate parameterisations of boundary conditions, data assimilation to reduce bias accumulations, higher resolution modelling, and more time- and space-dependent parameter and paleoclimate perturbations.

https://doi.org/10.5194/egusphere-2025-1616
Preprint. Discussion started: 10 April 2025

Code and data availability.

The open-access source code for PISM can be accessed and downloaded from https://github.com/pism/pism . The code specific to the PISM version used in this study, version 2.0.5, can be accessed from https://doi.org/10.5281/zenodo.7199611 .

All input data formatted for PISM (NetCDF file formats), along with shell scripts required to run each ensemble simulation (n=100), which together enable to reproduce the simulations presented in this study, as well as model output data and videos for the five overall best-fit simulations (which pass all sieves), are available for download from the following Zenodo repository: https://doi.org/10.5281/zenodo.15149359

Supplement.

The supplement related to this article is available online at: ……..

Author contributions.

JCE and TPML conceived and guided the study. Input from SLB and CDC contributed to the design of the modelling investigation. TPML prepared the input data products and conducted the modelling on High Performance Computer clusters with technical help from JCE and REA. SLB conducted the glacial-isostatic-adjustment model and earth model simulations required to produce the non-local relative-sea-level forcing input data. JCE conducted the installation of PISM on the University of Sheffield High Performance Computing clusters. JZ provided access to- and support in interpreting- the iCESM data used as input climate forcing, with technical help from SLB. TPML conducted the post-modelling data processing and quantitative model-data comparisons, with feedback from CDC and JCE, and TPML conducted all subsequent quantitative analyses. TPML wrote the manuscript, with feedback from JCE and SLB primarily, and other co-authors for subsequent drafts. TPML produced all maps, figures, and tables.

Competing interests.

The contact author has declared that none of the authors have any competing interests.

Acknowledgements.

We wish to thank all individuals who contributed support, ideas, and insightful discussions to this investigation including Joshua Cuzzone, Jason Briner, and members of the PALGLAC team including Christiaan R. Diemont, Anna L. C. Hughes, Stephen J. Livingstone, Remy L. J. Veness, Frances E. G. Butcher, Helen E. Dulfer, and Benjamin M. Boyes. We thank the University of Sheffield Research and Innovation team in IT Services for their work and vital support in using the University High Performance Computing clusters for all computation.

Financial support.

https://doi.org/10.5194/egusphere-2025-1616
Preprint. Discussion started: 10 April 2025

This study benefited from the PALGLAC team of researchers with funding from the European Research Council (ERC) under the European Union's Horizon 2020 research and innovation programme to Christopher D. Clark (Grant Agreement No. 787263), and which employed Tancrède P. M. Leger, Sarah L. Bradley, and Rosie E. Archer. The CESM project is supported primarily by the U.S. National Science Foundation (NSF). This material is based upon work supported by the NSF National Center for Atmospheric Research, which is a major facility sponsored by the NSF under Cooperative Agreement No. 1852977. Jeremy C. Ely has received support from a NERC independent fellowship award (grant no. NE/R014574/1).

https://doi.org/10.5194/egusphere-2025-1616
Preprint. Discussion started: 10 April 2025

References.

Albrecht, T. and Levermann, A.: Spontaneous ice-front retreat caused by disintegration of adjacent ice shelf in Antarctica, Earth Planet Sci Lett, 393, 26–30, https://doi.org/10.1016/j.epsl.2014.02.034, 2014.

Albrecht, T., Winkelmann, R., and Levermann, A.: Glacial-cycle simulations of the Antarctic Ice Sheet with the Parallel Ice Sheet Model (PISM)-Part 1: Boundary conditions and climatic forcing, Cryosphere, 14, 599–632, https://doi.org/10.5194/tc-14-599-2020, 2020.

Arndt, J. E., Jokat, W., and Dorschel, B.: The last glaciation and deglaciation of the Northeast Greenland continental shelf revealed by hydro-acoustic data, Quat Sci Rev, 160, 45–56, https://doi.org/10.1016/j.quascirev.2017.01.018, 2017.

Arnold, K. C. and MacKay, D. K.: Different methods of calculating mean daily temperatures, their effects on degree-day totals in the high Arctic and their significance to glaciology, Geogr Bull, 21, 123–129, 1964.

Aschwanden, A., Bueler, E., Khroulev, C., and Blatter, H.: An enthalpy formulation for glaciers and ice sheets, Journal of Glaciology, 58, 441–457, https://doi.org/10.3189/2012JoG11J088, 2012.

Aschwanden, A., Aðalgeirsdóttir, G., and Khroulev, C.: Hindcasting to measure ice sheet model sensitivity to initial states, Cryosphere, 7, 1083–1093, https://doi.org/10.5194/tc-7-1083-2013, 2013.

Aschwanden, A., Fahnestock, M. A., and Truffer, M.: Complex Greenland outlet glacier flow captured, Nat Commun, 7, 10524, https://doi.org/10.1038/ncomms10524, 2016.

Aschwanden, A., Fahnestock, M. A., Truffer, M., Brinkerhoff, D. J., Hock, R., Khroulev, C., Mottram, R., and Abbas Khan, S.: Contribution of the Greenland Ice Sheet to sea level over the next millennium, Sci Adv, 5, https://doi.org/10.1126/sciadv.aav9396, 2019.

Bennett, M. R.: Ice streams as the arteries of an ice sheet: their mechanics, stability and significance, Earth Sci Rev, 61, 309–339, https://doi.org/10.1016/S0012-8252(02)00130-7, 2003.

Bennike, O., Björck, S., Böcher, J., Hansen, L., Heinemeier, J., and Wohlfarth, B.: Early Holocene plant and animal remains from North-east Greenland, J Biogeogr, 26, 667–677, https://doi.org/10.1046/j.1365-2699.1999.t01-1-00315.x, 1999.

Berger, AndréL.: Long-Term Variations of Daily Insolation and Quaternary Climatic Changes, J Atmos Sci, 35, 2362–2367, https://doi.org/10.1175/1520-0469(1978)035<2362:LTVODI>2.0.CO;2, 1978.

Biette, M., Jomelli, V., Chenet, M., Braucher, R., Rinterknecht, V., and Lane, T.: Mountain glacier fluctuations during the Lateglacial and Holocene on Clavering Island (northeastern Greenland) from 10Be moraine dating, Boreas, 49, 873–885, https://doi.org/10.1111/bor.12460, 2020.

Born, A. and Robinson, A.: Modeling the Greenland englacial stratigraphy, Cryosphere, 15, 4539–4556, https://doi.org/10.5194/tc-15-4539-2021, 2021.

Bouttes, N., Lhardy, F., Quiquet, A., Paillard, D., Goosse, H., and Roche, D. M.: Deglacial climate changes as forced by different ice sheet reconstructions, Climate of the Past, 19, 1027–1042, https://doi.org/10.5194/cp-19-1027-2023, 2023.

Bradley, S. L., Reerink, T. J., Van De Wal, R. S. W., and Helsen, M. M.: Simulation of the Greenland Ice Sheet over two glacial-interglacial cycles: investigating a sub-ice-shelf melt parameterization and relative sea level forcing in an ice-sheet-ice-shelf model, Climate of the Past, 14, 619–635, https://doi.org/10.5194/cp-14-619-2018, 2018.

Bradley, S. L., Sellevold, R., Petrini, M., Vizcaino, M., Georgiou, S., Zhu, J., Otto-Bliesner, B. L., and Lofverstrom, M.: Surface mass balance and climate of the Last Glacial Maximum Northern Hemisphere ice sheets: simulations with CESM2.1, Climate of the Past, 20, 211–235, https://doi.org/10.5194/cp-20-211-2024, 2024.

https://doi.org/10.5194/egusphere-2025-1616
Preprint. Discussion started: 10 April 2025

Brady, E., Stevenson, S., Bailey, D., Liu, Z., Noone, D., Nusbaumer, J., Otto-Bliesner, B. L., Tabor, C., Tomas, R., Wong, T., Zhang, J., and Zhu, J.: The Connected Isotopic Water Cycle in the Community Earth System Model Version 1, J Adv Model Earth Syst, 11, 2547–2566, https://doi.org/10.1029/2019MS001663, 2019.

Braithwaite, R. J.: Positive degree-day factors for ablation on the Greenland ice sheet studied by energy-balance modelling, Journal of Glaciology, 41, 153–160, https://doi.org/10.1017/S0022143000017846, 1995.

Briner, J., Schaefer, J., Young, N., Keisling, B., Anandakrishnan, S., Kuhl, T., Boeckmann, G., MacGregor, J., Deconto, R., Morlighem, M., Winckler, G., and Walcott, C.: Introducing GreenDrill: Retrieving sub-glacial bedrock cores in North Greenland to test ice sheet response to interglacial warmth (and supporting your research?), in: AGU Fall Meeting Abstracts, C31A-07, 2021.

Briner, J. P., Kaufman, D. S., Bennike, O., and Kosnik, M. A.: Amino acid ratios in reworked marine bivalve shells constrain Greenland Ice Sheet history during the holocene, Geology, 42, 75–78, https://doi.org/10.1130/G34843.1, 2014.

Briner, J. P., Cuzzone, J. K., Badgeley, J. A., Young, N. E., Steig, E. J., Morlighem, M., Schlegel, N. J., Hakim, G. J., Schaefer, J. M., Johnson, J. V., Lesnek, A. J., Thomas, E. K., Allan, E., Bennike, O., Cluett, A. A., Csatho, B., de Vernal, A., Downs, J., Larour, E., and Nowicki, S.: Rate of mass loss from the Greenland Ice Sheet will exceed Holocene values this century, Nature, 586, 70–74, https://doi.org/10.1038/s41586-020-2742-6, 2020.

Bueler, E. and Brown, J.: Shallow shelf approximation as a "sliding law" in a thermomechanically coupled ice sheet model, J Geophys Res Earth Surf, 114, 1–21, https://doi.org/10.1029/2008JF001179, 2009.

Bueler, E., Lingle, C. S., and Brown, J.: Fast computation of a viscoelastic deformable Earth model for ice-sheet simulations, Ann Glaciol, 46, 97–105, https://doi.org/10.3189/172756407782871567, 2007.

Buizert, C., Gkinis, V., Severinghaus, J. P., He, F., Lecavalier, B. S., Kindler, P., Leuenberger, M., Carlson, A. E., Vinther, B., Masson-Delmotte, V., White, J. W. C., Liu, Z., Otto-Bliesner, B., and Brook, E. J.: Greenland temperature response to climate forcing during the last deglaciation, Science (1979), 345, 1177–1180, https://doi.org/10.1126/science.1254961, 2014.

Buizert, C., Keisling, B. A., Box, J. E., He, F., Carlson, A. E., Sinclair, G., and DeConto, R. M.: Greenland-Wide Seasonal Temperatures During the Last Deglaciation, Geophys Res Lett, 45, 1905–1914, https://doi.org/10.1002/2017GL075601, 2018.

Calov, R. and Greve, R.: A semi-analytical solution for the positive degree-day model with stochastic temperature variations, Journal of Glaciology, 51, 173–175, https://doi.org/10.3189/172756505781829601, 2005.

Calov, R., Robinson, A., Perrette, M., and Ganopolski, A.: Simulating the Greenland ice sheet under present-day and palaeo constraints including a new discharge parameterization, Cryosphere, 9, 179–196, https://doi.org/10.5194/tc-9-179-2015, 2015.

Clark, C. D., Ely, J. C., Hindmarsh, R. C. A., Bradley, S., Ignéczi, A., Fabel, D., Ó Cofaigh, C., Chiverrell, R. C., Scourse, J., Benetti, S., Bradwell, T., Evans, D. J. A., Roberts, D. H., Burke, M., Callard, S. L., Medialdea, A., Saher, M., Small, D., Smedley, R. K., Gasson, E., Gregoire, L., Gandy, N., Hughes, A. L. C., Ballantyne, C., Bateman, M. D., Bigg, G. R., Doole, J., Dove, D., Duller, G. A. T., Jenkins, G. T. H., Livingstone, S. L., McCarron, S., Moreton, S., Pollard, D., Praeg, D., Sejrup, H. P., Van Landeghem, K. J. J., and Wilson, P.: Growth and retreat of the last British–Irish Ice Sheet, 31 000 to 15 000 years ago: the BRITICE-CHRONO reconstruction, Boreas, 51, 699–758, https://doi.org/10.1111/bor.12594, 2022.

Clark, P. U. and Mix, A. C.: Ice sheets and sea level of the Last Glacial Maximum, Quat Sci Rev, 21, 1–7, https://doi.org/10.1016/S0277-3791(01)00118-4, 2002.

Cuffey, K. M. and Paterson, W. S. B.: The Physics of Glaciers, Academic Press, 2010.

Dalton, A. S., Dulfer, H. E., Margold, M., Heyman, J., Clague, J. J., Froese, D. G., Gauthier, M. S., Hughes, A. L. C., Jennings, C. E., Norris, S. L., and Stoker, B. J.: Deglaciation of the north American ice sheet complex in calendar

https://doi.org/10.5194/egusphere-2025-1616
Preprint. Discussion started: 10 April 2025

years based on a comprehensive database of chronological data: NADI-1, Quat Sci Rev, 321, 108345, https://doi.org/10.1016/j.quascirev.2023.108345, 2023.

van Dam, E. R., Husslage, B., den Hertog, D., and Melissen, H.: Maximin Latin Hypercube Designs in Two Dimensions, Oper Res, 55, 158–169, https://doi.org/10.1287/opre.1060.0317, 2007.

Dansgaard, W., Clausen, H. B., Gundestrup, N., Hammer, C. U., Johnsen, S. F., Kristinsdottir, P. M., and Reeh, N.: A New Greenland Deep Ice Core, Science (1979), 218, 1273–1277, https://doi.org/10.1126/science.218.4579.1273, 1982.

Davies, J., Mathiasen, A. M., Kristiansen, K., Hansen, K. E., Wacker, L., Alstrup, A. K. O., Munk, O. L., Pearce, C., and Seidenkrantz, M.-S.: Linkages between ocean circulation and the Northeast Greenland Ice Stream in the Early Holocene, Quat Sci Rev, 286, 107530, https://doi.org/10.1016/j.quascirev.2022.107530, 2022a.

Davies, J., Mathiasen, A. M., Kristiansen, K., Hansen, K. E., Wacker, L., Alstrup, A. K. O., Munk, O. L., Pearce, C., and Seidenkrantz, M.-S.: Linkages between ocean circulation and the Northeast Greenland Ice Stream in the Early Holocene, Quat Sci Rev, 286, 107530, https://doi.org/10.1016/j.quascirev.2022.107530, 2022b.

Edwards, T. L., Nowicki, S., Marzeion, B., Hock, R., Goelzer, H., Seroussi, H., Jourdain, N. C., Slater, D. A., Turner, F. E., Smith, C. J., McKenna, C. M., Simon, E., Abe-Ouchi, A., Gregory, J. M., Larour, E., Lipscomb, W. H., Payne, A. J., Shepherd, A., Agosta, C., Alexander, P., Albrecht, T., Anderson, B., Asay-Davis, X., Aschwanden, A., Barthel, A., Bliss, A., Calov, R., Chambers, C., Champollion, N., Choi, Y., Cullather, R., Cuzzone, J., Dumas, C., Felikson, D., Fettweis, X., Fujita, K., Galton-Fenzi, B. K., Gladstone, R., Golledge, N. R., Greve, R., Hattermann, T., Hoffman, M. J., Humbert, A., Huss, M., Huybrechts, P., Immerzeel, W., Kleiner, T., Kraaijenbrink, P., Le clec'h, S., Lee, V., Leguy, G. R., Little, C. M., Lowry, D. P., Malles, J.-H., Martin, D. F., Maussion, F., Morlighem, M., O'Neill, J. F., Nias, I., Pattyn, F., Pelle, T., Price, S. F., Quiquet, A., Radić, V., Reese, R., Rounce, D. R., Rückamp, M., Sakai, A., Shafer, C., Schlegel, N.-J., Shannon, S., Smith, R. S., Straneo, F., Sun, S., Tarasov, L., Trusel, L. D., Van Breedam, J., van de Wal, R., van den Broeke, M., Winkelmann, R., Zekollari, H., Zhao, C., Zhang, T., and Zwinger, T.: Projected land ice contributions to twenty-first-century sea level rise, Nature, 593, 74–82, https://doi.org/10.1038/s41586-021-03302-y, 2021.

Ely, J. C., Clark, C. D., Small, D., and Hindmarsh, R. C. A.: ATAT 1.1, the Automated Timing Accordance Tool for comparing ice-sheet model output with geochronological data, Geosci Model Dev, 12, 933–953, https://doi.org/10.5194/gmd-12-933-2019, 2019.

Ely, J. C., Clark, C. D., Bradley, S. L., Gregoire, L., Gandy, N., Gasson, E., Veness, R. L. J., and Archer, R.: Behavioural tendencies of the last British–Irish Ice Sheet revealed by data–model comparison, J Quat Sci, 39, 839–871, https://doi.org/10.1002/jqs.3628, 2024.

Erb, M. P., Mckay, N. P., Steiger, N., Dee, S., Hancock, C., Ivanovic, R. F., Gregoire, L. J., and Valdes, P.: Reconstructing Holocene temperatures in time and space using paleoclimate data assimilation, Climate of the Past, 18, 2599–2629, https://doi.org/10.5194/cp-18-2599-2022, 2022.

Fausto, R. S., Ahlstrøm, A. P., Van As, D., Bøggild, C. E., and Johnsen, S. J.: A new present-day temperature parameterization for Greenland, Journal of Glaciology, 55, 95–105, https://doi.org/10.3189/002214309788608985, 2009.

Fleming, K. and Lambeck, K.: Constraints on the Greenland Ice Sheet since the Last Glacial Maximum from sea-level observations and glacial-rebound models, Quat Sci Rev, 23, 1053–1077, https://doi.org/10.1016/j.quascirev.2003.11.001, 2004.

Franke, S., Bons, P. D., Westhoff, J., Weikusat, I., Binder, T., Streng, K., Steinhage, D., Helm, V., Eisen, O., Paden, J. D., Eagles, G., and Jansen, D.: Holocene ice-stream shutdown and drainage basin reconfiguration in northeast Greenland, Nat Geosci, 15, 995–1001, https://doi.org/10.1038/s41561-022-01082-2, 2022.

Funder, S., Kjeldsen, K. K., Kjær, K. H., and Ó Cofaigh, C.: The Greenland Ice Sheet During the Past 300,000 Years: A Review, in: Developments in Quaternary Science, vol. 15, 699–713, https://doi.org/10.1016/B978-0-444-53447-7.00050-7, 2011a.

https://doi.org/10.5194/egusphere-2025-1616
Preprint. Discussion started: 10 April 2025

Funder, S., Kjeldsen, K. K., Kjær, K. H., and Ó Cofaigh, C.: The Greenland Ice Sheet During the Past 300,000 Years: A Review, in: Developments in Quaternary Science, vol. 15, 699–713, https://doi.org/10.1016/B978-0-444-53447-7.00050-7, 2011b.

Gandy, N., Astfalck, L. C., Gregoire, L. J., Ivanovic, R. F., Patterson, V. L., Sherriff-Tadano, S., Smith, R. S., Williamson, D., and Rigby, R.: De-Tuning Albedo Parameters in a Coupled Climate Ice Sheet Model to Simulate the North American Ice Sheet at the Last Glacial Maximum, J Geophys Res Earth Surf, 128, https://doi.org/10.1029/2023JF007250, 2023.

GEBCO Bathymetric Compilation Group 2022: The GEBCO_2022 Grid - a continuous terrain model of the global oceans and land, 2022.

Goelzer, H., Robinson, A., Seroussi, H., and van de Wal, R. S. W.: Recent Progress in Greenland Ice Sheet Modelling, Curr Clim Change Rep, 3, 291–302, https://doi.org/10.1007/s40641-017-0073-y, 2017.

Goelzer, H., Nowicki, S., Payne, A., Larour, E., Seroussi, H., Lipscomb, W. H., Gregory, J., Abe-Ouchi, A., Shepherd, A., Simon, E., Agosta, C., Alexander, P., Aschwanden, A., Barthel, A., Calov, R., Chambers, C., Choi, Y., Cuzzone, J., Dumas, C., Edwards, T., Felikson, D., Fettweis, X., Golledge, N. R., Greve, R., Humbert, A., Huybrechts, P., Le Clec'H, S., Lee, V., Leguy, G., Little, C., Lowry, D., Morlighem, M., Nias, I., Quiquet, A., Rückamp, M., Schlegel, N. J., Slater, D. A., Smith, R., Straneo, F., Tarasov, L., Van De Wal, R., and Van Den Broeke, M.: The future sea-level contribution of the Greenland ice sheet: A multi-model ensemble study of ISMIP6, Cryosphere, 14, 3071–3096, https://doi.org/10.5194/tc-14-3071-2020, 2020.

Gowan, E. J.: Paleo sea-level indicators and proxies from Greenland in the GAPSLIP database and comparison with modelled sea level from the PaleoMIST ice-sheet reconstruction, GEUS Bulletin, 53, 1–17, https://doi.org/10.34194/geusb.v53.8355, 2023.

Grootes, P. M., Stuiver, M., White, J. W. C., Johnsen, S., and Jouzel, J.: Comparison of oxygen isotope records from the GISP2 and GRIP Greenland ice cores, Nature, 366, 552–554, https://doi.org/10.1038/366552a0, 1993.

Håkansson, L., Briner, J., Alexanderson, H., Aldahan, A., and Possnert, G.: 10Be ages from central east Greenland constrain the extent of the Greenland ice sheet during the Last Glacial Maximum, Quat Sci Rev, 26, 2316–2321, https://doi.org/10.1016/j.quascirev.2007.08.001, 2007.

He, C., Liu, Z., Otto-Bliesner, B. L., Brady, E. C., Zhu, C., Tomas, R., Buizert, C., and Severinghaus, J. P.: Abrupt Heinrich Stadial 1 cooling missing in Greenland oxygen isotopes, Sci Adv, 7, 1007–1023, https://doi.org/10.1126/sciadv.abh1007, 2021a.

He, C., Liu, Z., Otto-Bliesner, B. L., Brady, E. C., Zhu, C., Tomas, R., Clark, P. U., Zhu, J., Jahn, A., Gu, S., Zhang, J., Nusbaumer, J., Noone, D., Cheng, H., Wang, Y., Yan, M., and Bao, Y.: Hydroclimate footprint of pan-Asian monsoon water isotope during the last deglaciation, Sci Adv, 7, 1–12, https://doi.org/10.1126/sciadv.abe2611, 2021b.

Hellmer, H., Jacobs, S. S., and Jenkins, A.: Oceanic erosion of a floating Antarctic glacier in the Amundsen Sea, in: American Geophysical Union, 1998.

Hogan, K. A., Ó Cofaigh, C., Jennings, A. E., Dowdeswell, J. A., and Hiemstra, J. F.: Deglaciation of a major palaeo-ice stream in Disko Trough, West Greenland, Quat Sci Rev, 147, 5–26, https://doi.org/10.1016/j.quascirev.2016.01.018, 2016.

Holland, D. M. and Jenkins, A.: Modeling Thermodynamic Ice–Ocean Interactions at the Base of an Ice Shelf, J Phys Oceanogr, 29, 1787–1800, https://doi.org/10.1175/1520-0485(1999)029<1787:MTIOIA>2.0.CO;2, 1999.

Huybrechts, P.: Sea-level changes at the LGM from ice-dynamic reconstructions of the Greenland and Antarctic ice sheets during the glacial cycles, Quat Sci Rev, 21, 203–231, https://doi.org/10.1016/S0277-3791(01)00082-8, 2002.

Huybrechts, P. and de Wolde, J.: The Dynamic Response of the Greenland and Antarctic Ice Sheets to Multiple-Century Climatic Warming, J Clim, 12, 2169–2188, https://doi.org/10.1175/1520-0442(1999)012<2169:TDROTG>2.0.CO;2, 1999.

https://doi.org/10.5194/egusphere-2025-1616
Preprint. Discussion started: 10 April 2025

Hvidberg, C. S., Grinsted, A., Dahl-Jensen, D., Khan, S. A., Kusk, A., Andersen, J. K., Neckel, N., Solgaard, A., Karlsson, N. B., Kjær, H. A., and Vallelonga, P.: Surface velocity of the Northeast Greenland Ice Stream (NEGIS): assessment of interior velocities derived from satellite data by GPS, Cryosphere, 14, 3487–3502, https://doi.org/10.5194/tc-14-3487-2020, 2020.

Iman, R. L.: Latin Hypercube Sampling, in: Encyclopedia of Quantitative Risk Analysis and Assessment, Wiley, https://doi.org/10.1002/9780470061596.risk0299, 2008.

Jennings, A. E., Sheldon, C., Cronin, T. M., Francus, P., Stoner, J., and Andrews, J.: The holocene history of nares strait: transition from Glacial Bay to Arctic- Atlantic Throughflow, Oceanography, 24, 26–41, https://doi.org/10.5670/oceanog.2011.52, 2011.

Jennings, A. E., Andrews, J. T., Ó Cofaigh, C., Onge, G. S., Sheldon, C., Belt, S. T., Cabedo-Sanz, P., and Hillaire-Marcel, C.: Ocean forcing of Ice Sheet retreat in central west Greenland from LGM to the early Holocene, Earth Planet Sci Lett, 472, 1–13, https://doi.org/10.1016/j.epsl.2017.05.007, 2017.

Joughin, I., Smith, B., Howat, I., and Scambos, T.: MEaSUREs Greenland Ice Sheet Velocity Map from InSAR Data, Version 2, 2018a.

Joughin, I., Smith, B., Howat, I., and Scambos, T.: MEaSUREs Greenland Ice Sheet Velocity Map from InSAR Data, Version 2, 2018b.

Katrine Elnegaard Hansen, Lorenzen, J., Davies, J., Wacker, L., Pearce, C., and Seidenkrantz, M.-S.: Deglacial to Mid Holocene environmental conditions on the northeastern Greenland shelf, western Fram Strait, Quat Sci Rev, 293, 107704, https://doi.org/10.1016/j.quascirev.2022.107704, 2022a.

Katrine Elnegaard Hansen, Lorenzen, J., Davies, J., Wacker, L., Pearce, C., and Seidenkrantz, M.-S.: Deglacial to Mid Holocene environmental conditions on the northeastern Greenland shelf, western Fram Strait, Quat Sci Rev, 293, 107704, https://doi.org/10.1016/j.quascirev.2022.107704, 2022b.

Kendall, R. A., Mitrovica, J. X., and Milne, G. A.: On post-glacial sea level - II. Numerical formulation and comparative results on spherically symmetric models, Geophys J Int, 161, 679–706, https://doi.org/10.1111/j.1365-246X.2005.02553.x, 2005.

Keys, R.: Cubic convolution interpolation for digital image processing, IEEE Trans Acoust, 29, 1153–1160, https://doi.org/10.1109/TASSP.1981.1163711, 1981.

Khan, S. A., Sasgen, I., Bevis, M., van Dam, T., Bamber, J. L., Wahr, J., Willis, M., Kjær, K. H., Wouters, B., Helm, V., Csatho, B., Fleming, K., Bjørk, A. A., Aschwanden, A., Knudsen, P., and Munneke, P. K.: Geodetic measurements reveal similarities between post–Last Glacial Maximum and present-day mass loss from the Greenland ice sheet, Sci Adv, 2, https://doi.org/10.1126/sciadv.1600931, 2016.

Khroulev, C. and The PISM authors: PISM, a Parallel Ice Sheet Model v1.2: User's Manual., 2020.

Lambeck, K., Rouby, H., Purcell, A., Sun, Y., and Sambridge, M.: Sea level and global ice volumes from the Last Glacial Maximum to the Holocene, Proceedings of the National Academy of Sciences, 111, 15296–15303, https://doi.org/10.1073/pnas.1411762111, 2014.

Lambeck, K., Purcell, A., and Zhao, S.: The North American Late Wisconsin ice sheet and mantle viscosity from glacial rebound analyses, Quat Sci Rev, 158, 172–210, https://doi.org/10.1016/j.quascirev.2016.11.033, 2017.

Larsen, N. K., Funder, S., Linge, H., Möller, P., Schomacker, A., Fabel, D., Xu, S., and Kjær, K. H.: A Younger Dryas re-advance of local glaciers in north Greenland, Quat Sci Rev, 147, 47–58, https://doi.org/10.1016/j.quascirev.2015.10.036, 2016.

Larsen, N. K., Søndergaard, A. S., Levy, L. B., Olsen, J., Strunk, A., Bjørk, A. A., and Skov, D.: Contrasting modes of deglaciation between fjords and inter-fjord areas in eastern North Greenland, Boreas, 49, 903–917, https://doi.org/10.1111/bor.12475, 2020.

https://doi.org/10.5194/egusphere-2025-1616
Preprint. Discussion started: 10 April 2025

Lecavalier, B. S., Milne, G. A., Vinther, B. M., Fisher, D. A., Dyke, A. S., and Simpson, M. J. R.: Revised estimates of Greenland ice sheet thinning histories based on ice-core records, Quat Sci Rev, 63, 73–82, https://doi.org/10.1016/j.quascirev.2012.11.030, 2013.

Lecavalier, B. S., Milne, G. A., Simpson, M. J. R., Wake, L., Huybrechts, P., Tarasov, L., Kjeldsen, K. K., Funder, S., Long, A. J., Woodroffe, S., Dyke, A. S., and Larsen, N. K.: A model of Greenland ice sheet deglaciation constrained by observations of relative sea level and ice extent, Quat Sci Rev, 102, 54–84, https://doi.org/10.1016/j.quascirev.2014.07.018, 2014.

Leger, T. P. M., Clark, C. D., Huynh, C., Jones, S., Ely, J. C., Bradley, S. L., Diemont, C., and Hughes, A. L. C.: A Greenland-wide empirical reconstruction of paleo ice sheet retreat informed by ice extent markers: PaleoGrIS version 1.0, Climate of the Past, 20, 701–755, https://doi.org/10.5194/cp-20-701-2024, 2024.

Leger, T. P. M., Jouvet, G., Kamleitner, S., Mey, J., Herman, F., Finley, B. D., Ivy-Ochs, S., Vieli, A., Henz, A., and Nussbaumer, S. U.: A data-consistent model of the last glaciation in the Alps achieved with physics-driven AI, Nat Commun, 16, 848, https://doi.org/10.1038/s41467-025-56168-3, 2025.

Levermann, A., Albrecht, T., Winkelmann, R., Martin, M. A., Haseloff, M., and Joughin, I.: Kinematic first-order calving law implies potential for abrupt ice-shelf retreat, Cryosphere, 6, 273–286, https://doi.org/10.5194/tc-6-273-2012, 2012.

Lingle, C. S. and Clark, J. A.: A numerical model of interactions between a marine ice sheet and the solid earth: Application to a West Antarctic ice stream, J Geophys Res Oceans, 90, 1100–1114, https://doi.org/10.1029/JC090iC01p01100, 1985.

Liu, Z., Otto-Bliesner, B. L., He, F., Brady, E. C., Tomas, R., Clark, P. U., Carlson, A. E., Lynch-Stieglitz, J., Curry, W., Brook, E., Erickson, D., Jacob, R., Kutzbach, J., and Cheng, J.: Transient Simulation of Last Deglaciation with a New Mechanism for Bølling-Allerød Warming, Science (1979), 325, 310–314, https://doi.org/10.1126/science.1171041, 2009.

Lloyd, J. M., Ribeiro, S., Weckström, K., Callard, L., Ó Cofaigh, C., Leng, M. J., Gulliver, P., and Roberts, D. H.: Ice-ocean interactions at the Northeast Greenland Ice stream (NEGIS) over the past 11,000 years, Quat Sci Rev, 308, 108068, https://doi.org/10.1016/j.quascirev.2023.108068, 2023.

Lofverstrom, M., Fyke, J. G., Thayer-Calder, K., Muntjewerf, L., Vizcaino, M., Sacks, W. J., Lipscomb, W. H., Otto-Bliesner, B. L., and Bradley, S. L.: An Efficient Ice Sheet/Earth System Model Spin-up Procedure for CESM2-CISM2: Description, Evaluation, and Broader Applicability, J Adv Model Earth Syst, 12, https://doi.org/10.1029/2019MS001984, 2020.

Lüthi, D., Le Floch, M., Bereiter, B., Blunier, T., Barnola, J.-M., Siegenthaler, U., Raynaud, D., Jouzel, J., Fischer, H., Kawamura, K., and Stocker, T. F.: High-resolution carbon dioxide concentration record 650,000–800,000 years before present, Nature, 453, 379–382, https://doi.org/10.1038/nature06949, 2008.

Ma, Q., Shi, X., Scholz, P., Sidorenko, D., Lohmann, G., and Ionita, M.: Revisiting climate impacts of an AMOC slowdown: dependence on freshwater locations in the North Atlantic, Sci Adv, 10, 3243, https://doi.org/10.1126/sciadv.adr3243, 2024.

Mankoff, K. D., Solgaard, A., Colgan, W., Ahlstrøm, A. P., Khan, S. A., and Fausto, R. S.: Greenland Ice Sheet solid ice discharge from 1986 through March 2020, Earth Syst Sci Data, 12, 1367–1383, https://doi.org/10.5194/essd-12-1367-2020, 2020.

Marienfeld, P.: Faziesvariationen glazialmariner Sedimente im Scoresby-Sund, Ost-Grönland, Zentralblatt für Geologie und Paläontologie, 1, 1739–1749, 1990.

Martin, T., Biastoch, A., Lohmann, G., Mikolajewicz, U., and Wang, X.: On Timescales and Reversibility of the Ocean's Response to Enhanced Greenland Ice Sheet Melting in Comprehensive Climate Models, Geophys Res Lett, 49, https://doi.org/10.1029/2021GL097114, 2022.

https://doi.org/10.5194/egusphere-2025-1616
Preprint. Discussion started: 10 April 2025

Martos, Y. M., Jordan, T. A., Catalán, M., Jordan, T. M., Bamber, J. L., and Vaughan, D. G.: Geothermal Heat Flux Reveals the Iceland Hotspot Track Underneath Greenland, Geophys Res Lett, 45, 8214–8222, https://doi.org/10.1029/2018GL078289, 2018.

Menard, H. W. and Smith, S. M.: Hypsometry of ocean basin provinces, J Geophys Res, 71, 4305–4325, https://doi.org/10.1029/JZ071i018p04305, 1966.

Meredith, M., Sommerkorn, M., Cassotta, S., Derksen, C., Ekaykin, A., Hollowed, A., Kofinas, G., Mackintosh, A., Melbourne-Thomas, J., Muelbert, M. M. C., Ottersen, G., Pritchard, H., and Schuur, E. A. G.: Polar regions. Chapter 3, IPCC Special Report on the Ocean and Cryosphere in a Changing Climate, 203–320 pp., 2019.

Millan, R., Mouginot, J., Rabatel, A., and Morlighem, M.: Ice velocity and thickness of the world's glaciers, Nat Geosci, 15, https://doi.org/10.1038/s41561-021-00885-z, 2022.

Mitrovica, J. X. and Milne, G. A.: On post-glacial sea level: I. General theory, Geophys J Int, 154, 253–267, https://doi.org/10.1046/j.1365-246X.2003.01942.x, 2003.

Morlighem, M., Rignot, E., Mouginot, J., Seroussi, H., and Larour, E.: Deeply incised submarine glacial valleys beneath the Greenland ice sheet, Nat Geosci, 7, 418–422, https://doi.org/10.1038/ngeo2167, 2014.

Morlighem, M., Williams, C. N., Rignot, E., An, L., Arndt, J. E., Bamber, J. L., Catania, G., Chauché, N., Dowdeswell, J. A., Dorschel, B., Fenty, I., Hogan, K., Howat, I., Hubbard, A., Jakobsson, M., Jordan, T. M., Kjeldsen, K. K., Millan, R., Mayer, L., Mouginot, J., Noël, B. P. Y., O'Cofaigh, C., Palmer, S., Rysgaard, S., Seroussi, H., Siegert, M. J., Slabon, P., Straneo, F., van den Broeke, M. R., Weinrebe, W., Wood, M., and Zinglersen, K. B.: BedMachine v3: Complete Bed Topography and Ocean Bathymetry Mapping of Greenland From Multibeam Echo Sounding Combined With Mass Conservation, Geophys Res Lett, 44, 11,051-11,061, https://doi.org/10.1002/2017GL074954, 2017a.

Morlighem, M., Williams, C. N., Rignot, E., An, L., Arndt, J. E., Bamber, J. L., Catania, G., Chauché, N., Dowdeswell, J. A., Dorschel, B., Fenty, I., Hogan, K., Howat, I., Hubbard, A., Jakobsson, M., Jordan, T. M., Kjeldsen, K. K., Millan, R., Mayer, L., Mouginot, J., Noël, B. P. Y., O'Cofaigh, C., Palmer, S., Rysgaard, S., Seroussi, H., Siegert, M. J., Slabon, P., Straneo, F., van den Broeke, M. R., Weinrebe, W., Wood, M., and Zinglersen, K. B.: BedMachine v3: Complete Bed Topography and Ocean Bathymetry Mapping of Greenland From Multibeam Echo Sounding Combined With Mass Conservation, Geophys Res Lett, 44, 11,051-11,061, https://doi.org/10.1002/2017GL074954, 2017b.

Motyka, R. J., Truffer, M., Fahnestock, M., Mortensen, J., Rysgaard, S., and Howat, I.: Submarine melting of the 1985 Jakobshavn Isbrae floating tongue and the triggering of the current retreat, J Geophys Res Earth Surf, 116, n/a-n/a, https://doi.org/10.1029/2009JF001632, 2011.

NIU, L., LOHMANN, G., HINCK, S., GOWAN, E. J., and KREBS-KANZOW, U.: The sensitivity of Northern Hemisphere ice sheets to atmospheric forcing during the last glacial cycle using PMIP3 models, Journal of Glaciology, 65, 645–661, https://doi.org/10.1017/jog.2019.42, 2019.

NorthGRIPMembers, Andersen, K. K., Azuma, N., Barnola, J.-M., Bigler, M., Biscaye, P. E., Caillon, N., Chappellaz, J., Clausen, H. B., Dahl-Jensen, D., Fischer, H., Flückiger, J., Fritzsche, D., Fujii, Y., Goto-Azuma, K., Grønvold, K., Gundestrup, N. S., Hansson, M., Huber, C., Hvidberg, C. S., Johnsen, S. J., Jonsell, U., Jouzel, J., Kipfstuhl, S., Landais, A., Leuenberger, M., Lorrain, R., Masson-Delmotte, V., Miller, H., Motoyama, H., Narita, H., Popp, T., Rasmussen, S. O., Raynaud, D., Rothlisberger, R., Ruth, U., Samyn, D., Schwander, J., Shoji, H., Siggaard-Andersen, M.-L., Steffensen, J.-P. P., Stocker, T., Sveinbjörnsdóttir, A. E., Svensson, A., Takata, M., Tison, J.-L., Thorsteinsson, T., Watanabe, O., Wilhelms, F., White, J. W. C., and Siggard-Andersen, M.-L.: High-resolution record of Northern Hemisphere climate extending into the last interglacial period., Nature, 431, 147–151, https://doi.org/10.1038/nature02805, 2004.

Ó Cofaigh, C., Dowdeswell, J. A., Jennings, A. E., Hogan, K. A., Kilfeather, A., Hiemstra, J. F., Noormets, R., Evans, J., McCarthy, D. J., Andrews, J. T., Lloyd, J. M., and Moros, M.: An extensive and dynamic ice sheet on the west greenland shelf during the last glacial cycle, Geology, 41, 219–222, https://doi.org/10.1130/G33759.1, 2013a.

https://doi.org/10.5194/egusphere-2025-1616
Preprint. Discussion started: 10 April 2025

Ó Cofaigh, C., Dowdeswell, J. A., Jennings, A. E., Hogan, K. A., Kilfeather, A., Hiemstra, J. F., Noormets, R., Evans, J., McCarthy, D. J., Andrews, J. T., Lloyd, J. M., and Moros, M.: An extensive and dynamic ice sheet on the west greenland shelf during the last glacial cycle, Geology, 41, 219–222, https://doi.org/10.1130/G33759.1, 2013b.

Oerlemans, J., Anderson, B., Hubbard, A., Huybrechts, P., Jóhannesson, T., Knap, W. H., Schmeits, M., Stroeven, A. P., van de Wal, R. S. W., Wallinga, J., and Zuo, Z.: Modelling the response of glaciers to climate warming, Clim Dyn, 14, 267–274, https://doi.org/10.1007/s003820050222, 1998.

Osman, M. B., Tierney, J. E., Zhu, J., Tardif, R., Hakim, G. J., King, J., and Poulsen, C. J.: Globally resolved surface temperatures since the Last Glacial Maximum, Nature, 599, 239–244, https://doi.org/10.1038/s41586-021-03984-4, 2021.

Patterson, V. L., Gregoire, L. J., Ivanovic, R. F., Gandy, N., Owen, J., Smith, R. S., Pollard, O. G., Astfalck, L. C., and Valdes, P. J.: Contrasting the Penultimate Glacial Maximum and the Last Glacial Maximum (140 and 21 ka) using coupled climate–ice sheet modelling, Climate of the Past, 20, 2191–2218, https://doi.org/10.5194/cp-20-2191-2024, 2024.

Peltier, W. R., Argus, D. F., and Drummond, R.: Space geodesy constrains ice age terminal deglaciation: The global ICE-6G_C (VM5a) model, J Geophys Res Solid Earth, 120, 450–487, https://doi.org/10.1002/2014JB011176, 2015.

Pittard, M. L., Whitehouse, P. L., Bentley, M. J., and Small, D.: An ensemble of Antarctic deglacial simulations constrained by geological observations, Quat Sci Rev, 298, 107800, https://doi.org/10.1016/j.quascirev.2022.107800, 2022.

Plach, A., Nisancioglu, K. H., Langebroek, P. M., Born, A., and Le clec'h, S.: Eemian Greenland ice sheet simulated with a higher-order model shows strong sensitivity to surface mass balance forcing, Cryosphere, 13, 2133–2148, https://doi.org/10.5194/tc-13-2133-2019, 2019.

Pritchard, H. D., Ligtenberg, S. R. M., Fricker, H. A., Vaughan, D. G., van den Broeke, M. R., and Padman, L.: Antarctic ice-sheet loss driven by basal melting of ice shelves, Nature, 484, 502–505, https://doi.org/10.1038/nature10968, 2012.

Quiquet, A., Roche, D. M., Dumas, C., Bouttes, N., and Lhardy, F.: Climate and ice sheet evolutions from the last glacial maximum to the pre-industrial period with an ice-sheet–climate coupled model, Climate of the Past, 17, 2179–2199, https://doi.org/10.5194/cp-17-2179-2021, 2021.

Rasmussen, S. O., Abbott, P. M., Blunier, T., Bourne, A. J., Brook, E., Buchardt, S. L., Buizert, C., Chappellaz, J., Clausen, H. B., Cook, E., Dahl-Jensen, D., Davies, S. M., Guillevic, M., Kipfstuhl, S., Laepple, T., Seierstad, I. K., Severinghaus, J. P., Steffensen, J. P., Stowasser, C., Svensson, A., Vallelonga, P., Vinther, B. M., Wilhelms, F., and Winstrup, M.: A first chronology for the North Greenland Eemian Ice Drilling (NEEM) ice core, Climate of the Past, 9, 2713–2730, https://doi.org/10.5194/cp-9-2713-2013, 2013.

Rasmussen, S. O., Dahl-Jensen, D., Fischer, H., Fuhrer, K., Hansen, S. B., Hansson, M., Hvidberg, C. S., Jonsell, U., Kipfstuhl, S., Ruth, U., Schwander, J., Siggaard-Andersen, M.-L., Sinnl, G., Steffensen, J. P., Svensson, A. M., and Vinther, B. M.: Ice-core data used for the construction of the Greenland Ice-Core Chronology 2005 and 2021 (GICC05 and GICC21), Earth Syst Sci Data, 15, 3351–3364, https://doi.org/10.5194/essd-15-3351-2023, 2023.

Rieckh, T., Born, A., Robinson, A., Law, R., and Gülle, G.: Design and performance of ELSA v2.0: an isochronal model for ice-sheet layer tracing, Geosci Model Dev, 17, 6987–7000, https://doi.org/10.5194/gmd-17-6987-2024, 2024.

Rinterknecht, V., Jomelli, V., Brunstein, D., Favier, V., Masson-Delmotte, V., Bourlès, D., Leanni, L., and Schläppy, R.: Unstable ice stream in Greenland during the Younger Dryas cold event, Geology, 42, 759–762, https://doi.org/10.1130/G35929.1, 2014.

Ritz, C.: EISMINT Intercomparison Experiment: Comparison of existing Greenland models., Laboratoire de Glaciologie et de Géophysique de l'Environnement, Saint Martin d'Hères, France, 1997.

https://doi.org/10.5194/egusphere-2025-1616
Preprint. Discussion started: 10 April 2025

Roberts, D. H., Lane, T. P., Jones, R. S., Bentley, M. J., Darvill, C. M., Rodes, A., Smith, J. A., Jamieson, S. S. R., Rea, B. R., Fabel, D., Gheorghiu, D., Davidson, A., Cofaigh, C. Ó., Lloyd, J. M., Callard, S. L., and Humbert, A.: The deglacial history of 79N glacier and the Northeast Greenland Ice Stream, Quat Sci Rev, 336, 108770, https://doi.org/10.1016/j.quascirev.2024.108770, 2024a.

Roberts, D. H., Lane, T. P., Jones, R. S., Bentley, M. J., Darvill, C. M., Rodes, A., Smith, J. A., Jamieson, S. S. R., Rea, B. R., Fabel, D., Gheorghiu, D., Davidson, A., Cofaigh, C. Ó., Lloyd, J. M., Callard, S. L., and Humbert, A.: The deglacial history of 79N glacier and the Northeast Greenland Ice Stream, Quat Sci Rev, 336, 108770, https://doi.org/10.1016/j.quascirev.2024.108770, 2024b.

Rogozhina, I., Martinec, Z., Hagedoorn, J. M., Thomas, M., and Fleming, K.: On the long-term memory of the Greenland ice sheet, J Geophys Res Earth Surf, 116, 1–16, https://doi.org/10.1029/2010JF001787, 2011.

Rovere, A., Stocchi, P., and Vacchi, M.: Eustatic and Relative Sea Level Changes, Curr Clim Change Rep, 2, 221–231, https://doi.org/10.1007/s40641-016-0045-7, 2016.

Sbarra, C. M., Briner, J. P., Graham, B. L., Poinar, K., Thomas, E. K., and Young, N. E.: Evidence for a more extensive Greenland Ice Sheet in southwestern Greenland during the Last Glacial Maximum, Geosphere, 18, 1316–1329, https://doi.org/10.1130/GES02432.1, 2022a.

Sbarra, C. M., Briner, J. P., Graham, B. L., Poinar, K., Thomas, E. K., and Young, N. E.: Evidence for a more extensive Greenland Ice Sheet in southwestern Greenland during the Last Glacial Maximum, Geosphere, 18, 1316–1329, https://doi.org/10.1130/GES02432.1, 2022b.

Seguinot, J. and Rogozhina, I.: Daily temperature variability predetermined by thermal conditions over ice-sheet surfaces, Journal of Glaciology, 60, 603–605, https://doi.org/10.3189/2014JoG14J036, 2014.

Seroussi, H., Nowicki, S., Simon, E., Abe-Ouchi, A., Albrecht, T., Brondex, J., Cornford, S., Dumas, C., Gillet-Chaulet, F., Goelzer, H., Golledge, N. R., Gregory, J. M., Greve, R., Hoffman, M. J., Humbert, A., Huybrechts, P., Kleiner, T., Larour, E., Leguy, G., Lipscomb, W. H., Lowry, D., Mengel, M., Morlighem, M., Pattyn, F., Payne, A. J., Pollard, D., Price, S. F., Quiquet, A., Reerink, T. J., Reese, R., Rodehacke, C. B., Schlegel, N. J., Shepherd, A., Sun, S., Sutter, J., Van Breedam, J., Van De Wal, R. S. W., Winkelmann, R., and Zhang, T.: InitMIP-Antarctica: An ice sheet model initialization experiment of ISMIP6, Cryosphere, 13, 1441–1471, https://doi.org/10.5194/tc-13-1441-2019, 2019.

Simonsen, S. B., Barletta, V. R., Colgan, W. T., and Sørensen, L. S.: Greenland Ice Sheet Mass Balance (1992–2020) From Calibrated Radar Altimetry, Geophys Res Lett, 48, 1–10, https://doi.org/10.1029/2020GL091216, 2021.

Simpson, M. J. R., Milne, G. A., Huybrechts, P., and Long, A. J.: Calibrating a glaciological model of the Greenland ice sheet from the Last Glacial Maximum to present-day using field observations of relative sea level and ice extent, Quat Sci Rev, 28, 1631–1657, https://doi.org/10.1016/j.quascirev.2009.03.004, 2009.

Sinclair, G., Carlson, A. E., Mix, A. C., Lecavalier, B. S., Milne, G., Mathias, A., Buizert, C., and DeConto, R.: Diachronous retreat of the Greenland ice sheet during the last deglaciation, Quat Sci Rev, 145, 243–258, https://doi.org/10.1016/j.quascirev.2016.05.040, 2016.

Sinet, S., von der Heydt, A. S., and Dijkstra, H. A.: AMOC Stabilization Under the Interaction With Tipping Polar Ice Sheets, Geophys Res Lett, 50, https://doi.org/10.1029/2022GL100305, 2023.

Smith-Johnsen, S., de Fleurian, B., Schlegel, N., Seroussi, H., and Nisancioglu, K.: Exceptionally high heat flux needed to sustain the Northeast Greenland Ice Stream, Cryosphere, 14, 841–854, https://doi.org/10.5194/tc-14-841-2020, 2020.

Søndergaard, A. S., Larsen, N. K., Steinemann, O., Olsen, J., Funder, S., Egholm, D. L., and Kjær, K. H.: Glacial history of Inglefield Land, north Greenland from combined in situ 10Be and 14C exposure dating, Climate of the Past, 16, 1999–2015, https://doi.org/10.5194/cp-16-1999-2020, 2020.

Stein, M.: Large Sample Properties of Simulations Using Latin Hypercube Sampling, Technometrics, 29, 143–151, https://doi.org/10.1080/00401706.1987.10488205, 1987.

https://doi.org/10.5194/egusphere-2025-1616
Preprint. Discussion started: 10 April 2025

Swift, D. A., Persano, C., Stuart, F. M., Gallagher, K., and Whitham, A.: A reassessment of the role of ice sheet glaciation in the long-term evolution of the East Greenland fjord region, Geomorphology, 97, 109–125, https://doi.org/10.1016/j.geomorph.2007.02.048, 2008.

Tabone, I., Blasco, J., Robinson, A., Alvarez-Solas, J., and Montoya, M.: The sensitivity of the Greenland Ice Sheet to glacial–interglacial oceanic forcing, Climate of the Past, 14, 455–472, https://doi.org/10.5194/cp-14-455-2018, 2018.

Tadono, T., Ishida, H., Oda, F., Naito, S., Minakawa, K., and Iwamoto, H.: Precise Global DEM Generation by ALOS PRISM, ISPRS Annals of the Photogrammetry, Remote Sensing and Spatial Information Sciences, II–4, 71–76, https://doi.org/10.5194/isprsannals-II-4-71-2014, 2014.

Tarasov, L., Dyke, A. S., Neal, R. M., and Peltier, W. R.: A data-calibrated distribution of deglacial chronologies for the North American ice complex from glaciological modeling, Earth Planet Sci Lett, 315–316, 30–40, https://doi.org/10.1016/j.epsl.2011.09.010, 2012.

The IMBIE Team: Mass balance of the Greenland Ice Sheet from 1992 to 2018, Nature, 579, 233–239, https://doi.org/10.1038/s41586-019-1855-2, 2019.

Tierney, J. E., Zhu, J., King, J., Malevich, S. B., Hakim, G. J., and Poulsen, C. J.: Glacial cooling and climate sensitivity revisited, Nature, 584, 569–573, https://doi.org/10.1038/s41586-020-2617-x, 2020.

Tulaczyk, S., Kamb, W. B., and Engelhardt, H. F.: Basal mechanics of Ice Stream B, west Antarctica: 2. Undrained plastic bed model, J Geophys Res Solid Earth, 105, 483–494, https://doi.org/10.1029/1999JB900328, 2000.

van Kampenhout, L., Lenaerts, J. T. M., Lipscomb, W. H., Lhermitte, S., Noël, B., Vizcaíno, M., Sacks, W. J., and van den Broeke, M. R.: Present-Day Greenland Ice Sheet Climate and Surface Mass Balance in CESM2, J Geophys Res Earth Surf, 125, https://doi.org/10.1029/2019JF005318, 2020.

Vinther, B. M., Buchardt, S. L., Clausen, H. B., Dahl-Jensen, D., Johnsen, S. J., Fisher, D. A., Koerner, R. M., Raynaud, D., Lipenkov, V., Andersen, K. K., Blunier, T., Rasmussen, S. O., Steffensen, J. P., and Svensson, A. M.: Holocene thinning of the Greenland ice sheet, Nature, 461, 385–388, https://doi.org/10.1038/nature08355, 2009.

Winkelmann, R., Martin, M. A., Haseloff, M., Albrecht, T., Bueler, E., Khroulev, C., and Levermann, A.: The Potsdam Parallel Ice Sheet Model (PISM-PIK) – Part 1: Model description, Cryosphere, 5, 715–726, https://doi.org/10.5194/tc-5-715-2011, 2011.

Yan, Q., Zhang, Z., Gao, Y., Wang, H., and Johannessen, O. M.: Sensitivity of the modeled present-day Greenland Ice Sheet to climatic forcing and spin-up methods and its influence on future sea level projections, J Geophys Res Earth Surf, 118, 2174–2189, https://doi.org/10.1002/jgrf.20156, 2013.

Yang, H., Krebs-Kanzow, U., Kleiner, T., Sidorenko, D., Rodehacke, C. B., Shi, X., Gierz, P., Niu, L., Gowan, E. J., Hinck, S., Liu, X., Stap, L. B., and Lohmann, G.: Impact of paleoclimate on present and future evolution of the Greenland Ice Sheet, PLoS One, 17, 1–21, https://doi.org/10.1371/journal.pone.0259816, 2022.

Yu, L., Gao, Y., and Otterå, O. H.: The sensitivity of the Atlantic meridional overturning circulation to enhanced freshwater discharge along the entire, eastern and western coast of Greenland, Clim Dyn, 46, 1351–1369, https://doi.org/10.1007/s00382-015-2651-9, 2016.

Zhu, J., Liu, Z., Brady, E., Otto-Bliesner, B., Zhang, J., Noone, D., Tomas, R., Nusbaumer, J., Wong, T., Jahn, A., and Tabor, C.: Reduced ENSO variability at the LGM revealed by an isotope-enabled Earth system model, Geophys Res Lett, 44, 6984–6992, https://doi.org/10.1002/2017GL073406, 2017.

Zoet, L. K. and Iverson, N. R.: A slip law for glaciers on deformable beds, Science (1979), 368, 76–78, https://doi.org/10.1126/science.aaz1183, 2020.